

*Aki Koskela*

UTILISATION OF LIGNIN-  
BASED BIOCARBON IN  
PYROMETALLURGICAL  
APPLICATIONS

UNIVERSITY OF OULU GRADUATE SCHOOL;  
UNIVERSITY OF OULU,  
FACULTY OF TECHNOLOGY





ACTA UNIVERSITATIS OULUENSIS  
C Technica 882

*AKI KOSKELA*

**UTILISATION OF LIGNIN-BASED  
BIOCARBON IN  
PYROMETALLURGICAL  
APPLICATIONS**

Academic dissertation to be presented with the assent of the Doctoral Programme Committee of Technology and Natural Sciences of the University of Oulu for public defence in the OP auditorium (L10), Linnanmaa, on 12 May 2023, at 12 noon

UNIVERSITY OF OULU, OULU 2023

Copyright © 2023  
Acta Univ. Oul. C 882, 2023

Supervised by  
Professor Timo Fabritius  
Doctor Hannu Suopajarvi

Reviewed by  
Professor Merete Tangstad  
Doctor Elsayed Mousa

Opponent  
Professor Ari Jokilaakso

ISBN 978-952-62-3667-4 (Paperback)  
ISBN 978-952-62-3668-1 (PDF)

ISSN 0355-3213 (Printed)  
ISSN 1796-2226 (Online)

Cover Design  
Raimo Ahonen

PUNAMUSTA  
TAMPERE 2023

## **Koskela, Aki, Utilisation of lignin-based biocarbon in pyrometallurgical applications.**

University of Oulu Graduate School; University of Oulu, Faculty of Technology

*Acta Univ. Oul. C 882, 2023*

University of Oulu, P.O. Box 8000, FI-90014 University of Oulu, Finland

### ***Abstract***

Pyrometallurgical processes in the iron and steel industry are energy intensive. Therefore, sustainability in terms of CO<sub>2</sub> emissions is highly dependent on the choice of fuel. Large quantities of carbon are used in pyrometallurgical processes, for example in slag foaming, iron oxide reduction or as an alloying element. Currently, the majority of the used carbon originates from fossil sources.

The most important properties that are generally required from carbonaceous materials in pyrometallurgical applications are mechanical strength, sufficient apparent density and suitable reactivity. The properties of industrially produced metallurgical coke works as a great reference for evaluation of these properties, since metallurgical coke is used in multiple pyrometallurgical applications in different forms: coke dust is used as a foaming agent and carburiser in the electric arc furnace (EAF) process, and coke lumps are used as a reducing agent and structural bed material in the blast furnace (BF) process and as a reducing agent in submerged arc furnace (SAF) process.

This thesis focuses on the utilisation of hydrolysis lignin as a raw material for the production of biocarbon that could be utilised as a carbonaceous material in pyrometallurgical applications to substitute fossil-based carbon. Based on the results of this thesis, it was discovered that the structure of lignin-based biocarbon can be modified using the chosen treatment methods, briquetting and high pyrolysis temperature. With these treatment methods, the important properties (mechanical strength, apparent density and reactivity) were improved and modified, with the compressive strength property of biocarbon even surpassing that of metallurgical coke.

*Keywords:* biocarbon, biocoke, biomass, carbonization, hydrolysis lignin, properties, pyrolysis



## **Koskela, Aki, Ligniinipohjaisen biohiilen käyttö metallurgisissa sovelluksissa.**

Oulun yliopiston tutkijakoulu; Oulun yliopisto, Teknillinen tiedekunta

*Acta Univ. Oul. C 882, 2023*

Oulun yliopisto, PL 8000, 90014 Oulun yliopisto

### ***Tiivistelmä***

Terästeollisuuden pyrometallurgiset prosessit ovat energiaintensiivisiä. Sen vuoksi terästeollisuuden ekologisuus CO<sub>2</sub> päästöjen osalta on erittäin riippuvainen polttoainevalinnasta. Suuria määriä hiiltä käytetään pyrometallurgisissa prosesseissa, esimerkiksi kuonan kuohutuksessa, raudan oksidien pelkistyksessä tai seosaineena. Nykyään suurin osa käytetystä hiilestä on lähtöisin fossiilisista lähteistä.

Pyrometallurgisissa prosesseissa käytettäviltä hiilimateriaaleilta vaadittuja tärkeimpiä ominaisuuksia ovat mekaaninen lujuus, riittävä näennäistiheys ja sopiva reaktiivisuus. Teollisesti valmistetun metallurgisen koksen ominaisuudet sopivat hyvin näiden ominaisuuksien vertailukohdaksi, sillä koksia käytetään useissa eri sovelluksissa eri muodoissa: koksipölyä käytetään kuonan kuohutusaineena ja hiilen tuojana valokaariuuniprosessissa, palakoksia pelkistimenä ja rakenteellisena petimateriaalina masuunissa sekä pelkistimenä uppokaariuunissa.

Tämä työ keskittyy hydrolyysiligniinin hyötykäyttöön raaka-aineena biohiilen ja biokoksen valmistuksessa, joita voidaan käyttää hiilen tuojana pyrometallurgisissa sovelluksissa korvaamaan fossiilista lähteistä tuotettua hiiltä. Tämän työn tulosten perusteella hydrolyysiligniini-pohjaisen biohiilen rakennetta pystyttiin muokkaamaan valituilla käsittelymenetelmillä, briketoinnilla ja korkealla pyrolyysilämpötilalla. Näillä menetelmillä biohiilen tärkeitä ominaisuuksia (mekaaninen lujuus, näennäistiheys ja reaktiivisuus) saatiin parannettua siten, että biohiilen puristuslujuus oli jopa suurempi kuin metallurgisella koksilla.

*Asiasanat:* biohiili, biokoksi, biomassa, hiillestys, hydrolyysiligniini, ominaisuudet, pyrolyysi



*Dedicated to my beloved family*



## Preface

This work was carried out at the Process Metallurgy Research Unit, University of Oulu from spring 2017 to autumn 2022. The research was conducted as part of several projects: Fundamentals of formation and properties of metallurgical coke (FFPMC) funded by the Academy of Finland, Biostart, which was a customer-financed research project, Carbotech, funded by the European Regional Development Fund (ERDF), and TOCANEM, funded by Business Finland. The research and writing work for the compilation part was performed as part of the TOCANEM project, while the research work and the writing of the original papers was performed as part of the other mentioned projects.

I would like to thank my thesis supervisors Professor Timo Fabritius from the Process Metallurgy Research Unit and Dr Hannu Suopajärvi from Sapotech for his guidance, support and patience during this process. They provided me with an interesting and important topic for research. This has been a great opportunity for me to develop my expertise as a researcher.

I would like to thank the co-authors of the original research papers. I feel that their contribution to the original research papers have resulted in a great amount of added value for each research topic.

Great thanks to all my colleagues at the Process Metallurgy Research Unit. Special thanks to Tommi Kokkonen and Riku Mattila, who have provided their technical support and know-how to each of the original research papers.

I would also like to thank Professor Merete Tangstad from Norwegian University of Science and Technology and Dr. Elsayed Mousa from Swerim AB for reviewing this thesis and for their comments.

Finally, I owe my deepest gratitude to my family. Their support has been inexpressibly important, especially at those times when the stress seemed to get the better of me.

Oulu, 31.3.2023

Aki Koskela



## Abbreviations

ARR	Apparent reaction rate
ASTM	American Society for Testing and Materials
BET	Brunauer-Emmett-Teller
BF	Blast furnace
BOF	Basic oxygen furnace
CHP	Combined heat and power
CRI	Coke reactivity index
CSR	Coke strength after reaction
db.	Dry basis
ddpm	Dial divisions per minute
DFT	Density functional theory
EAF	Electric arc furnace
FSI	Free swelling index
GHG	Greenhouse gas
IMDC	Inert maceral derived component
IUPAC	International Union of Pure and Applied Chemistry
LOM	Light optical microscopy
MS	Mass spectrometer
NIST	National Institute of Standards and Technology
SSA	Specific surface area
TGA	Thermogravimetric analysis



## List of original publications

This thesis is based on the following publications, which are referred to throughout the text by their Roman numerals:

- I Koskela, A., Suopajarvi, H., Mattila, O., Uusitalo, J., & Fabritius, T. (2019). Lignin from bioethanol production as a part of a raw material blend of a metallurgical coke. *Energies*, 12(8), 1533. <https://doi.org/10.3390/en12081533>
- II Koskela, A., Heikkilä, A., Bergna, D., Salminen, J., & Fabritius, T. (2021). Effects of briquetting and high pyrolysis temperature on hydrolysis lignin char properties and reactivity in CO-CO<sub>2</sub>-N<sub>2</sub> conditions. *Minerals*, 11(2), 187. <https://doi.org/10.3390/min11020187>
- III Koskela, A., Suopajarvi, H., & Fabritius, T. (2022). Interaction between coal and lignin briquettes in co-carbonization. *Fuel*, 324, 124823. <https://doi.org/10.1016/j.fuel.2022.124823>
- IV Koskela, A., Suopajarvi, H., Uusitalo, J., & Fabritius, T. (2023). Evolution of biocarbon strength and structure during gasification in CO<sub>2</sub> containing gas atmosphere. *Fuel Communications*, 14, 100082. <https://doi.org/10.1016/j.jfueco.2022.100082>

The author was the main author of all the presented papers. The author planned and performed most of the experiments and data processing. The analysis of the results was done by the author.



# Contents

<b>Abstract</b>	
<b>Tiivistelmä</b>	
<b>Preface</b>	<b>9</b>
<b>Abbreviations</b>	<b>11</b>
<b>List of original publications</b>	<b>13</b>
<b>Contents</b>	<b>15</b>
<b>1 Introduction</b>	<b>17</b>
1.1 Outline and objective of the study .....	18
<b>2 Metallurgical coke</b>	<b>23</b>
2.1 Properties of coal .....	23
2.2 Coking coal .....	24
2.2.1 Physical properties of coking coal.....	25
2.2.2 Chemical properties of coking coal .....	26
2.2.3 Coking properties .....	27
2.2.4 Stability of the quality .....	28
2.3 Coke quality .....	29
2.4 Bio-based material as part of a coking blend .....	30
<b>3 Lignin</b>	<b>31</b>
3.1 Hydrolysis lignin.....	31
3.2 Lignin structure .....	32
3.3 Pyrolysis of lignin .....	32
<b>4 Materials and methods</b>	<b>35</b>
4.1 The effect of hydrolysis lignin addition on the formation and properties of biocoke.....	35
4.1.1 Coke preparation .....	36
4.1.2 Interaction between coking coal and hydrolysis lignin- based materials .....	38
4.2 Hydrolysis lignin-based reductants for substitution of fossil- based reductants .....	40
4.2.1 Structural changes and gasification reactivity of pyrolysed hydrolysis lignin .....	42
4.2.2 Evolution of biocarbon structure and mechanical strength at different levels of gasification .....	43
<b>5 Results of biocoke formation and properties</b>	<b>47</b>
5.1 Chemical composition of biocoke raw materials .....	47

5.2	Chemical composition of biocarbons .....	50
5.3	Coking properties of coal .....	51
5.4	Volatile release during co-carbonisation .....	52
5.5	Released devolatilisation products of hydrolysis lignin .....	55
5.6	Properties of biocokes .....	57
5.6.1	Visual evaluation of the produced biocokes .....	57
5.6.2	Compression strength of biocokes .....	60
5.6.3	Reactivity of the biocokes .....	63
5.6.4	Structure of the surface of biocokes .....	64
5.7	Interaction during co-carbonisation.....	68
5.7.1	Volumetric changes of hydrolysis lignin-based briquettes during co-carbonisation .....	69
<b>6</b>	<b>Results of biocarbon formation and properties</b>	<b>73</b>
6.1	Chemical composition.....	73
6.2	The effect of pyrolysis conditions on the solid biocarbon yield.....	76
6.3	The structure of biocarbons.....	79
6.4	High temperature reactivity of biocarbons .....	81
6.4.1	Dynamic reactivity tests .....	81
6.4.2	Isothermal reactivity tests at the level of 20% mass loss.....	83
6.4.3	Inhibitive effect of CO on the gasification of biocarbon and nut coke.....	86
6.4.4	Gasification to higher levels of mass loss.....	88
6.5	Structural changes during gasification .....	92
6.6	Compressive strength of biocarbons and nut coke .....	94
6.7	Relationship between the level of gasification, structural changes and compressive strength .....	99
<b>7</b>	<b>Evaluation of the results</b>	<b>103</b>
<b>8</b>	<b>Conclusions and future research</b>	<b>107</b>
8.1	Conclusions .....	107
8.2	Future research .....	111
	<b>References</b>	<b>113</b>
	<b>Original publications</b>	<b>123</b>

# 1 Introduction

The iron and steel industry is undergoing a period of transition towards an era of direct reduction, where hydrogen will be used as a reducing agent of iron instead of carbonaceous materials, e.g. metallurgical coke. Meanwhile, the conventional blast furnace (BF) basic oxygen furnace (BOF) process route is considered to produce too many greenhouse gas (GHG) emissions, mainly carbon dioxide (CO<sub>2</sub>) (Patisson & Mirgaux, 2020; Spreitzer & Schenk, 2019; Vogl et al., 2018). However, the transition stage towards hydrogen-based steelmaking will still take years from now, and the BF-BOF steelmaking route will be dominant in the global steelmaking industry during this period. The partial replacement of fossil-based carbon in BF and other pyrometallurgical processes that require carbon would accelerate the transition towards fossil neutrality in the steelmaking industry.

Despite the transition towards hydrogen-based iron and steelmaking, carbon will still play a role in various applications in this industry: as a foaming agent in the electric arc furnace (EAF), as a carburiser of the carbon steel grades from hydrogen reduced iron and as a fuel in sintering process, just to name few of these applications (Echterhof, 2021; Mousa et al., 2016; Robinson et al., 2020; Sakaranaho et al., 2018). These applications do not require such high standards for the properties of carbonaceous materials that are required from metallurgical coke in the BF process, but there are similarities in the requirements of all these applications. In general, suitable reactivity, sufficient strength and apparent density are required from the carbonaceous materials in pyrometallurgical processes. These are also the properties that are addressed to be the most important when considering the challenges in the utilisation of biocarbon as a carbon source in pyrometallurgical processes (Jeguirim & Limousy, 2019; Kumar & Gupta, 1997; Lu et al., 2012; Marcos et al., 2019).

Lignin is the second abundant plant polymer after cellulose. The lignin content in coniferous wood species (softwood) is generally higher (26–34%, dry basis) than that of deciduous (hardwood) species (23–30%, dry basis) (Rowell et al., 2012). When considering the major components in woody biomass (cellulose, hemicellulose and lignin), lignin has the highest solid yield in the pyrolysis process, mainly due to the complex, branch-chained aromatic structure. The binding energy of the chemical bonds in lignin structure cover a wide range, thus the thermal degradation of lignin occurs in a wide temperature range (Yang et al., 2007). Its relatively high solid yield, aromatic carbon structure and adhesive nature (Mili et al., 2022) are the properties that make lignin a desirable raw material for biocarbon

production through thermochemical processing, i.e. pyrolysis for metallurgical applications to substitute for fossil-based carbonaceous materials.

## **1.1 Outline and objective of the study**

The primary objective of this study was to develop a hydrolysis lignin-based biocarbon-containing product that could be utilised in pyrometallurgical processes. The sub-objectives were to provide vital information about the behaviour of the raw material lignin in pyrolysis and the main properties (gasification reactivity and compressive strength) of the chosen biocarbons. Also, information about how the selected pre-treatment methods affected the main properties and structure were in the scope of this study. The pre-treatment methods were chosen based on the desired properties of the biomaterial-containing carbon products. However, the motivation was to keep the pre-treatment methods simple, so that their implementation would be easy. The research within this thesis can be divided into two different branches: Publications I and III investigate the usage of hydrolysis lignin and hydrolysis lignin-based biocarbon as part of a coking blend in biocoke production. Publications II and IV represent the other branch, in which the focus is on the utilisation of hydrolysis lignin-based biocarbons as an individual substitution for fossil-based carbon in pyrometallurgical processes. The objectives of the two branches of the research work in this thesis are as follows:

Utilisation of lignin and lignin-based biocarbons as a part of a coking blend in biocoke production:

- To find out the effect of the pyrolysis of hydrolysis lignin on its behaviour during the coking process.
- The addition of non-pyrolysed and pyrolysed lignin into a coking blend and the effect on the properties of produced biocoke.
- The changes in the reactivity, compressive strength, and porous structure of coke as a function of addition of non-pyrolysed and pyrolysed hydrolysis lignin.
- To evaluate the interaction of coal-hydrolysis lignin and coal hydrolysis lignin-based biocarbon blends during co-carbonisation, and the effect of the pyrolysis temperature of biocarbon on the interaction.
- The physical (dilatation-shrinking behaviour) and chemical (amount of volatile release and gaseous compounds) interaction of biocarbon with the surrounding material matrix during the coking process.

Biocarbon as an individual carbon source to substitute fossil-based carbon in the pyrometallurgical processes:

1. To evaluate suitable hydrolysis lignin pre-treatment methods to improve the properties of biocarbon for utilisation in pyrometallurgical processes.
2. To evaluate the impact of the chosen pre-treatment methods, grinding, briquetting and high pyrolysis temperature on the cold compressive strength, gasification reactivity and structure of the biocarbons.
3. To investigate the effect of gasification on hydrolysis lignin-based biocarbons: structural changes, development of gasification reaction rate and evolution of compressive strength at different stages of gasification.

The main objectives and the contribution of each publication is presented in Fig. 1. The main objectives of the publications are focused on the co-carbonisation of hydrolysis lignin-based biocarbon and coking coal, the structural changes of the produced carbonaceous materials, and their pyrometallurgical properties i.e. mechanical strength and reactivity.

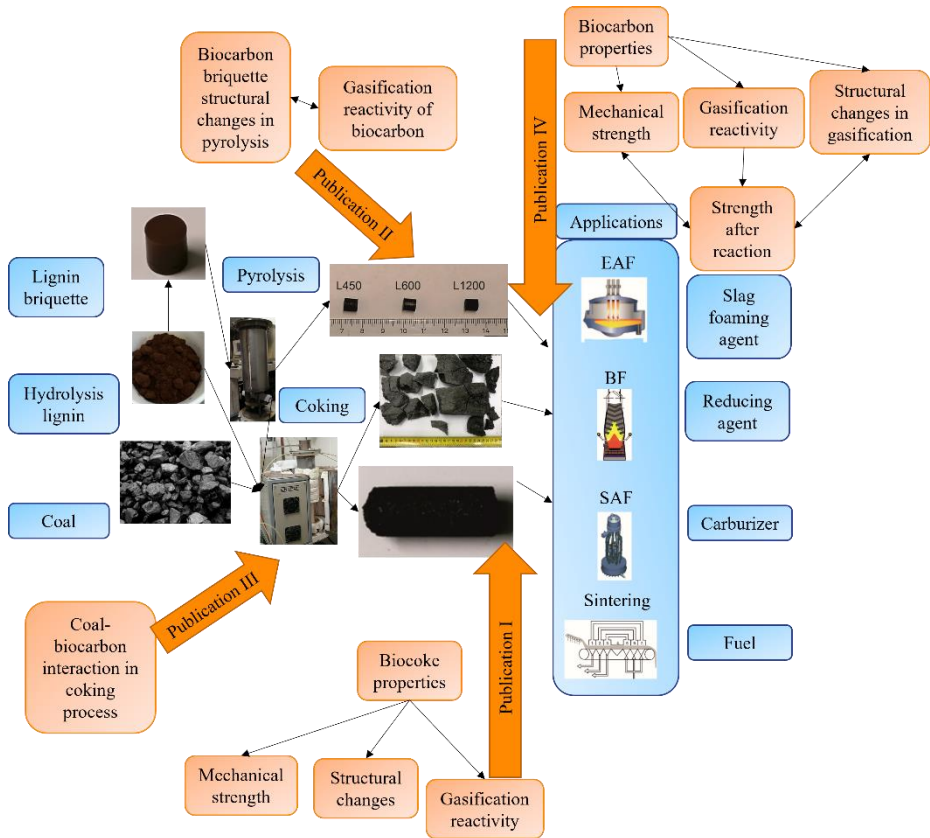


**Fig. 1. General idea of the original publications and the thesis.**

The two branches of the research in this thesis and the contribution of each publication on the objective of this study is presented in Fig. 2.

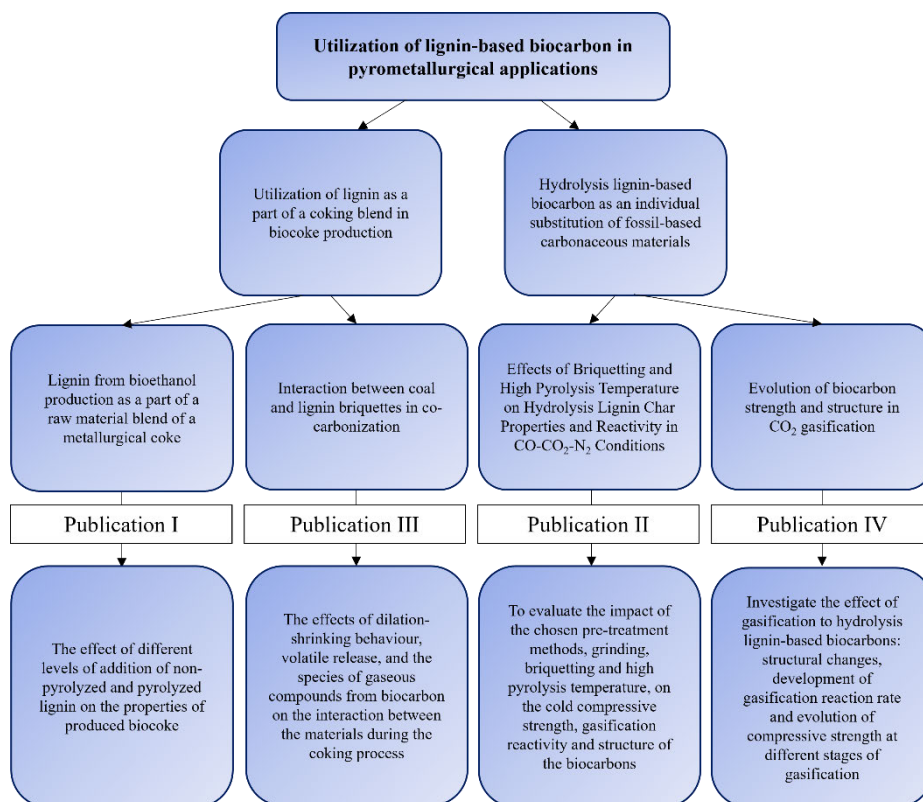


**Fig. 2. The two branches of the study.**

The reference material in the experiments was either industrially produced metallurgical nut coke or laboratory-made coke that is produced from good quality coking coal. Each experiment was also repeated with the reference material so that the properties of the hydrolysis lignin-based biocarbon products could be sufficiently evaluated. Besides the coking coal and metallurgical coke, graphite was also used as a reference additive in the coke-making. This was done for evaluation of the inert behaviour of hydrolysis lignin-based biocarbon as a partial replacement of coking coal in the coke making process.



## 2 Metallurgical coke

Carbon is required in various pyrometallurgical applications and for different purposes. The requirements for the properties of the carbonaceous materials are set not only by the application itself, but also by the storing and transportation. Furthermore, the requirements in a specific application are set by the function of the carbon material, the configuration of the application, i.e. how the carbon material is fed into the process, and what the process conditions are. However, similarities between these requirements exist, with high mechanical strength, suitable reactivity and sufficient apparent density being the most important properties from the carbonaceous materials. In this study, the evaluation of the properties of biocoke and biocarbon has been performed by using metallurgical coke as a reference, thus the most significant properties of metallurgical coke are under investigation.

### 2.1 Properties of coal

Coal is a complex sedimentary rock that is composed of plant residues that originate from a swampy depositional environment to form peat and has further gone through metamorphism to form higher rank coal. The coal rank further indicates the degree of metamorphism of each carbonaceous material (Geerdes et al., 2015; Ward & Suárez-Ruiz, 2008). The simplified illustration of the degree of metamorphism, according to the American Society for Testing and Materials (ASTM), is presented in Fig. 3 (Flores, 2014; Schweinfurth, 2009). The ASTM coal rank classification is based on multiple parameters, including heating value, volatile matter, moisture, ash and fixed carbon. Besides the coal rank, there are also two other parameters for defining the properties of coal: coal type and coal grade (Suárez-Ruiz & Ward, 2008; Ward & Suárez-Ruiz, 2008).

The peat originates from mixtures of different types of plant components (wood, leaves, algae, etc.), fragments or other materials derived from those components. These organic materials are referred to as macerals and they are the constituents that coal is microscopically composed of. The mixture of macerals reflects the variations in the coal type (Suárez-Ruiz & Ward, 2008; Ward & Suárez-Ruiz, 2008).

Coal grade indicates the level of contamination of plant debris by inorganic material before and after burial and during coalification. Coal grade is an independent indicator of the properties of coal; thus, it is not affected by the rank

or type of coal. A high-grade coal has a low mineral matter content, while the mineral matter content of low-grade coal is high (Suárez-Ruiz & Ward, 2008; Ward & Suárez-Ruiz, 2008).

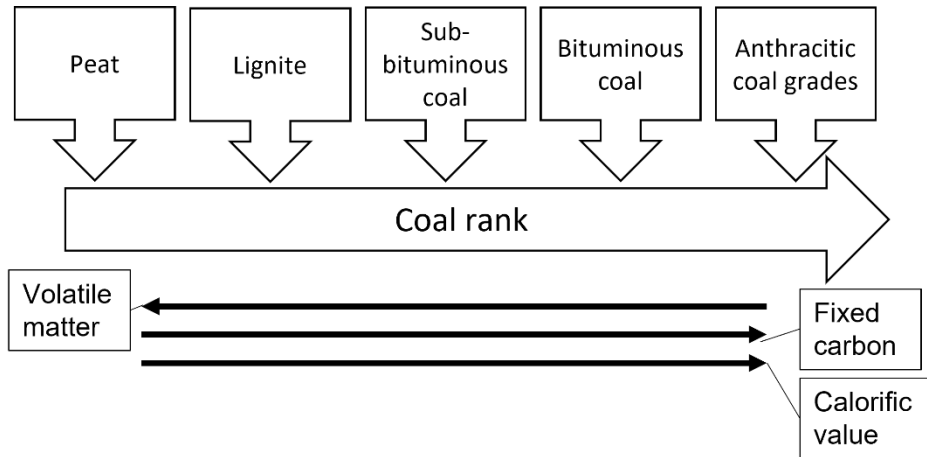


**Fig. 3. Coal rank.**

## **2.2 Coking coal**

Coking coals, or metallurgical coals, are classified, based on coal rank, i.e. degree of metamorphism, into high-, medium- and low-volatile coking coals (Schweinfurth, 2009). When considering coal rank, the coking coals are in the bituminous coals and anthracite categories. However, prime coking coals are more expensive and less available than other coals (Kandiyoti et al., 2017). Also, individual coals typically lack all the necessary properties for good quality coke formation in the coking process (Kandiyoti et al., 2017). Therefore, cokes are produced from coal blends that consist not only of prime coking coals but also other coals from a wide rank range. Typically, coking blends are formed from three to seven different coals. The coking blends are formed in a way where the lack of a certain property of one coal fraction is compensated by the properties of other coal fractions. The different properties of coking coals can be classified into physical properties, chemical properties, coking properties and stability of the quality (Gerdes et al., 2015; Suarez-Ruiz et al., 2018; Yang et al., 2014)

## **2.2.1 Physical properties of coking coal**

Density, grain size, petrography, ash, volatiles and moisture are the most important physical properties of coking coal (Yang et al., 2014). Coal petrography is a technique used to define the degree of carbonisation of coal and the coal maceral composition. Macerals can be divided into three different groups: vitrinite, exinite and inertinite. Macerals originate from different sources; thus, the maceral groups have some characteristic differences. Vitrinite originates from lignocellulosic tissues that have lost their cellular vegetable structure through gelification caused by bacterial activity (Loison et al., 1989a). In low-rank coals, the materials of similar origin to vitrinite are called huminite. In general, huminite macerals are regarded as low-rank precursors of the vitrinite group components (Ward, 2003). Liptinite is derived from organisms and organs that are relatively poor in oxygen. Inertinite is considered to be an inert or unreactive component during the coking process. Macerals in the inertinite group show negligible fluidity during coking, although the degree of thermal stability varies between different inertinite components (Patrick, 1974). Inertinite originates from residues of wood components that are either partly burnt or have undergone a lengthy aerobic oxidation before burial. However, the cellular structure corresponding to plant vessels can be identified from inertinites.

The density of coking coals depends on the maceral composition. Liptinite is the lightest maceral group, the density typically being between 1.1 and 1.25. The density of vitrinite increases with the coal rank from 1.2 to 1.7, while the macerals in the inertinite group are the densest, with a typical density varying between 1.4 and 2.0 (Loison et al., 1989a).

The particle size of coal affects the quality of coke in many ways. In the coal blends the coal particle size should be suitable and constantly monitored because too small a particle size decreases the resolidification temperature, thus propagating the fissure formation on the structure of coke (Loison et al., 1989c). On the other hand, large inert maceral-derived components (IMDC) may cause local weak points in the structure of coke (Andriopoulos et al., 2003). The fine crushing of high-volatile coking coal and inertinite has also been found to have a decreasing impact on coking pressure and the strength of produced coke (Konno et al., 2020).

The optimisation of moisture content of coking coal has multiple positive impacts on the coke formation and coking process itself. The optimum moisture content of coking coal is approximately 6–10 wt.% (Kato & Seiji, 2009; Krebs et al., 1996; Nomura et al., 2004). Higher moisture content leads to higher energy

consumption, thus lower energy efficiency in the coking process (Yan et al., 2020). Low moisture content also increases the coal bulk density in the coke oven, improving the proximity of the coal particles, thus improving the mechanical strength of produced coke. The increased bulk density also increases the coking pressure, which should be adjusted and controlled by optimising the coal blending ratios (Nomura et al., 2004). The formation of carbon deposits on oven walls has also found to decrease, as the moisture content was elevated up to 8 wt.%. When the moisture content was further increased above 8 wt.% the carbon deposition rate increased sharply (Krebs et al., 1996).

The macerals composition of coal determines the amount and composition of released volatiles from coal, thus the development of coal fluidity during the coking process. The volatile release from liptinites is the highest, but the proportion of them in good quality coking coals is generally low. Vitrinite, on the other hand, is usually the most abundant maceral group, particularly in coals from the Northern Hemisphere. Therefore, vitrinite is the maceral group that has the biggest effect on the coking properties of coals. Vitrinite surrounds other macerals and minerals in coal, forming a matrix that has a tendency to swell, agglomerate and fuse during carbonisation.

### ***2.2.2 Chemical properties of coking coal***

The chemistry of coking coal affects the quality of produced coke. Coking coal chemistry is related to the maceral composition and the mineral constituents in coal. The mineral matter in coal can be classified into two different categories based on the origin. Inherent mineral matter originates from the vegetables from which the coal is formed. The content of inherent mineral in coal is usually less than 1% and it is chemically bound to the organic matter of coal. Adventitious mineral matter originates from multiple sources. They are the minerals that are deposited at the same time as the plant debris and show as inclusions crossing the empty spaces in coal structure (Loison et al., 1989a).

Sulphur can occur either as organic groups bound to the hydrocarbon material or as mineral compounds. Approximately 50–60% of the sulphur remains in the produced coke while the rest of the sulphur become devolatilised from the coal during the coking process. However, usually the sulphur content of cokes remain low, the sulphur content varying from 0.6–1.5% in cokes made in Europe and the US (Loison et al., 1989a, 1989b). In iron and steelmaking, in the BF process, whole sulphur will be released at around 1050 °C, but sulphur-bearing compounds such

as calcium sulphide (CaS) and barium sulphide (BaS) will survive BF conditions as solid phases and can later occur as sulphur-bearing inclusions in steels (Gornostayev et al., 2018; Jones et al., 2008; Wang et al., 2002).

The phosphorus mainly occurs as crystalline mineral particles in coal, but traces of phosphorus can also be associated with organic components as small particles only a few micrometres in diameter. The phosphorus mainly originates from the phospho-proteins in the plant debris, but volcanic debris, shells or faecal matter may also act as phosphorus sources of coals. Practically all the phosphorus of coking coals remains in the produced coke. Phosphorus content is generally low in coking coals, the global average being approximately 0.05% (500 ppm). However, high phosphorus content of coke is problematic in iron and steelmaking because in the BF process, for example, the phosphorus is transferred from coke to iron and thence to the resulting steel (Mahony et al., 1981; Ward et al., 1996).

The alkali content of coal, particularly potassium (K) and sodium (Na), have a significant impact on the mechanical strength and gasification reactivity of the produced coke. This is suggested to occur via intercalation of the alkali vapours with micro graphite crystals, thus causing expansion of the coke carbon matrix and subsequently causing the formation of cracks (Li et al., 2014, 2015). This so-called “peeling effect” has been found to correlate with the K content in alkalisated cokes (Li et al., 2015). Moreover, earlier findings show that Na does not readily intercalate into graphite, which means that in terms of coke-alkali interaction, the focus should be on the intercalation of K-bearing minerals into the coke matrix (Dresselhaus & Dresselhaus, 2002). According to (Gornostayev et al., 2016), the concentrations of mineral-related K compounds are not sufficient to cause noticeable reactions in the coke matrix during the coking process or in the upper parts of BF, but above 1100 °C, mineral-related K vapours will be available in noticeable amounts in the system.

### **2.2.3 Coking properties**

The coking properties of coal are namely plasticity, shrinking and swelling. These properties illustrate the coking ability of coals or coal blends and are related to the properties of produced coke. The coking properties are evaluated individually based on the results of the established testing methods of each coking property.

Plasticity illustrates the coal’s ability to soften and become plastic when heated, and in the end of the plastic phase, re-solidify into a coke. This is the nature of the melting and bonding behaviour of the coal in coking. Coal or coal-blend plasticity

is an indication of the softening, gas liberation, chemical reactions and re-solidification behaviour of coals in the coking process. The fluidity of the coal or coal blend in the plastic stage is a major factor in the determination of the coal plastic properties, thus it is widely used in evaluation of the proportions of each coal type in the blend.

Fluidity is part of the thermoplastic properties of coal, but is explained here in a separate section since its important role in the formation of coke from a blend of carbonaceous materials. The fluidity of coal is measured with a plastometer, which produces information about coal fluidity in a plastic phase, maximum fluidity and temperatures of initial softening, maximum fluidity and re-solidification. The development of maximum fluidity and the temperature range of the coal plastic stage is important for the formation of the organised, mechanically strong structure of coke.

Shrinking and swelling (contraction and dilatation) are measured with a dilatometer in which finely crushed coal is compressed into a pencil and then slowly heated up. As the coal passes the softening temperature, the pencil initially starts to contract (the pencil gets shorter), and then expands (the pencil gets longer) as the temperature is further elevated. The results consist of maximum dilatation and maximum contraction, which are given as a percentage of the initial pencil size. The other results from the test are the temperatures of softening, maximum contraction and maximum dilatation.

Coal swelling is also evaluated with the free swelling index (FSI), which is a threshold test and does not produce information about the contraction or dilatation behaviour of coal in the coal plastic stage. In the test, one gram of coal is heated to 800 °C and then the height and shape of coke lump is compared with the standard chart of different shapes and sizes of coke lumps. The sizes and shapes in the chart are rated and the rating prescribes whether the sample is hard coking coal, medium coking coal or weak coking coal.

#### **2.2.4 Stability of the quality**

Over the years, the consumption of metallurgical coke has reduced, especially in the BF process. The reduction of metallurgical coke consumption has not only set high quality standards for coke, but stability of the coke quality is also important (Lyalyuk et al., 2012).

Coke quality can be tested using different methods. Drum tests are a widely used technique to evaluate coke strength. Four different parameters, Irsid index 10

(I10), Irsid index 20(I20), Micum index 10 (M10) and Micum index 40 (M40) are obtained from different room temperature drum test techniques. These techniques are based on the standardised drum test methods (ISO 556:2020) (Li et al., 2014). In the 1970s new methods were introduced to measure coke reactivity (coke reactivity index, CRI) and coke strength after reaction (CSR). These testing methods have since been adopted as ASTM standard testing methods for evaluation of coke reactivity. CRI indicates the percentual weight loss of coke after reaction in CO<sub>2</sub> atmosphere at 1100 °C for 2h. CSR is measured after the CRI test. The sample is tumbled in an I-drum for 600 revolutions at 20 rpm and the cumulative percentage of +9.5 mm coke is denoted as CSR. In short, low CRI and high CSR are the measures of good quality coke, whereas high CRI and low CSR refer to low quality coke (Li et al., 2014). Besides the quality standards of metallurgical coke that are mentioned here, other standardised methods, such as in-house methods of different industrial operators and research organisations, also exist for the evaluation of coke quality.

The stability of coke can refer to two different things: either mechanical stability, which is based on the ASTM tumbler test (ASTM D3402/D3402M-16), or the uniformity coefficient, which is recommended by the Eastern Coal-Chemistry Institute (Lyalyuk et al., 2012; Mahoney et al., 2005). The uniformity coefficient K is the total number of determinations (n) minus the number of determinations with deviations exceeding the corresponding limits for each characteristic (n<sub>1</sub>) and the difference divided by the total number of determinations. Earlier it has been found that the fluctuations in coke properties are in relation to the fluctuations in coal characteristics (Lyalyuk et al., 2012).

### **2.3 Coke quality**

Considering the quality of metallurgical coke, the characteristics of the individual raw material fraction can be crucial because it can modify the characteristics of the whole raw material blend. This is also the case when biomass is added to the coking blend. The research findings so far suggest that the addition of different biomass-originating fractions to the coking blend inhibit the fluidity development of the coal, thus affecting the bonding of coal particles, and the anisotropic texture and porosity of coke. This further leads to modifications of coke mechanical strength and reactivity to CO<sub>2</sub> in high temperature processes (Diez et al., 2012). However, different ways to overcome the inhibitive effect of biomass on coal fluidity development have been suggested. The thermochemical treatment of biomass

(torrefaction or pyrolysis), particle size variations, agglomeration of the biomass and variation of heating rate during the coal plastic phase have been suggested and found to have a positive effect on the produced coke (Kokonya et al., 2013).

## **2.4 Bio-based material as part of a coking blend**

The addition of bio-based material to the coking blend has been recognised as a considerable possibility to mitigate fossil-based CO<sub>2</sub> emissions in the iron and steel industry (Suopajarvi et al., 2017). The utilisation of biomass, such as wood, in a coking blend is part of a short-term carbon cycle. In this cycle the produced CO<sub>2</sub> creates a carbon debt, which will be covered within a period of time by the CO<sub>2</sub> capture from new growing trees (Manousiouthakis & Choi, 2021). On the other hand, the use of fossil-based fuels interrupts the long-term carbon cycle by fastening it; i.e. the total carbon in the active cycle (short-term cycle) is increased. In the utilisation of biomass in a coking blend, the properties of the blend should not be harmed in a way that the produced coke does not fulfil the requirements that are set to it. In addition, coal and biomass should have chemical and physical interaction during the coking process in order to achieve a uniform coke structure such that the biomaterial particles do not appear as inclusions in the structure of coke. This being said, the species of biomass, and more specifically the released oxygen-bearing compounds from biomass will affect the coal fluidity development during the coking process. The magnitude of this effect is dependent on the oxygen functionality in the released compounds (Diez et al., 2012). Carbonisation of the biomass before mixing it with the coking blend has previously been found to decrease the coal fluidity inhibition effect (Diez et al., 2012) and the detrimental effect on coke properties, such as gasification reactivity and compression strength (Suopajarvi et al., 2017).

## 3 Lignin

Lignin is the second abundant plant polymer after cellulose. The lignin content in coniferous wood species (softwood) is generally higher (26–34%, dry basis) than that of deciduous (hardwood) species (23–30%, dry basis) (Rowell et al., 2012). Lignin is an adhering material that acts as a glue, binding cellulose and hemicellulose components together in the plant cell walls. Lignin adds strength and rigidity to plant stems for vertical growth, controls the fluid flow, and protects the plants against biochemical stresses by inhibiting enzymatic degradation of other plant components (Bergna et al., 2022; Khan et al., 2019; Mandlekar et al., 2018).

Industrially extracted lignin fractions are named based on the extraction method. The extracted lignins are classified as modified lignin or technical lignin (Chio et al., 2019). The most common technical lignins are Kraft lignin, hydrolysis lignin, soda lignin, liginosulfonate and organosolv lignin. New processes for lignin extraction from lignocellulosic biomass are also under development, like steam explosion and ammonia fibre expansion (Bergna et al., 2022; Berlin & Balakshin, 2014; Chakar & Ragauskas, 2004; De Carvalho & Colodette, 2017; Negi & Pandey, 2015). On a global scale, approximately 100 million tonnes of technical lignin are produced annually. The majority of the technical lignin is produced at pulp and paper facilities worldwide. However, it is estimated that the production of lignin as a by-product of biofuel production will significantly increase during the coming years. Currently, lignin side-streams are mainly considered as low-value waste and approximately 98% of the technical lignin is utilised as raw material in power and heat generation, while only 2% is used in the production of value-added products (Chio et al., 2019).

### 3.1 Hydrolysis lignin

Cellulosic ethanol plants represent the second generation of bioethanol production, whereas first-generation bioethanol production is based primarily on the fermentation of starch-based sugar. The main issue in the first-generation bioethanol production is that the raw material, starchy crops, e.g. corn, wheat, sugarcane juice and sugar beet, competes with food and land and it necessitates critical soil, water and nutrient conditions (Raj et al., 2022). Cellulosic ethanol represents the product of second-generation bioethanol production and is chemically identical to first-generation bioethanol. However, in contrast to the feedstock of first-generation bioethanol production, lignocellulosic biomass is

utilised in second-generation bioethanol production. The lignocellulosic biomass needs to be broken down (hydrolysed) into simpler sugars (Kemppainen et al., 2012; Mahmood et al., 2016). Currently, most of the cellulosic ethanol plants are demonstration plants, but also commercial plants exist. However, the majority of the commercial facilities are currently on hold, idle or inactive due to the technical and techno-economic challenges. One way to tackle the economic issues would be the commercialisation of the lignin by-product by generating value-added products out of it rather than using the lignin as a raw material in heat and power generation (Raj et al., 2022).

The term hydrolysis lignin refers to solid residue that is obtained as a by-product after hemicellulose extraction, acid or enzymatic hydrolysis of lignocellulosic biomass and subsequent sugar/lignin separation (Zevallos Torres et al., 2020). Compared to Kraft lignin, for example, hydrolysis lignin is sulphur-free and suffers only a little degradation, thus the structure resembles native lignin (Mahmood et al., 2016).

### **3.2 Lignin structure**

Lignin is an aromatic polymer derived from a number of precursor monomers but mainly of three monolignols: *p*-coumaryl alcohol, coniferyl alcohol and sinapyl alcohol. These monolignols differ in their degree of methoxylation. When incorporated into the lignin polymer, these monolignols produce *p*-hydroxyphenyl, guaiacyl and syringyl phenylpropanoid units. The amount of different phenylpropanoid units in lignins differ between plant species, with softwood lignin being mainly composed of guaiacyl and *p*-hydroxyphenyl (Boerjan et al., 2003). Softwood lignin has a complex, branched and cross-linked structure where approximately half of the cross-linkages involve aromatic rings, but also a significant number of linkages are located in the side chains (Balakshin et al., 2020). The activity of the chemical bonds of lignin cover a wide range, thus the thermal degradation of lignin occurs in a wide temperature range (100–900 °C) (Yang et al., 2007).

### **3.3 Pyrolysis of lignin**

The different stages of lignin pyrolysis can be considered from different perspectives based on thermogravimetric analysis (TGA), pyrolysis mechanisms

and structural changes. These perspectives are highly linked to each other and are dependent on the pyrolysis conditions.

Usually, the pyrolysis of lignin is described as a three-stage process (Collard & Blin, 2014; Li et al., 2020; Yu et al., 2021), but from the TGA point of view lignin pyrolysis can also be perceived as a two-stage process (Cao et al., 2013a; Hu et al., 2013; Huang et al., 2012; Liu et al., 2008). However, in (Cao et al., 2013a) and (Liu et al., 2008) the evaporation of water (drying) is considered as one of the pyrolysis stages, resulting in a total of three pyrolysis stages when combined with the two stages of actual pyrolysis. The structural rearrangement stage is also found for lignin in temperatures above 900 °C with a slight but observable mass loss (Cao et al., 2013a). In general, the two pyrolysis stages can be divided into primary pyrolysis stage and secondary pyrolysis stage, or the pyrolysis stage and carbonisation stage, depending on the author (Cao et al., 2013a; Evans & Milne, 1987; Kawamoto, 2017; Liu et al., 2008).

Based on the mechanisms, the pyrolysis of lignin can be divided into three different stages: 1) early stage of decomposition (< 375 °C); 2) extensive decomposition stage (375-450 °C) 2) char formation stage (> 450 °C) (Yu et al., 2021). In general, the pyrolysis conversion is considered as a superposition of three primary mechanisms: char formation, depolymerisation and fragmentation, and of secondary mechanism (Collard & Blin, 2014; Eom et al., 2012; Patwardhan et al., 2011; Van de Velden et al., 2010). The lignin degradation has been reported to occur in a wide temperature range (100–900 °C) (Yang et al., 2007); however, the main conversion step is in the range of 200 to 450 °C, with the highest decomposition rate usually in the range of 360–400 °C (Collard & Blin, 2014). The main decomposition stage of lignin is followed by char formation, which consists of the rearrangement of the aromatic compounds forming polycyclic aromatic structures, thus forming the skeleton of the char. This is the stage where most of the primary volatile compounds are released due to the instability of the propyl chains, some linkages between the monomer units, and methoxy substituents of the aromatic rings. The fragmentation of methoxy groups and breakage of the bonds between the monomers, however, mainly occur above 400 °C, whereas the conversion of the alkyl chains mainly occurs below 400 °C. The volatile compounds released in the decomposition stage, and due to the rearrangement reactions, are mainly low molecular weight and incondensable gases (Cao et al., 2013a; Collard & Blin, 2014; Liu et al., 2008).

From the perspective of biocarbon formation, lignin is a good raw material because of its aromatic structure. In general, the term biocarbon indicates a solid

residue with an aromatic polycyclic structure that is formed in a biomass conversion (Collard & Blin, 2014; McGrath et al., 2003; Pastorova et al., 1994). The biomass conversion process includes an intra- and intermolecular rearrangement reaction that leads to higher degree of structural reticulation, thus a higher degree of thermal stability of the biocarbon. The aromatic structures are already present in the lignin structure, thus the conversion process is simpler than in the case of polysaccharides (cellulose and hemicellulose) (Collard & Blin, 2014).

Lignin undergoes a lot of structural changes during pyrolysis, especially when the final pyrolysis temperature is high. One way to determine the level of carbonisation of lignin could be the determination of the fused aromatic rings within the lignin structure. Based on the C/H ratio at different stages of carbonisation of lignin, the lignin structure is close to naphthalene at 200 °C (two fused aromatic rings), similar to anthracene (three rings) at 300 °C, similar to pyrene (four rings) at 350 °C, and having 20 fused benzene rings at 550 °C. The growth of a fused ring structure and the degree of reticulation continues as the pyrolysis temperature is further elevated (Zhang et al., 2020). When the pyrolysis temperature is further elevated to 1200 °C, graphite-like substructures can be found from the structure of lignin (Haensel et al., 2009). This is in line with findings of (Otani et al., 1984), who studied the evolution of lignin structure at high temperatures. They detected a formation of small graphitic lamellae from the polymeric chains near 1000 °C, thus inducing a rapid change in electric conductivity from values typical of insulators to values of semiconductors. This is accompanied by the densification of the carbon matrix. When the pyrolysis temperature is further elevated, the carbon matrix evolves from amorphous carbon to a turbostratic structure, which is a graphite-like structure with a higher degree of disorientation. Meanwhile, the micropores grow but the pore number remains constant (Otani et al., 1984). Based on earlier findings, the different stages of the structural evolution of lignin in the pyrolysis process could be determined as follows: 1) bond-breaking and recombination stage, 2) the aromatisation stage and 3) the graphitisation stage (Haensel et al., 2009; Hu et al., 2013; Otani et al., 1984; Zhang et al., 2020; Zheng et al., 2022). The graphitisation stage covers the widest temperature range as the evolution of a graphite-like structure has been reported to continue up to 2400 °C (Otani et al., 1984).

## **4 Materials and methods**

The research work of this thesis was divided into two different branches, one of which is related to the hydrolysis lignin-based material addition to the coking blend in metallurgical coke production, and the other that deals with the properties of hydrolysis lignin-based biocarbon products. The research work from both branches started with the characterisations of the raw materials, continued with the characterisations of the products, and finally proceeded to a definition of the properties that are relevant from the pyrometallurgical perspective, i.e. the definition of the reactivity and mechanical strength of biocoke and biocarbon.

### **4.1 The effect of hydrolysis lignin addition on the formation and properties of biocoke**

Biocoke-related research is contributed to by publications I and III of this thesis. The effect of powdered (non-pyrolysed and pyrolysed) lignin on the properties of produced coke was investigated in Publication I and the interactions between coking coal and briquetted (non-pyrolysed and pyrolysed) lignin were the subject of research in Publication III.

Overall, the research activities of Publications I and III are listed in Table 1. The pathways of the research activities of the publications are similar, but the activities themselves differ from each other because of their different objectives. The more detailed introduction about research activities can be found from sections 4.1.1 in Publication I and 4.1.2 in Publication II. The raw materials for both publications were the same. The coking coal was received in non-ground form, and at approximately 9 wt.% moisture. Hydrolysis lignin was highly moist as received, the moisture content being approximately 50%. The hydrolysis lignin was dried to 5.3 wt.% moisture for preventing mould formation. Also, the treatments for hydrolysis lignin, e.g. grinding, is easier when the material is relatively dry.

**Table 1. Research activities and analyses of Publications I and III.**

Activity / Analysis	Publication I	Publication III
Grinding	x	x
Chemical analysis	x	x
Coking properties of coal	x	x
Briquetting		x
Pyrolysis temperatures [°C]	350	450; 600; 1200
Raw material blending	x	x
Coking	x	x
Thermogravimetric analysis	x	x
Mass spectrometry		x
Coke reactivity	x	
Coke kompression strength	x	
Optical microscopy	x	x
Image analysis	x	
Optical dilatometry		x

#### **4.1.1 Coke preparation**

The raw materials, hydrolysis lignin and coking coal, were ground and sieved before co-carbonisation (coking). The size range of non-pyrolysed and pyrolysed hydrolysis lignin was 125–250 µm, which has earlier been found to be suitable for charcoal when utilised in coke-making as part of a coking blend (Suopajarvi et al., 2017). Some 30% of the coking coal was ground and sieved to a < 0.5 mm size fraction and 70% to a 0.5–1.0 mm size fraction. Larger fractions were excluded because of the limited size of the laboratory-scale mini coke ovens. The heating rate in the pyrolysis of hydrolysis lignin was 5 °C/min, while the final temperature was 350 °C and the holding time was 8 h. The pyrolysed hydrolysis lignin was expected to have inert characteristics in the coal plastic phase. Therefore, also graphite powder was used as an additive in the coking blend to act as a reference inert material. The amounts of the additives in the blends were 5, 10 and 15 mass percentages in the coking blend. The amount of non-pyrolysed lignin was adjusted so that the bulk density would correspond to the blend of pyrolysed lignin and coking coal at a temperature of 350 °C, i.e. the higher volatile release of non-pyrolysed lignin in comparison to pyrolysed lignin was taken into account when adjusting the blends.

**Table 2. Studied coking blends (Modified under CC BY 4.0 license from Publication I @2019 Authors).**

Replacing Agent	Amount of Replacement [m.%]	Coal		Lignin [g]	Pyrolysed Lignin [g]	Graphite Powder	Targeted Bulk Density [kg/m <sup>3</sup> ]
		0.5–1.0 mm [g]	<0.5 mm [g]				
None	0	9.1	3.9	0	0	0	751.62
Lignin	5	9.1	3.25	1.11	0	0	778.5
Lignin	10	9.1	2.6	2.23	0	0	805.38
Lignin	15	9.1	1.95	3.34	0	0	832.26
Pyrolysed lignin	5	9.1	3.25	0	0.65	0	751.62
Pyrolysed lignin	10	9.1	2.6	0	1.3	0	751.62
Pyrolysed lignin	15	9.1	1.95	0	1.95	0	751.62
Graphite	5	9.1	3.25	0	0	0.65	751.62
Graphite	10	9.1	2.6	0	0	1.3	751.62
Graphite	15	9.1	1.95	0	0	1.95	751.62

The volatile release from the raw materials was analysed with TGA. The analysis was executed by simulating the coking conditions that were used in this research work, i.e. the heating rate (2.5 °C/min) and inert gas (nitrogen) were the same as in the coking experiments. The N<sub>2</sub> flow rate was 60 ml/min. The release of volatile matter helps to evaluate the interaction between the raw materials during the coking process. The effect of hydrolysis lignin on the properties of produced coke can therefore be evaluated.

The properties and quality of produced cokes were evaluated with high temperature reactivity tests and compression strength tests. The gasification reactivity tests were made in a gas atmosphere that is presented in Table 3. This gas atmosphere has been reported earlier in (Haapakangas et al., 2016) as “low-hydrogen shaft gas”. Both, dynamic and isothermal reactivity tests were conducted within this research. The isothermal reactivity tests were conducted at 1100 °C while the initial temperature in dynamic tests was 800 °C and the temperature was elevated to 1100 °C with a heating rate of 2 °C/min. The gas composition was kept static during the reactivity experiments.

**Table 3. Gas composition in the reactivity tests (Modified under CC BY 4.0 license from Publication I @2019 Authors).**

Gas Species	Share [vol.%]
N <sub>2</sub>	50
CO	27.9
CO <sub>2</sub>	17.1
H <sub>2</sub>	2.1
H <sub>2</sub> O	2.9

The cold strength of cokes was tested with compression strength tests that were conducted with a Gleeble 3800 thermomechanical simulator (Dynamic Systems Inc., New York, NY, USA). The force of the compression was elevated at a rate of 100 N/s, so that the time of compression was approximately 30 seconds at the point of fracture from the beginning of the compression.

The surface structures of the samples were studied using an Olympus BX51 (Olympus, Tokyo, Japan) optical microscope equipped with a polarising lens. The polarising lens was adjusted to different angles in order to observe the additive particles from the structure of the coke. A series of micrographs were taken from the coke surface with a camera that was coupled with the microscope. The micrographs were further analysed with Matlab-based image analysis software. For example, the porosity, pore size distribution and pore shape factors were determined with the image analysis software.

#### **4.1.2 Interaction between coking coal and hydrolysis lignin-based materials**

In this biocoke-related research, the lignin was ground, sieved and pressed into a briquette before pyrolysis. The height and diameter of the original non-pyrolysed hydrolysis lignin mini briquette were 9 mm and 8 mm, respectively.

Hydrolysis lignin mini briquettes were pyrolysed at three different temperatures, 450, 600 and 1200 °C. The choice of pyrolysis temperatures was based on the structural changes of hydrolysis lignin at different stages of thermochemical conversion. At 450 °C, most of the volatile compounds are devolatilised and the char formation begins at this temperature, thus the number of fused aromatic rings in the polycyclic ring structures is somewhere between 4 and 20 rings (Yu et al., 2021; Zhang et al., 2020). At 600 °C the thermal degradation stage is over, and the fused polycyclic structures are larger than 20 rings. Also, the

ring structures start to become more organised and more of these structures begin to form, thus the structure of biocarbon increasingly resembles amorphous carbon (Toloue Farrokh et al., 2018; Zhang et al., 2020). Ultimately, at 1200 °C amorphous carbon structures are predominant and even graphitic substructures can be found from hydrolysis lignin biocarbon (Haensel et al., 2009; Otani et al., 1984).

The release of volatile matter from the raw materials of the coking blend was analysed with TGA, Netzsch STA 449 F3 Jupiter (Netzsch-Gerätebau GmbH, Selb, Germany) which was coupled with a Netzsch QMS 403 C quadrupole mass spectrometer (Netzsch-Gerätebau GmbH, Selb, Germany). The raw materials in the coking blend were coking coal (Coal), hydrolysis lignin briquette (HLIG), and hydrolysis lignin briquettes that were pyrolysed at 450 °C (L450), 600 °C (L600) and 1200 °C (L1200). The heating rate in the experiments was 5 °C/min and the temperature range from room temperature to 1200 °C. The final temperature in this TGA and MS experiment was the same as that subsequently applied in the co-carbonisation (coking) experiments. The mass spectra of the compounds that were released during the carbonisation were obtained from an  $m/z$  range of 0 to 250. The  $m/z$  range was chosen so that major gaseous pyrolysis products of softwood lignin could be identified (Zhao et al., 2014). Also, these products have previously been reported to inhibit the fluidity development of coal (Diez et al., 2012). The MS signals of hydrolysis lignin degradation products were compared and characterised with the MS signals that are available in the database of the library of the National Institute of Standards and Technology (NIST) Chemistry Webbook (U.S. Secretary of Commerce, 2022).

The dilatation-shrinking behaviour of hydrolysis lignin-based briquettes was investigated with an optical dilatometer. The heating rate was 5 °C/min, the final temperature 1200 °C and N<sub>2</sub> was used as a protective gas with a flow rate of 2 l/min. The conditions in optical dilatometry investigations were set so that the heating rate, final temperature and protective gas were similar to those in the coking experiments.

The coking experiments were executed with a custom-made coking device that simulates the heat transfer from the coke oven walls to the centre of the oven. The coke oven was heated with an Entech model ETF 75/17V gradient furnace (Entech AB Ängelholm, Sweden). Industrial coke ovens are usually heated from the oven walls. Therefore, the heating in the experiments was conducted by only heating the lower chamber of the gradient furnace. The bottom of the custom-made coke oven illustrates the oven walls, whereas the top of the coke bed simulates the centre of the coke oven. The height of the coke bed containing the hydrolysis lignin briquette (or biocarbon briquette) was 200 mm. The custom-made coke oven and the gradient

furnace are presented in Fig. 4. Bio-based briquettes were placed at three different levels in a vertical direction on the coal bed. The heights of the bio-based briquette locations were 30 mm, 70 mm and 100 mm. The cross-sectional arrangement of the briquettes is presented in Fig. 4. A more detailed description of the equipment and the experimental conditions can be found in (Koskela et al., 2022a).

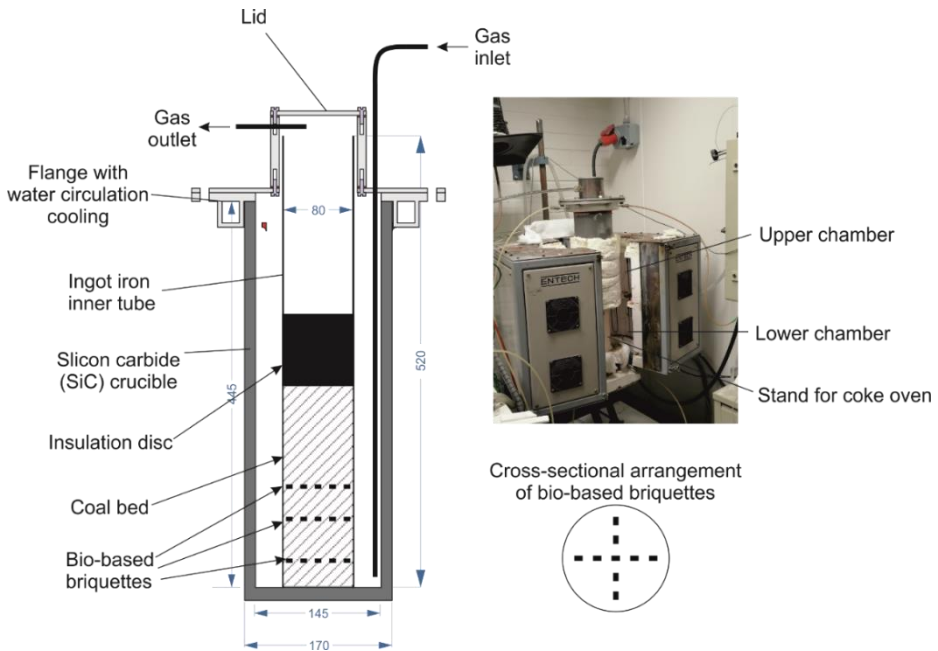


**Fig. 4. Coke oven and gradient furnace (Modified under CC BY 4.0 license from Publication III @2022 Authors).**

## 4.2 Hydrolysis lignin-based reductants for substitution of fossil-based reductants

The objective of this branch of research is to directly replace metallurgical coke or other fossil-based carbonaceous material in pyrometallurgical processes either partially or completely, depending on the process. The dependence on the process is due to the different requirements of each process on the properties of carbonaceous material. For example, in the BF process metallurgical coke has three roles: 1) to act as a chemical reducing agent; 2) as a fuel to bring heat to the process to cover the demand of the endothermic reactions like direct reduction of wüstite

(FeO) with carbon (C); and 3) as a solid structural bed material for iron burden that provides a permeable matrix for ascending gases and descending iron melt and slag (Díez et al., 2002). These different roles require high mechanical strength, suitable reactivity, high carbon content and high mechanical strength after reaction. Also, the high density of carbonaceous material is related to the strength and reactivity properties of coke. When carbonaceous material is used for slag foaming in EAF, the requirements are not as high as in the BF process. However, properties such as density and reactivity of the carbonaceous materials have been addressed to affect the slag foaming phenomena, i.e. low density results in low penetration depth of the carbon material on the slag bath, and overly high reactivity leads to premature combustion of the carbon, thus reducing the interaction between carbon and FeO (Echterhof, 2021; Marcos et al., 2019). Moreover, mechanical strength is required from the carbonaceous material during transportation and storing, because the extensive formation of fine powder may cause problems such as dusting or accumulation on the conveyors.

Reactivity has previously been associated with the surface area, porosity and crystalline structure of the carbonaceous materials (Diez & Borrego, 2013; Huo et al., 2014). Considering the properties of lignin and their evolution during carbonisation, agglomeration and subsequent slow pyrolysis at high temperatures were chosen for the treatment methods of lignin. The goal was to develop a biocarbon product that is comparable to metallurgical nut coke in terms of main properties, density, reactivity and mechanical strength.

This branch of research in this thesis is contributed to by Publications II and IV. The evolution of the hydrolysis lignin biocarbon surface area, porosity, density and gaseous products during pyrolysis were investigated in Publication II. Also, preliminary tests on biocarbon reactivity in a gas atmosphere containing CO<sub>2</sub> at high temperatures were performed as part of Publication II. In Publication IV, the evolution of structural changes of hydrolysis lignin-based biocarbon in gasification and the effect of these changes on the properties (reactivity and mechanical strength) of biocarbon were investigated. In both publications, industrially produced metallurgical nut coke was used as a reference material. This helps with the evaluation of the suitability of biocarbons for pyrometallurgical processes.

#### **4.2.1 Structural changes and gasification reactivity of pyrolysed hydrolysis lignin**

As explained above, the structure of lignin-based biocarbon is built on the existing aromatic rings that are fused to one another, thus forming unified structures of dozens of rings. The number of rings and the degree of organisation of the ring structures increases as a function of temperature, which leads to the formation of turbostratic structure above 1000 °C. The stages of evolution of the biocarbon structure were considered within this publication, thus three different final temperatures were applied in the slow pyrolysis of hydrolysis lignin briquettes: 450, 600 and 1200 °C. Also, briquetting of the hydrolysis lignin prior to pyrolysis was a choice based on the evolution of the biocarbon structure during the pyrolysis. The hypothesis behind this was that the briquetting would enable the formation of larger fused aromatic substructures, which further contributes to the denser, stronger and less reactive biocarbon formation during the pyrolysis.

The behaviour of hydrolysis lignin in the pyrolysis process was studied with a Netzsch STA 449 F3 Jupiter TGA (Netzsch-Gerätebau GmbH, Selb, Germany) which was coupled with a Netzsch QMS 403 C quadrupole mass spectrometer (Netzsch-Gerätebau GmbH, Selb, Germany). The mass loss and mass loss rate data combined with mass spectrometry data of the released volatile matter helps with the understanding of the thermal degradation behaviour of hydrolysis lignin. The heating rate and the final temperature in the experiment were 5 °C/min and 1200 °C, respectively. These conditions correspond to the heating rate and the final temperature range of the pyrolysis experiments that were carried out in this study. Argon (Ar) was used as an inert gas in the experiments, while N<sub>2</sub> was used in the pyrolysis experiments. The reasoning behind the choice of Ar for the TGA-MS experiments was to avoid the overlapping of the signals of releasing volatile compounds (e.g. ethylene, C<sub>2</sub>H<sub>4</sub>, and carbon monoxide, CO) with the inert gas at an m/z value of 28. The m/z scanning width of MS was 100, ranging from 0 to 100. Therefore, only compounds with relatively low molecular weight were identified. Different gas components were identified based on the MS signal library of National Institute of Standards and Technology (NIST) Chemistry Webbook (U.S. Secretary of Commerce, 2022). However, the analysis results were also compared with the results of existing literature concerning lignocellulosic biomass pyrolysis.

The proximate analyses of biocarbon products and metallurgical nut coke were performed with a Netzsch STA 449 F3 Jupiter TGA by following the procedure that is reported in (Cassel & Menard, 2012).

The apparent density measurements are based on the external volume and the mass of the sample. In this study, the external volume of the hydrolysis lignin-based briquettes was defined with a vernier caliper and the mass with an analytical scale. The briquettes were regularly shaped (cylindrical), thus the use of vernier caliper was applicable in this case (Basu, 2010).

The determination of specific surface area (SSA), pore size distribution and pore volume was done with ASAP 2020 and 3Flex physisorption instruments by Micromeritics Instruments Corporation, Georgia, USA. The experimental procedure is explained in detail in (Koskela et al., 2021). The SSA was calculated based on the Brunauer-Emmet-Teller (BET) algorithm (Naderi, 2015). The pore size distribution was calculated using the density-functional-theory (DFT) model, assuming slit-like pores (Figueroa-Gerstenmaier et al., 2014; Ryu et al., 1998). The different-sized pores were categorised according to the International Union of Pure and Applied Chemistry (IUPAC) notation (micropores < 2 nm, mesopores 2 nm < 50 nm, macropores > 50 nm) (Thommes et al., 2015).

The reactivity of the samples was determined with dynamic high-temperature reactivity tests in a gas atmosphere containing CO, CO<sub>2</sub> and N<sub>2</sub>. The volumetric percentages of CO, CO<sub>2</sub> and N<sub>2</sub> in the reactive gas atmosphere were 25, 25 and 50, respectively (Babich et al., 2009). A Netzsch STA 449 F3 Jupiter TGA was used in these experiments. The heating rate in these dynamic high-temperature reactivity tests was 10 °C/min, from 30 °C to 1350 °C. The dynamic reactivity tests were performed in a wide temperature range to reveal the threshold temperature of carbon gasification as well as the reactivity of the samples at high temperatures (Babich et al., 2009).

#### ***4.2.2 Evolution of biocarbon structure and mechanical strength at different levels of gasification***

In Publication IV, the focus was on the evolution of biocarbon and metallurgical nut coke properties (strength and structure) during gasification. This includes the study of the effect of different gas atmospheres on the gasification reaction and reaction rate and the effect of pyrolysis temperature on the hydrolysis lignin-based biocarbon mechanical strength and gasification reaction rate. Also, the effect of the level of gasification on the biocarbon and metallurgical nut coke structure and strength was studied.

The pyrolysis temperatures of the hydrolysis lignin-based biocarbons were 600, 900 and 1200 °C. The reasoning behind the chosen pyrolysis temperatures is based

on the earlier results in Publication II (Koskela et al., 2021) considering the reactivity and porous structure development of hydrolysis lignin-based biocarbons, and the evolution of the structure of lignin during the pyrolysis that was found from the literature review of this thesis (Section 3.1.2 “Pyrolysis of lignin”). At 600 °C the degradation stage of lignin is complete, and the formation of more organised aromatic structures with sub-structures of a larger number of fused aromatic rings has begun (Toloue Farrokh et al., 2018; Zhang et al., 2020). At 900 °C, amorphous structures are predominant in the lignin biocarbon structure but graphitic sub-structures have not yet formed (Otani et al., 1984). At 1200 °C, graphitic sub-structures can be identified from the lignin structure and the degree of orientation of the biocarbon structure has evolved from amorphous structure towards a turbostratic structure (Haensel et al., 2009; Otani et al., 1984).

The gasification experiments for three different biocarbon briquettes (sample names: L600, L900 and L1200) and metallurgical nut coke (sample name: coke) were performed with a custom-made TGA in three different reactive gas atmospheres. The detailed presentation about the custom-made TGA is reported previously in (Haapakangas et al., 2016) and (Suopajarvi et al., 2017). Three different gas components (CO<sub>2</sub>, CO and N<sub>2</sub>) with varying amounts were used in the reactivity tests. The volumetric percentages of different gas components of different experimental programmes are presented in Table 4. The temperature of the isothermal reactivity tests was kept constant at 1000 °C.

**Table 4. Experimental programmes of the reactivity tests (Modified under CC BY 4.0 license from Publication IV @2022 Authors) .**

	Programme 1	Programme 2	Programme 3
CO [vol.%]	25	0	0
CO <sub>2</sub> [vol.%]	25	25	100
N <sub>2</sub> [vol.%]	50	75	0
Temperature [°C]	1000	1000	1000

The high temperature reactivity of all the samples was tested with programme 1 in which the reactive gas atmosphere consisted of 25, 25 and 50 volumetric percentages of CO, CO<sub>2</sub> and N<sub>2</sub>, respectively. The level of mass loss was fixed at 20% at this stage. At the second stage (programme 2 from Table 4), the CO was replaced with N<sub>2</sub>, i.e. the level of CO was decreased to 0 vol.% while the volumetric percentage of N<sub>2</sub> was elevated from 50 to 75 vol.%. At the third stage (experimental programme 3 from Table 4), the reactive gas atmosphere consisted of 100 vol.%

CO<sub>2</sub>. The purpose of the experiments in the second and third stages was to determine the inhibitive effect of CO on the gasification reaction rate (second stage) and the accelerating effect of the increase of CO<sub>2</sub> concentration on the gasification reaction rate. The evaluation of these effects was done by comparing the results of second and third stage with the results of first stage. Only L1200 and coke samples were tested in the conditions of programmes 2 and 3 (second and third stages). At the third stage, the samples were gasified to four different levels of volatile-free mass loss, i.e. the experiment was stopped when the mass loss of the samples reached the levels of 20, 30, 40 and 50% from the initial volatile-free mass. These levels of gasification were selected based on the typical mass loss levels of metallurgical coke in CRI tests (Haapakangas et al., 2016).

For determination of the structural changes of L1200 and coke samples during the gasification reaction, these samples were gasified to the different levels of mass loss, after which the structure of the sample surface was micrographed with an Olympus DSX1000 digital microscope (Olympus Corporation, Shinjuku, Tokyo, Japan) equipped with a DSX10-XLOB10X high-resolution objective lens. Once the samples were micrographed, gasification was continued to the next level and the samples were micrographed again. The mass loss levels in this experiment were 20, 30, 40 and 50% from the initial volatile-free sample mass.

The mechanical strength of the gasified and non-gasified samples was evaluated using compression strength tests, which were performed with a Gleeble 3800 thermomechanical simulator (Dynamic Systems, Inc. Austin, Texas, USA). The samples were compressed until they were crushed. The compression was programmed so that the strain of the sample was increased by 0.1 mm per second, which ultimately led to a compression period of approximately 30 s until the samples were crushed.

The surfaces of gasified and non-gasified samples were micrographed with an Olympus DSX1000 digital microscope (Olympus Corporation, Shinjuku, Tokyo, Japan) equipped with a DSX10-XLOB10X high-resolution objective lens. All the sample types (L600, L900, L1200 and coke) in a non-gasified state were micrographed. Also, all the sample types that were gasified to a level of 20% mass loss from initial volatile-free mass were micrographed. Only the sample types L1200 and coke were gasified to mass loss levels of 30, 40 and 50% and micrographed after gasification. The L1200 sample was chosen from the biocarbon samples for these further experiments because the gasification reaction rate was closest to that of nut coke. The chosen mass loss levels are close to those of industrially produced metallurgical coke experiences in CRI tests (Haapakangas et

al., 2016). All the micrographs were further analysed with the Fiji open-source java-based image processing package.

The experimental procedure of the gasification experiments that were combined with the compression strength tests, optical microscopy and image analysis are presented in Table 5.

**Table 5. Treatments of biocarbon and nut coke samples.**

Treatment / experiment	L600	L900	L1200	Nut coke
Pyrolysis temperature [°C]	600	900	1200	
Gasification to 20% mass loss	x	x	x	x
Gasification to 30% mass loss			x	x
Gasification to 40% mass loss			x	x
Gasification to 50% mass loss			x	x
Compression strength of the non-gasified samples	x	x	x	x
Compression strength of the gasified samples	x	x	x	x
Optical microscopy of non-gasified samples	x	x	x	x
Optical microscopy of gasified samples	x	x	x	x
Image analysis of the micrographs	x	x	x	x

## **5 Results of biocoke formation and properties**

This chapter is based on the research work that has been carried out within Publications I and III of this thesis. The scope is within the definition of suitability of hydrolysis lignin and hydrolysis lignin-based biocarbon as part of coking blend in metallurgical coke making. The most important properties of the produced biocokes will be determined in this chapter. These properties include the gasification reactivity and determination of compression strength. These properties were chosen to be measured for determination of the performance of biocokes in industrial pyrometallurgical processes. Coke with a single coking coal in the coking blend was used as a reference material in the experiment. Also, the reasons for the properties of biocoke were investigated by analysing the interaction between coking coal and biomaterial during the coking process.

### **5.1 Chemical composition of biocoke raw materials**

The major differences between the chemical compositions of coking coal and hydrolysis lignin are the oxygen content, volatile matter, ash and fixed carbon content (Table 6). The trace element composition of coking coal and hydrolysis lignin also differ considerably from each other. The major trace elements in coking coal ash are silicon dioxide ( $\text{SiO}_2$ ) and aluminium oxide ( $\text{Al}_2\text{O}_3$ ), while calcium oxide ( $\text{CaO}$ ), sodium oxide ( $\text{Na}_2\text{O}$ ), potassium oxide ( $\text{K}_2\text{O}$ ) and phosphorus pentoxide ( $\text{P}_2\text{O}_5$ ) are the major components in hydrolysis lignin ash.

**Table 6. Chemical properties of coking coal and hydrolysis lignin (Modified under CC BY 4.0 license from Publication I @2019 Authors).**

Analysis	Properties	Coking coal	Hydrolysis lignin
Total moisture (105 °C) [m.%]		9.02	5.3
Ultimate analysis [m.%], db.	C	79.90	62.10
	H	4.82	6.06
	O	2.88	30.40
	N	2.20	1.04
	S	0.56	0.13
Proximate analysis [m.%], db.	Volatile matter	22.69	66.26
	Ash content	9.64	0.20
	Fixed Carbon	67.67	33.54
Ash composition [%], db.	CaO	0.77	24.30
	MgO	0.54	4.70
	SiO <sub>2</sub>	65.20	4.30
	Al <sub>2</sub> O <sub>3</sub>	26.37	1.70
	Na <sub>2</sub> O	0.38	12.10
	K <sub>2</sub> O	0.94	7.70
	Fe <sub>2</sub> O <sub>3</sub>	3.45	4.90
	P <sub>2</sub> O <sub>5</sub>	0.47	16.10
	TiO <sub>2</sub>	1.56	0.04

The different trace element composition results in a more acidic coking coal ash and basic hydrolysis lignin ash in terms of basicity index or alkalinity index (Solar et al., 2021). Calcium and potassium in particular have previously been found to catalyse the Boudouard reaction, i.e. they increase the reaction rate of the carbonaceous material to CO<sub>2</sub> at high temperatures (Ding et al., 2014; Habibi et al., 2013; Hussein et al., 2017). In the BF process this may be detrimental because highly reactive coke might cause early breakage of cokes under chemical, thermal and mechanical burden, causing a collapse of the structural coke bed, thus leading to non-uniform distribution of heat, ascending gases and descending melts (slag and pig iron). On the other hand, less acidic coke would decrease the need for flux in the BF operation for increasing the basicity of the slag that is generated in the process (Solar et al., 2021). Also, the amount of coking coal ash is 48.2 times higher than that of hydrolysis lignin, thus the actual amount of single trace element species of hydrolysis lignin ash is considerably lower than that of coking coal. To summarise, the addition of hydrolysis lignin into the coking blend has a decreasing

effect on the total ash amount of the produced coke, thus compensating the non-favourable composition of the ash of hydrolysis lignin. The amounts of main trace elements of hydrolysis lignin and coking coal ash are presented in Table 7 as percentages in ash and as total amounts, i.e. grams per one kilogram of raw material.

**Table 7. Percentages and absolute amounts of main trace elements of hydrolysis lignin (Modified under CC BY 4.0 license from Publication III @2022 Authors).**

	Coking coal				Hydrolysis lignin			
	CaO	K <sub>2</sub> O	Na <sub>2</sub> O	P <sub>2</sub> O <sub>5</sub>	CaO	K <sub>2</sub> O	Na <sub>2</sub> O	P <sub>2</sub> O <sub>5</sub>
Percentage in ash [%]	0.77	0.94	0.38	0.47	24.30	7.70	12.10	16.10
Total amount [g/kg <sub>mat</sub> ]	0.74	0.91	0.37	0.45	0.49	0.15	0.24	0.32

The lower oxygen content of coking coal (bituminous coal) is a result of the formation and evolution of coal over the years under pressure and heat in the absence of oxygen in the earth's crust. The molecular structure of coking coal and hydrolysis lignin is presented in Fig. 5 (Cho et al., 2012; Mathews & Chaffee, 2012; Wisler, 1984). The coking coal structure consists of aromatic ring structures that contain a greater number of aromatic rings than hydrolysis lignin. Smaller ring structures of hydrolysis lignin are mainly connected with ether bonding. Furthermore, the mechanism of pyrolysis of lignin has been reported to initially include the loss of ether linkages (Cho et al., 2012), i.e. the oxygen content of hydrolysis lignin is highly related to the amount of volatile matter.

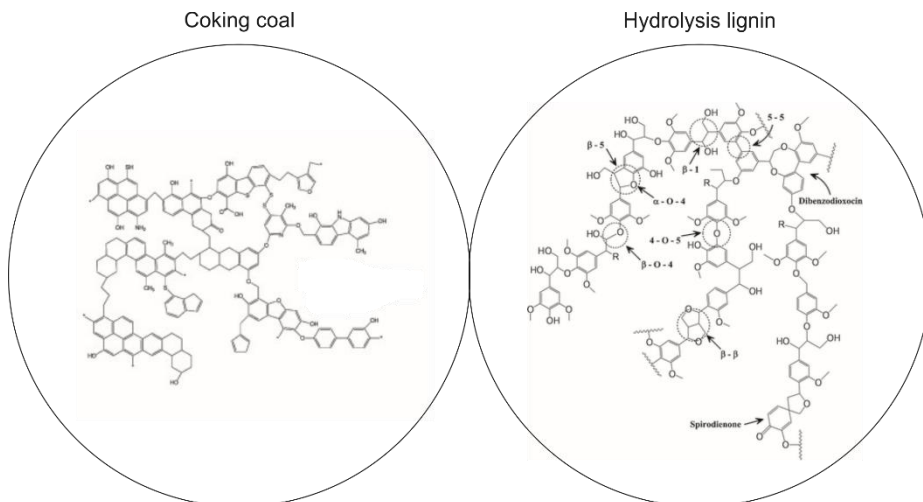


**Fig. 5. Structure of coking coal and hydrolysis lignin. Modified from Cho et al., 2012; Mathews & Chaffee, 2012; Wisler, 1984.**

## 5.2 Chemical composition of biocarbons

The chemical composition of the hydrolysis lignin evolves through thermochemical conversion during the pyrolysis. The chemical composition of hydrolysis lignin-based biocarbons is presented in Table 8. The mass-based solid yields in the pyrolysis of L350 (350 °C), L450 (450 °C), L600 (600 °C) and L1200 (1200 °C) were 58.3, 44.4, 39.3 and 34.7%, respectively. The major changes in the elemental composition of hydrolysis lignin-based biomass are the considerable decrease in the oxygen and hydrogen contents and an increase in the elemental carbon content. This also shows as a substantial decrease in the volatile matter content (from 66.26 to 1.43%) and as an increase in the fixed carbon content (from 33.54 to 97.21%) between dried hydrolysis lignin and L1200 biocarbon.

**Table 8. Chemical composition of hydrolysis lignin-based biocarbons (Modified under CC BY 4.0 license from Publication III @2022 Authors).**

Analysis	Properties	Hydrolysis lignin	L350	L450	L600	L1200
Total Moisture (105 °C) [m.%]		5.3	1.8	1.25	0.66	0.3
Ultimate analysis [m.%], db.	C	62.1	75.8	83.25	87.10	96.23
	H	6.06	4.4	3.96	2.15	0.09
	O	30.4	17.8	9.74	7.39	2.16
	N	1.04	1.4	1.17	1.23	0.16
	S	0.13	0.09	0.00	0.00	0.00
Proximate analysis [m.%], db.	Volatile matter	66.26	28.67	18.22	7.99	1.43
	Ash content	0.2	0.5	1.89	2.13	1.36
	Fixed Carbon	33.54	70.83	79.89	89.88	97.21

### 5.3 Coking properties of coal

The coking properties of coking coal are presented in Table 9. The coking coal in the experiments of this thesis was a medium-volatile coking coal with a maximum fluidity of 457 dial divisions per minute (ddpm). The coking coal had so-called self-coking capability, i.e. the thermoplastic properties of this single coal were suitable for the formation of coke during the coking process.

**Table 9. Plastic properties of coking coal (Modified under CC BY 4.0 license from Publication III @2022 Authors).**

Gieseler plastometer values of coal	
Softening temperature [°C]	422
Temperature of max. fluidity [°C]	459
Resolidification temperature [°C]	490
Maximum fluidity [ddpm]	457
Other plastic properties of coal	
FSI	8.00
Roga index	73.00
G value	1.04
Y value [mm]	14.00

## 5.4 Volatile release during co-carbonisation

The volatile release of individual raw materials (coking coal, L350 and hydrolysis lignin) in coking conditions is presented in Fig. 6. The mass loss of the samples is presented with a line and symbols, while the mass loss rates are presented only with lines whose colours correspond the colour of mass loss curves of each sample. The coal softening temperature (422 °C) and coal resolidification temperature (490 °C) are marked with a dashed line, while the temperature of maximum fluidity (459 °C) is presented with a dotted line. Most of the release of volatiles of hydrolysis lignin occurs before the coking coal softening, while only 7.6% of the total volatile release occurs during the coal plastic phase. Meanwhile, 20.0% of the total volatile release of L350 and 39.5% of the total volatile release of coking coal occur during the coal plastic phase. The volatile release of graphite powder was also analysed with TGA, but there was no detectable mass loss in the testing conditions. The result was expected since the graphite composition was 99.9% carbon. Meanwhile, the release of volatiles before the coal plastic phase was 79.7, 42.7 and 16.8% for hydrolysis lignin, L350 and coking coal, respectively. The gas release before the coal plastic phase leads to the formation of gaseous species that contribute to the fluidity development already in the coal softening stage before the formed gaseous compounds exit the system. In the case of hydrolysis lignin or hydrolysis lignin-based biocarbon (L350), the devolatilisation products are rich in oxygen. The oxygen-rich compounds act as inhibitive species to coal fluidity development. Besides the amount of oxygen-rich components, the functionality of the oxygen also influences the modification of the coal fluidity development. The oxygen-rich additives mainly affect the maximum fluidity development, while the temperatures of softening, maximum fluidity and resolidification remain almost unchanged. The oxygen functionalities contribute to the condensation of the fluidity promoting substances in the coking blend, thus facilitating the resolidification of the fluid mass into semi coke (Diez et al., 2012; Díez et al., 2005)

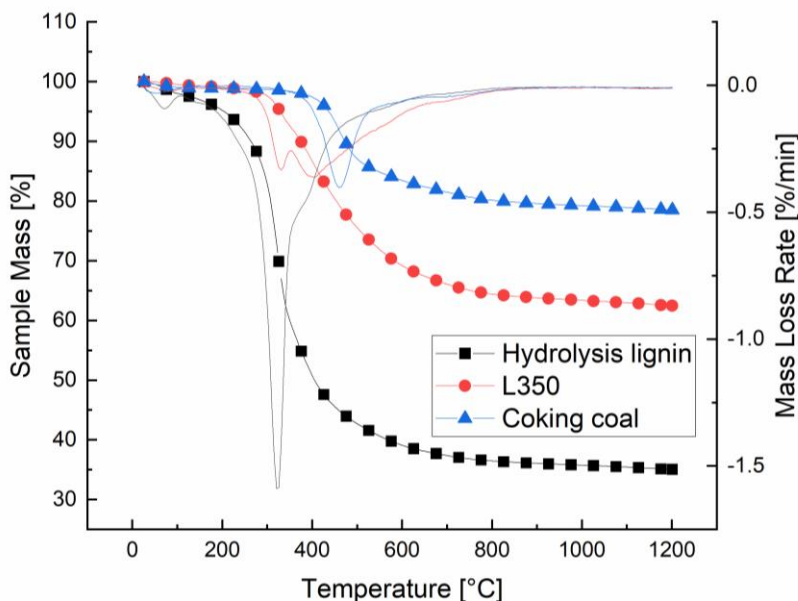


**Fig. 6. Volatile release of coking coal, hydrolysis lignin and L350 (Reprinted under CC BY 4.0 license from Publication I @2019 Authors).**

The mass loss of hydrolysis lignin (HLIG), L450, L600, L1200 briquettes and coking coal is presented in Fig. 7. The results show that HLIG loses most of its mass (51.07%) before the coal thermoplastic phase, thus generating a substantial amount of oxygen-bearing components that negatively will affect coal fluidity development (Diez et al., 2012; Mochizuki & Tsubouchi, 2019). Meanwhile, the mass losses of L450, L600 and L1200 were 3.77, 1.87 and 0.56% at this stage, respectively. The total mass losses of HLIG, L450, L600 and L1200 were 63.95, 20.24, 9.57 and 1.61 during the whole experiment, respectively. During the coal plastic phase, the mass loss of HLIG, L450, L600 and L1200 samples were 4.96, 1.41, 0.31 and 0.08%, respectively. The results indicate that the pyrolysis of the hydrolysis lignin briquettes modifies the sample chemistry so that the amount of devolatilisation products decrease as the pyrolysis temperature is elevated.

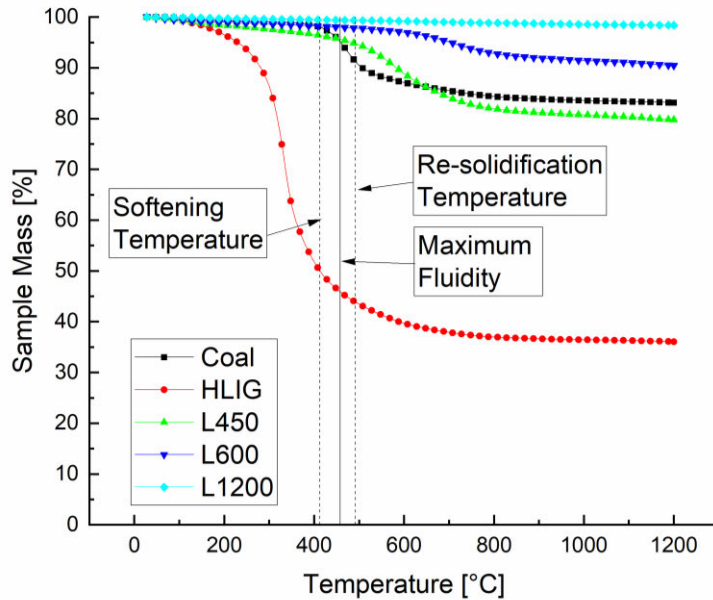


**Fig. 7. The devolatilisation of hydrolysis lignin-based briquettes and coking coal (Reprinted under CC BY 4.0 license from Publication III @2022 Authors).**

The mass loss rates of HLIG, L450, L600, L1200 and coking coal are presented in Fig. 8. The main peak of mass loss of HLIG can be found at 333 °C, which is well before the softening of the coking coal (422 °C). One notable thing is that the main peak of HLIG in Fig. 8 is considerably higher than that of hydrolysis lignin in Fig. 6. This is due to the higher heating rate of the experiment where HLIG was tested. However, the thermal degradation of HLIG continues through the coal thermoplastic phase, thus producing oxygen-bearing devolatilisation products from the beginning of the coal softening and through the coal thermoplastic phase. This will inhibit coal fluidity development as the oxygen-bearing substances react with the fluid components of the coking blends, which leads to a viscous, low fluid system, and thus disordered and weak structure of resulting coke (Diez et al., 2012). The biocarbon samples L450 and L600 peaked at a higher temperature after the coal thermoplastic stage. However, the development of the peaks of L450 and L600 begin before the coal resolidification temperature (490 °C). Also, the coal devolatilisation stage is not over when the peaks of L450 and L600 occur at 573 °C

and 715 °C, respectively. This means that possible gas-gas interaction between the biocarbon (L450 or L600) and coking coal originating gaseous compounds can occur during co-carbonisation (Díaz et al., 2012). On the other hand, a major gas release from the biocarbons inside the solidified coke matrix may remain trapped, thus promoting the formation of macropores inside the matrix (Casal et al., 2021). The L1200 sample did not show any considerable mass loss peaks during the experiment, but the mass reduced steadily throughout the experiment.

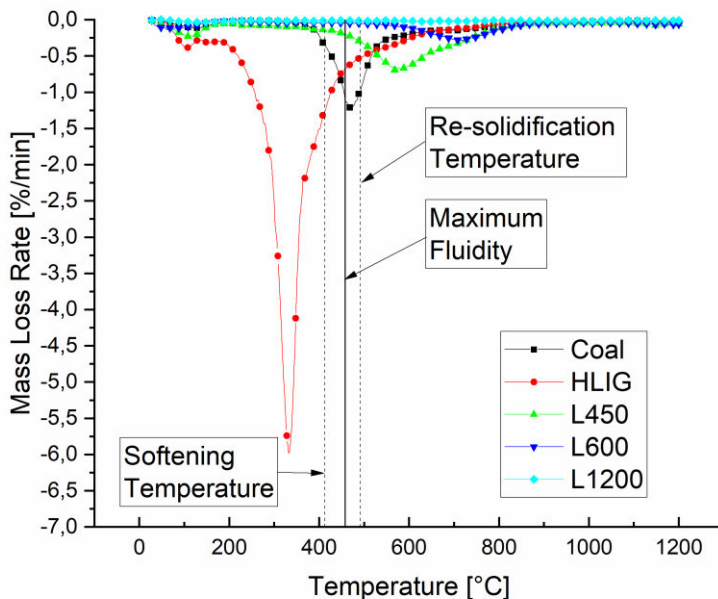


**Fig. 8. Mass loss rates of the samples during the co-carbonisation (Reprinted under CC BY 4.0 license from Publication III @2022 Authors).**

## 5.5 Released devolatilisation products of hydrolysis lignin

The functionality of the oxygen bearing functional groups has been reported to be the dominant factor in the development of coal fluidity, besides the total amount of oxygen (Diez et al., 2012). In (Diez et al., 2012) syringol (2,6-dimethoxyphenol) was reported as a representative thermal degradation product of alkali lignin. This may be the case with alkali lignin or hardwood lignin. However, the relative syringol content in the gaseous thermal degradation product blend of softwood

lignin is considerably lower than that of hardwood lignin (Zhao et al., 2014). The hydrolysis lignin that was used in the coking experiments in this thesis was extracted from softwood, thus the content of softwood thermal degradation products is more relevant. The typical groups of products from thermal degradation of softwood lignin are guaiacol (2-methoxy-phenol), syringol, phenols (phenol and 1,2,3-benzenetriol), catechol (1,2-benzenediol) and aromatic hydrocarbons, with guaiacol being the major type of compound (Zhao et al., 2014). These thermal degradation products were identified based on their MS signals in this study. The  $m/z$  signals of guaiacol ( $m/z$  values of 53, 81, 109 and 124), syringol (93, 96, 111 and 139), phenol (39, 65, 66, 94), 1,2,3-benzenetriol (52, 80, 108 and 126) and catechol (64, 81, 92 and 110) are presented in Fig. 9. The intensities of the peaks were normalised to 100% because the peak intensities varied notably from each other, thus the detection of the peaks with low intensities would have been hard without normalisation. The main peak of the release of these compounds are in a narrow temperature range, from 360 to 375 °C.

The peak of phenol and 1,2,3-benzenetriol can be found at 360 °C, while the peaks of guaiacol, syringol and catechol occurred at 375 °C. The release of these compounds occurs 27 °C and 42 °C after the main peak in the mass loss rate of HLIG and 62 °C and 47 °C before coal softening temperature (422 °C). With a heating rate of 5 °C/min, this would mean that these compounds are released approximately 10 minutes before the coal begins to soften. However, in the coking experiments, the HLIG samples are placed inside the coal bed, thus the devolatilisation products may still be in the co-carbonisation system when the coal starts to soften. Moreover, these products were devolatilised at lower temperatures than the final temperatures of the pyrolysis of the hydrolysis lignin-based biocarbons (L450, L600 and L1200). This was further confirmed by the MS results, which indicated that the devolatilisation products presented in Fig. 9 were not released from the coking of biocarbons.

The results suggest that the biocarbons do not have an inhibiting effect on the coal fluidity development through the chemical reactions of the devolatilisation products. However, biocarbons may have an inhibitive effect on the fluidity development of coal through adsorption of fluid components that originate from coal. In this study, the adsorption had no to only a minor effect on coal fluidity development because the amount of HLIG, L450, L600 or L1200 was so small in comparison to the surrounding coal blend. This was also the case with possible absorption. These phenomena were, however, addressed and were contributory

factors to why the surface area of hydrolysis lignin-based biocarbons was reduced by briquetting before the pyrolysis.

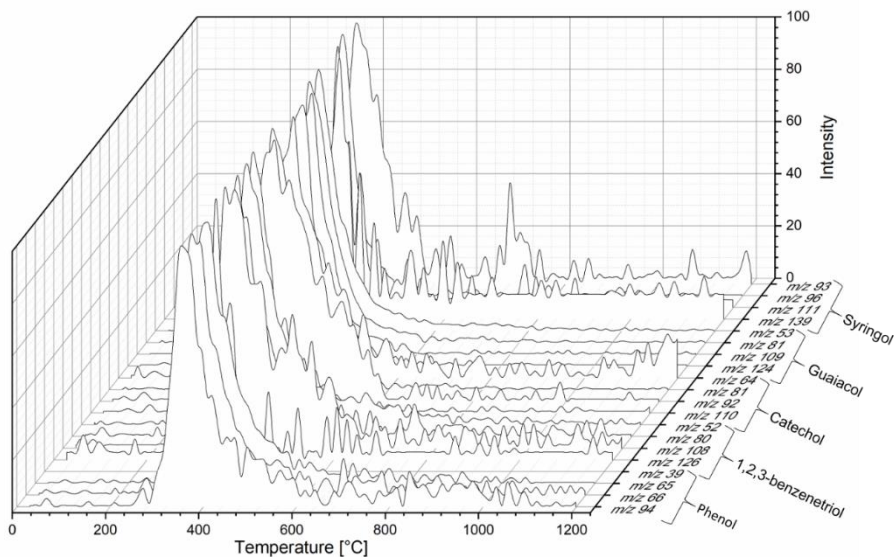


**Fig. 9. Mass spectrometry signals of HLIG in the coking process (Reprinted under CC BY 4.0 license from Publication III @2022 Authors).**

## 5.6 Properties of biocokes

### 5.6.1 Visual evaluation of the produced biocokes

The biocokes containing different amounts of non-pyrolysed hydrolysis lignin or pyrolysed lignin are presented in Fig. 10. The sample name “Reference” refers to the sample that was coked from a single coking and was not blended with anything. Sample names with “Lig” refer to the cokes that were produced from the blends of coking coal and non-pyrolysed hydrolysis lignin powder. “PrLig” refers, correspondingly, to the coke samples that were produced from the blends of coking coal and pyrolysed hydrolysis lignin powder. The number in the suffix of the sample name refers to the weight percentage of each additive in the blend. For example, PrLig15 contained 85% of coking coal and 15% of pyrolysed hydrolysis lignin in the blend. The weight percentages are calculated in relation to the total

weight of the blend. Macroscopically, the Reference sample was cylindrical-shaped, well coked and was not sensitive to abrasion. As the amount of non-pyrolised hydrolysis lignin was elevated in the blend, the height of the samples decreased, the cylinder shape was a little deformed, and more fines were released from the cokes under abrasion. This was also the case with the PrLig samples but the effect of bio-based additive on the physical appearance of the cokes was lighter than in the case of Lig samples.

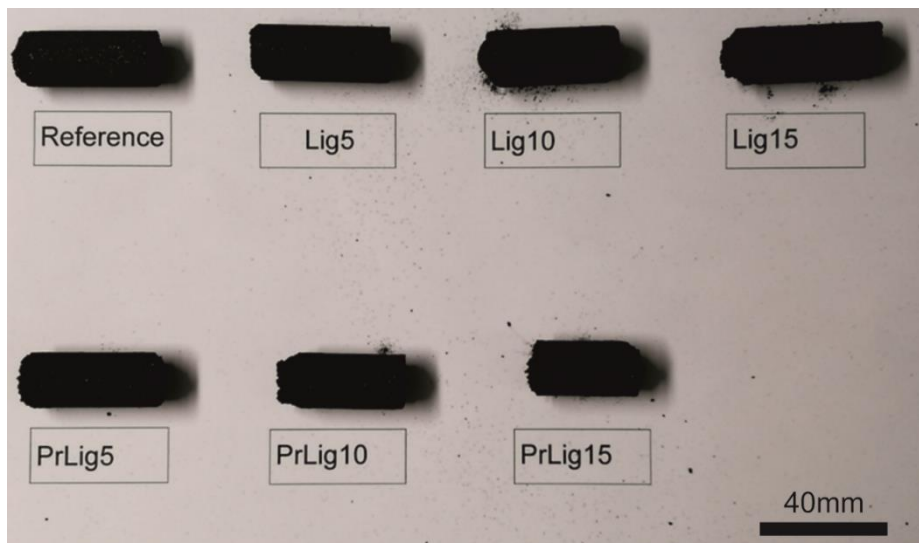


**Fig. 10. Mini biocokes (Reprinted under CC BY 4.0 license from Publication I @2019 Authors).**

The cokes containing HLIG, L450, L600 and L1200 briquettes are presented in Fig. 11. Although all the cokes were well formed and well resistant against abrasion, a higher number of formations of large cracks were observed in the cokes containing HLIG or L1200 than in the cokes that included either L450 or L600 briquettes. This also shows in Fig. 11 as the cokes including HLIG or L1200 briquettes came out of the coke oven in more numerous lumps than the two other cokes. The TGA results (Figs. 7 and 8), the MS results (Fig. 9) and visual investigation of the coke samples (Fig. 11) indicate that the mechanism of the crack formation was different between the cokes containing HLIG and L1200. In the case of HLIG containing cokes, the cracks were formed in the proximity of the HLIG briquettes but not directly in the interface of the coke and the HLIG briquette. The crack formation in this case is

assumed to originate from the local inhibition of coal fluidity during the thermoplastic phase, thus leading to formation of local weak points in the coke structure. Ultimately this has led to the formation of cracks during the contraction of coke. In the case of L1200 containing coke, the crack formation occurred at the interface of L1200 briquettes and surrounding coke. On the other hand, L1200 did not have a significant release of gaseous compounds during the coal thermoplastic phase, thus gas-gas interaction between the coal and L1200 briquettes was non-existent. The adsorption of the coal devolatilisation products inside the porous structure of L1200 briquettes would be a considerable option for how these two materials interact during the co-carbonisation process. However, Fig. 11 shows that this has not been the case between L1200 and coking coal.

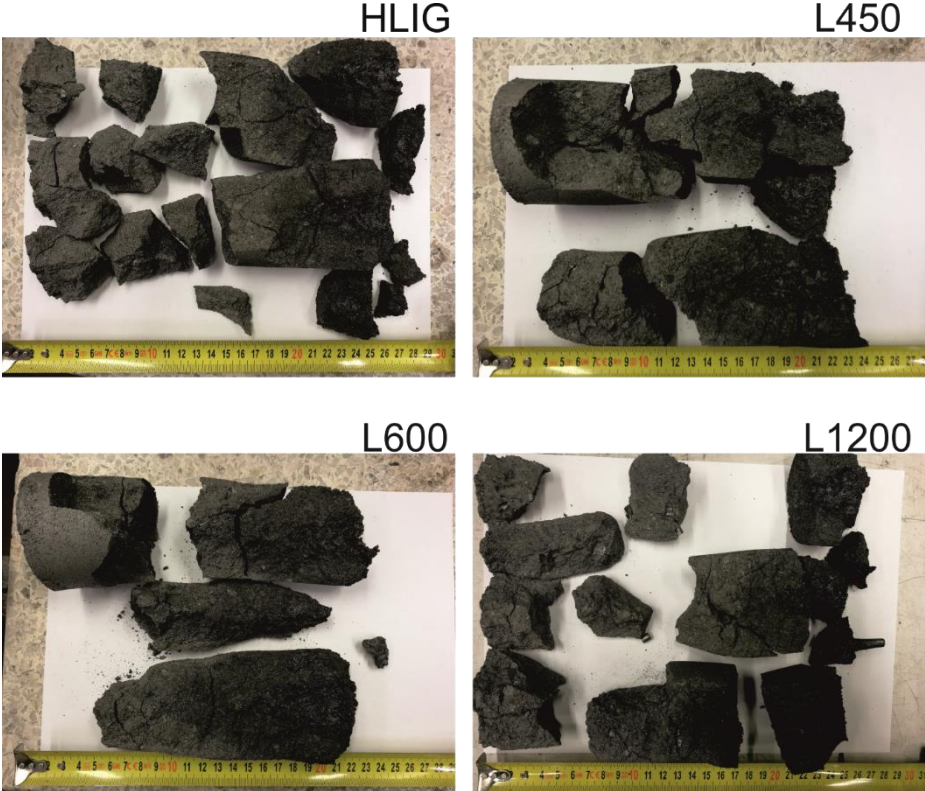


**Fig. 11. Biocokes from the blends of coking coal and hydrolysis lignin-based briquettes (Reprinted under CC BY 4.0 license from Publication III @2022 Authors).**

### 5.6.2 Compression strength of biocokes

The average compression strength, standard deviation and variability index of the compression strength test results are presented in Table 10. The values in Table 10 are calculated from the results of the compression of ten individual samples of each sample type. The reference samples were mechanically the strongest with highest standard deviation but with moderate variability index. The compression strength test results confirmed the visual observations that were made earlier. The strength of cokes decreased when the amount of hydrolysis lignin-based materials was increased in the coking blend. Furthermore, pyrolysis of hydrolysis lignin at 350 °C before blending with coking coal decreased the negative effect of this bio-based additive on the mechanical strength of produced coke. However, the compressive strength of pyrolysed lignin-containing cokes also decreased as the amount of this bio-based additive was increased in the blend. Graphite was the third additive in the coking blends. The mechanical strength of graphite-containing cokes (Graph) and the development of the compression strength of these cokes when the amount of additive is increased in the blend resemble those of pyrolysed lignin-containing cokes (PrLig). However, the drop in the strength of graphite-containing cokes is not as drastic as pyrolysed lignin-containing cokes when the amount of these additives is increased in the blends.

Also, the variability indices of the cokes containing pyrolysed lignin resemble those of graphite-containing cokes with corresponding amounts of additive material in the blend. This indicates a similar effect of these additives on the mechanical strength properties of coke. This is not the case with the samples containing non-pyrolysed lignin. Besides the considerably lower mechanical strength of these samples, the variability index lowers when the amount of hydrolysis lignin is increased in the blend, i.e. the heterogeneity of these samples decreases as the amount of additive in the blend is increased.

**Table 10. Summary of the compression strength results of biocokes (Modified under CC BY 4.0 license from Publication I @2019 Authors).**

Sample	Average strength [MPa]	Standard Deviation [MPa]	Variability Index
Reference	19.21	2.06	10.75
Lig5	4.76	1.59	33.46
Lig10	1.84	0.17	9.33
Lig15	1.30	0.07	5.65
PrLig5	8.17	1.54	18.91
PrLig10	3.22	1.01	31.26

Sample	Average strength [MPa]	Standard Deviation [MPa]	Variability Index
PrLig15	1.69	0.26	15.26
Graph5	9.77	3.28	33.55
Graph10	7.40	1.93	26.14
Graph15	5.14	1.96	38.07

The stress-strain curves of the compressions of different biocoke samples are presented in Fig. 12. The curves in Fig. 12 are from single compressions and were chosen based on the representativeness of the curve. The representativeness was evaluated based on how well the strength and strain at the fracture point of each compression corresponded to the average values of each sample batch.

The curve of the compression of Reference coke had the main peak at an early stage of the compression, before 5% strain. The peak was followed by step-like drops in the strength, thus indicating a layer-by-layer fracture of the structure. This type of behaviour under compression is typical for metallurgical coke (Haapakangas et al., 2014). The samples containing 5% of different additive materials (Lig5, PrLig5 and Graph5) had a similar peak at an early stage in the compression. However, the drop in the strength of Lig5 after the point of fracture was not step-like, but the strength decreased steadily until the sample was crushed. The behaviour of the PrLig5 and Graph5 samples, on the other hand, showed clear step-like characteristics after the point of fracture. Furthermore, the breaking behaviour of Lig and PrLig samples changed considerably as the amount of bio-based material in the coking blend was increased to 10 and 15%. This change showed as decreased strength, as a drift of strain at the point of fracture and as a change in the shape of stress-strain from a clear peak to a round curve without a clear point of fracture. The result indicates that at lower hydrolysis lignin-based addition levels the structure is oriented and layered, while at higher addition levels the structure becomes more disoriented. The similar effect on the breaking behaviour was not observed as the amount of graphite was increased in the coking blends.

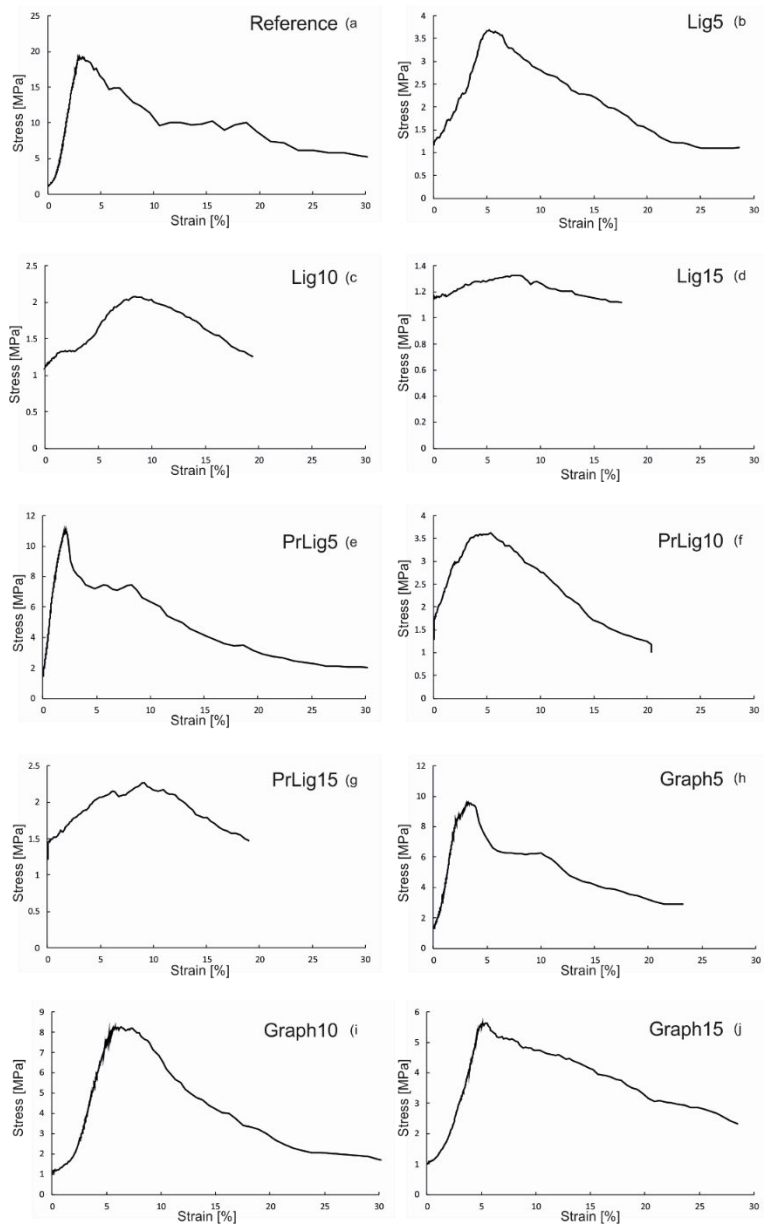


**Fig. 12. Stress-strain behaviour of biocokes (Reprinted under CC BY 4.0 license from Publication I @2019 Authors).**

### **5.6.3 Reactivity of the biocokes**

The reactivity of the biocokes, reference coke and graphite-containing cokes are presented in Fig. 13. Reference was the least reactive of all the samples, with 21.4% mass loss during the two-hour isothermal reactivity experiment. However, the reactivity of Graph15 and Graph10 were not considerably higher than that of Reference: 21.9 and 22.7% respectively. The mass loss of the samples containing 5% of additive material, Lig5, PrLig5 and Graph5 lost 23.7, 24.4 and 23.1% of their mass in the experiment, respectively. The effect of hydrolysis lignin-based material on the reactivity of the cokes is the opposite of the effect of graphite. While further increases in graphite (samples Graph10 and Graph15) in the cokes had a suppressive effect on the reactivity in comparison to Graph5, the further increase of non-pyrolsed and pyrolsed lignin just further increased the reactivity of coke. The samples containing pyrolsed lignin (PrLig5, PrLig10 and PrLig15) were slightly more reactivity than those containing corresponding amounts of non-pyrolsed lignin (Lig5, Lig10 and Lig15). The difference between the reactivities of the corresponding samples were not, however, that high.

The higher reactivity of the biocokes has been explained earlier by the following factors: the ash composition of the raw materials, oxygen content, the inhibition of fluidity development in the carbonised blend, the presence of porous isotropic particles from the biomass, functionality of the biomass material, and the microporosity of the cokes. The significance of these factors is dependent on the relative impact of other factors. For example, (Babich et al., 2009) discovered that the effect of microporosity on the CRI of cokes decreases and ultimately disappears as the amount of alkali in the system is increased.

Other than microporosity, the total number of pores, the number of larger pores and the shape of the pores also influence the reactivity of coke. Larger pores have better accessibility for reactive gas to enter the inner structure of coke and further react with the active sites (graphite crystallite edges). Also, the catalytic components tend to concentrate on the large pores, thus promoting the coke gasification (Nomura et al., 2007). Surface area is one notable characteristic contributing the reactivity of cokes. The irregularly shaped pores have larger edge length and surface area than the pores with corresponding volume but more regular shape (Diez & Borrego, 2013).

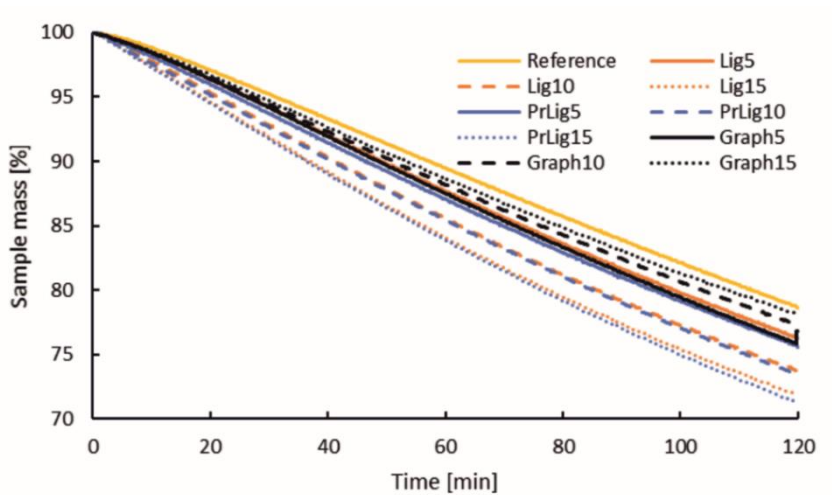
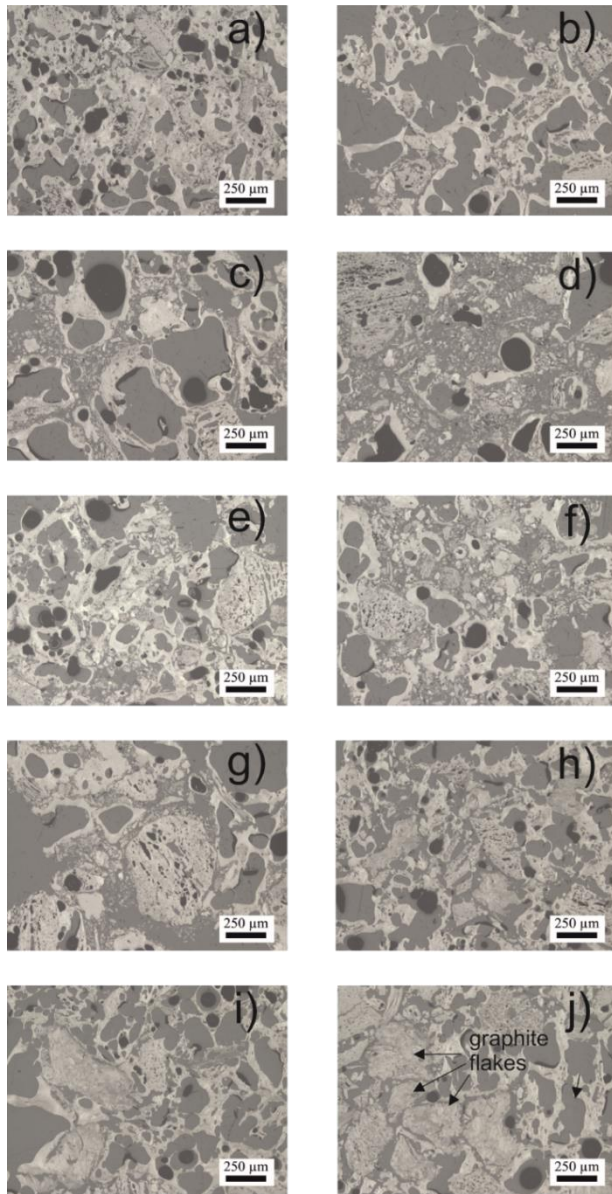


Fig. 13. Reactivity of the biocokes (Reprinted under CC BY 4.0 license from Publication I @2019 Authors).

#### 5.6.4 Structure of the surface of biocokes

The light optical microscopy (LOM) images of the biocokes, graphite containing cokes and Reference coke are presented in Fig. 14. The Reference coke (a), PrLig5 (e), Graph5 (h), Graph10 (i) and Graph15 (j) had a compact structure including medium sized elliptical pores. Lig5 had more open structure with larger sized pores and smaller cell wall thickness. As the amount of non-pyrolised or pyrolised lignin in coke was increased from 5% to 10 and 15%, the pore size enlarges with an increase of fine formation. This fine material can be found from the enlarged pores of Lig10, Lig15, PrLig10 and PrLig15. This fine material could not be observed in the LOM images of graphite containing samples (Graph5, Graph10 and Graph15). The porous structure of graphite containing cokes evolved as the amount of graphite was increased. The pores enlarged and the fusion of pores seems to be increased from sample Graph5 to Graph10. When the graphite content in coke was further increased to 15% (Graph15), the graphite flakes were accumulated inside the enlarged pores of coke. This explains the decrease in the reactivity of cokes when the amount of graphite in coke was increased. However, due to the poor interaction between coal and graphite in the coal thermoplastic phase, the linkages between graphite and the surrounding coke matrix are weak. This showed as a decrease in coke compression strength as a function of graphite addition level.



**Fig. 14. LOM images from coke samples: (a) Reference sample; (b) Lig5; (c) Lig10; (d) Lig15; (e) PrLig5; (f) PrLig10; (g) PrLig15; (h) Graph5; (i) Graph10; (j) Graph15 (Reprinted under CC BY 4.0 license from Publication I @2019 Authors).**

The micrographs in Fig. 14 were analysed and analysis results regarding the number of pores, pore size distribution and pore shape factor are collected in Table 11. There are different shape factors for defining the shape of the pores, but the Feret ratio was chosen for defining pore shapes in this work. It describes the ratio between the lowest and highest diameter of the pore. In practice, the Feret ratio is a ratio between the lowest and highest diameter of the pore with a value of 1 meaning a perfect circle, and a value of 0 referring to an infinitely elongated pore (Koskela et al., 2022b).

The uniform distribution of small pores is a structural characteristic that promotes better strength properties of coke (Andriopoulos et al., 2003). However, the increase in the total number of pores and pore area percentage are characteristics that decrease the strength of coke. The non-uniform pore distribution through the structure of coke is also a structural characteristic that has a decreasing effect on the strength of coke. The mechanism behind this reasoning is that the high local porosity creates local weak points, which lead to the formation of cracks under mechanical stress. The local weak point of coke is also promoted by pore connectedness and small cell wall thicknesses between the pores. The local weakness of coke is also related to the pore shape factor because a pore with low Feret ratio value has notably higher pore edge length than the pores with corresponding volume but a higher Feret ratio value. Higher edge length may lead to smaller cell wall thicknesses between pores, and elongated pores may promote crack formation in the direction of the elongation.

**Table 11. Image analysis results of biocokes (Modified under CC BY 4.0 license from Publication I @2019 Authors)**

Pore Edge Length [mm]	Reference	Lig5	Lig10	Lig15	PrLig5	PrLig10	PrLig15	Graph5	Graph10	Graph15
	Number of Pores									
0.01–0.20	1971	923	2062	2482	2305	2879	2233	1897	2120	2313
0.20–0.41	147	73	114	122	141	104	100	114	145	116
0.41–0.82	56	39	44	51	79	63	45	49	62	76
0.82–1.22	13	5	19	19	23	18	8	21	24	21
1.22–1.63	7	4	9	10	8	4	9	7	7	14
1.63–8.5	8	11	13	13	14	14	6	15	10	15
	Pore Shape Factor									
0.01–0.20	0.94	0.93	0.92	0.91	0.92	0.92	0.91	0.94	0.93	0.93
0.20–0.41	0.75	0.75	0.64	0.63	0.66	0.65	0.67	0.73	0.73	0.69
0.41–0.82	0.61	0.65	0.63	0.52	0.57	0.52	0.59	0.63	0.62	0.59
0.82–1.22	0.52	0.52	0.51	0.50	0.48	0.50	0.67	0.53	0.50	0.50
1.22–1.63	0.50	0.56	0.48	0.46	0.45	0.56	0.65	0.35	0.45	0.42
1.63–8.5	0.35	0.50	0.45	0.30	0.39	0.37	0.37	0.41	0.39	0.34

The number of pores did not explain the differences in the addition levels of different additives, the results in reactivity tests or differences in the strength test results. However, the pore shape factors of the smallest pores (pore edge length 0.01–0.2 mm) and largest pores (1.63–8.5 mm) correlated directly with the strength test results. However, large pores with elongated shape are considered to have a more significant effect on the strength of coke than mis-shaped small pores, because the pore area of an individual large pore is considerably higher than that of a small pore. The correlation between the compression strength and the pore shape factor of large pores of Lig, PrLig and Graph samples were 0.79, 0.95 and 0.97. Despite the high correlation, the shape of the large pores is not considered to be the only structural characteristic affecting the coke strength. High pore area percentage, number of the pores, the distribution of the porosity and so on affect the strength of coke (Koskela et al., 2022b).

## 5.7 Interaction during co-carbonisation

The LOM images of HLIG, L450, L600 and L1200-containing coke samples, micrographed under an X20 objective lens, are presented in Fig. 15. The micrographs are taken from the interface of the hydrolysis lignin-based briquettes and surrounding coke matrix in order to reveal the interaction of the two materials. The micrographs indicate that HLIG, L450 and L600 had chemical interaction with coking coal during the coking process, because these materials are fused to the coke matrix. However, L600 has separated from the surrounding coke matrix, having only a thin layer of coke on the surface of the briquette. This is an indication of the contraction of the L600 briquette after the coal solidification. The structure of coke near to the HLIG briquette is open, containing large, fused pores that may be caused by local fluidity inhibition by the devolatilisation products from HLIG during the coal thermoplastic phase. In the case of L1200, chemical interaction with coke cannot be observed as the materials clearly have their own separate surfaces without a joint interface. This leads to the formation of local weak points on the interfaces of coke and L1200 because the binding mechanism between these materials is based on the adsorption and further solidification of coal inside the pores of L1200, thus forming points of mechanical interlocking between the two materials (Kaliyan & Morey, 2010).

The micrographs (Fig. 15) indicate that the coking coal and hydrolysis lignin-based briquettes interact through gas-gas interaction, thus overlapping of the devolatilisation stages between the materials is required during the co-carbonisation for the formation of a fused interface.

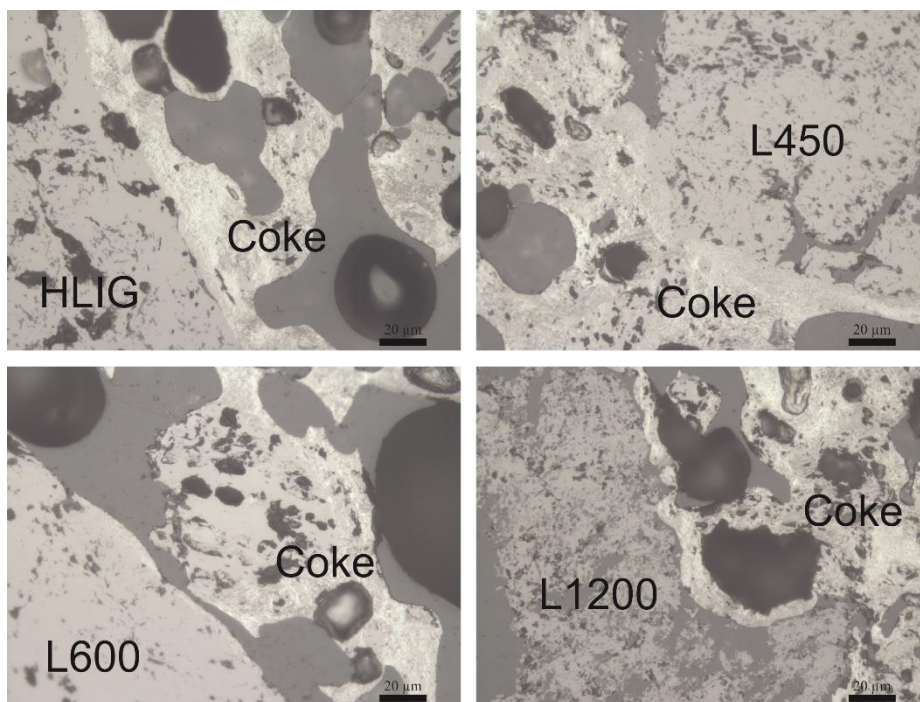


**Fig. 15. Interfaces of coke and hydrolysis lignin-based briquettes (Reprinted under CC BY 4.0 license from Publication III @2022 Authors).**

### ***5.7.1 Volumetric changes of hydrolysis lignin-based briquettes during co-carbonisation***

As was observed from the micrograph of L600 and coke interface (Fig. 15), the surfaces of the two materials were separated from each other during the co-carbonisation, with only a thin layer of coke on the surface of L600. This indicates a contraction or combined dilatation and contraction of the L600 briquette during the co-carbonisation. Earlier, lignin was found to undergo volumetric changes during the thermal treatment (Kifani-Sahban et al., 1997).

The volumetric changes of HLIG, L450, L600 and L1200 briquettes in the coking conditions is presented in Fig. 16. The contraction of HLIG briquette begins at approximately 220 °C, which is also the point where the thermal degradation peak (Fig. 8) of HLIG begins. Most of the lignin contraction occurred before the coke solidification temperature (490 °C), thus the volumetric change of HLIG is

not supposed to have a major effect on the formation of the joint interface with coke. The L450 briquette did not undergo volumetric changes at the early stage of the co-carbonisation. However, the volume of the sample starts to decrease approximately at the temperature of 490 °C, which is also the temperature where the coal was re-solidified. The contraction stage cannot only be associated with the thermal degradation of L450 because the thermal degradation stage ends somewhere between 450 and 550 °C and the contraction of L450 ended approximately at 820 °C. This indicates that lignin also contracts at its charring stage as the aromatic structure becomes more organised. However, this is not fully supported by the volumetric changes of L600 during the experiment. Slight variation in the L600 volume can be detected after 600 °C but a clear trend of contraction is missing. However, the L600 sample started to show a trend of dilation at approximately 700 °C and the dilation continued until the final temperature (1200 °C) of the co-carbonisation. L1200, on the other hand, did not contract during the co-carbonisation but started to dilate at approximately 700 °C and the trend of dilation continued until the final temperature of the experiment. The post-experiment measurements of sample height and diameter revealed that all the biocarbon samples shrunk when they cooled down to room temperature. The results suggest that L600 and L1200 stretch the solidified coke matrix at high temperatures of the co-carbonisation and the surrounding coke matrix does not follow the contraction of the briquettes during the cool-down stage. This conclusion is supported by the findings from the micrographs (Fig. 15) as the L600 and L1200 were separated from the surrounding coke matrix.

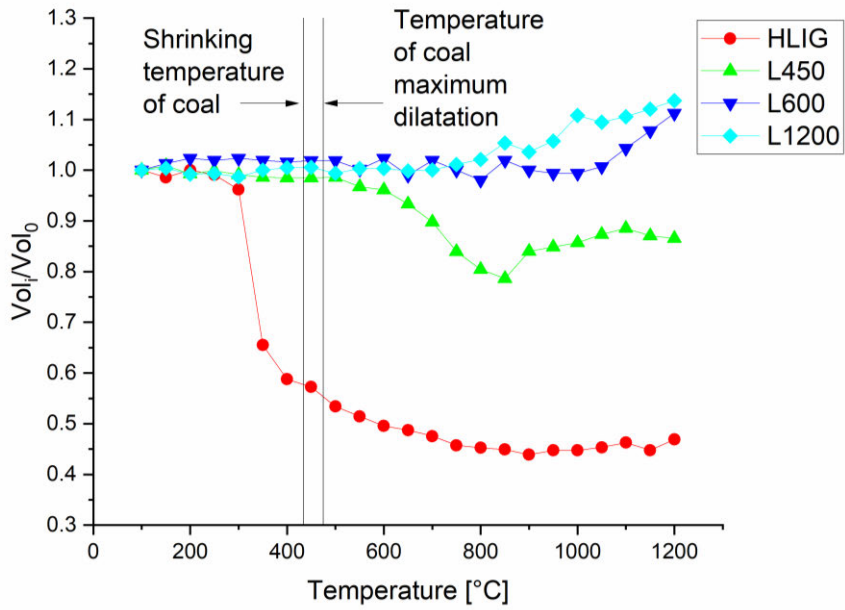


**Fig. 16. Volumetric changes of hydrolysis lignin-based briquettes during co-carbonisation (Reprinted under CC BY 4.0 license from Publication III @2022 Authors).**



## 6 Results of biocarbon formation and properties

This chapter is based on the research work that has been done within Publications II and IV of this thesis. The scope is within the definition of hydrolysis lignin-based biocarbon properties that are relevant in terms of the utilisation of biocarbon in pyrometallurgical processes for the substitution of fossil-based carbonaceous materials. The most relevant properties include chemical reactivity at high-temperatures and the determination of compression strength to define the performance of biocarbons in industrial pyrometallurgical processes. Also, the basic characterisation of the biocarbons is introduced in this chapter.

### 6.1 Chemical composition

The chemical composition of the raw material hydrolysis lignin is presented in Table 12. The chemical composition slightly differs from that of Table 5 in Section 5.1 “Chemical composition of biocoke raw materials”, because the materials are from different sample batches. The trace element composition of hydrolysis lignin ash is left out of Table 12 because the trace element characteristics were similar to those presented in Table 5 and the effect of the trace element composition was explained earlier in Section 5.1 “Chemical composition of biocoke raw materials”.

**Table 12. Chemical composition of hydrolysis lignin (Modified under CC BY 4.0 license from Publication IV @2022 Authors).**

Analysis	Properties	Hydrolysis lignin	Standard / Analysis method
Total Moisture (105 °C) [m.%]		5.3	SFS-EN 14774-2, CEN/TS 15414-2, ISO 589
Ultimate analysis [m.%], db.	C	61.0	SFS-EN ISO 16948, SFS-EN 15407, ISO29541
	H	6.1	SFS-EN ISO 16948, SFS-EN 15407, ISO29541
	O	31.9	SFS-EN ISO 16993
	N	0.7	SFS-EN ISO 16948, SFS-EN 15407, ISO29541
	S	0.1	ASTM D 4239 (mod), SFS-EN ISO 16994
Proximate analysis [m.%], db.	Volatile matter	70.9	SFS-EN ISO 18123, SFS-EN 15402, ISO 562
	Ash content	0.2	SFS-EN ISO 18122, SFS-EN 15403, ISO 1171
	Fixed Carbon	28.9	Determined by difference

The proximate analysis of hydrolysis lignin, lignin-based biocarbons and metallurgical nut coke are presented in Table 13. The ultimate analysis of lignin-based biocarbon briquettes (L600, L900 and L1200) is presented in Table 14. The different stages of carbonisation can be seen as differences in fixed carbon content and volatile matter. This is natural because the higher pyrolysis temperature increases the degree of carbonisation, and a greater amount of volatiles are removed when the pyrolysis temperature is increased. L450 has a lower fixed carbon content than nut coke, but when the pyrolysis temperature is elevated further to 600 °C (sample L600) the fixed carbon content of biocarbon exceeds that of nut coke. The biggest differences between the biocarbon samples and nut coke are the volatile matter content and ash content. Nut coke contains considerably higher ash content and is less volatile than biocarbons. These chemical properties can contribute to the differences in the reactivity and strength of biocarbons and nut coke.

**Table 13. Proximate analysis of the biocarbons (Modified under CC BY 4.0 license from Publication II @2021 Authors).**

Sample	Total Moisture (105 °C), [m.%]	Volatile matter [m.%], db.	Ash content [m.%], db.	Fixed Carbon [m.%], db.
Hydrolysis lignin	55.4	70.9	0.2	28.9
L450	1.25	18.7	2.01	79.29
L600	0.66	8.22	2.19	89.58
L900	0.71	5.33	2.13	92.55
L1200	0.30	1.53	1.3	97.16
Nut coke	6.00	0.14	11.45	88.41

The results of proximate and ultimate analysis show that the oxygen content and volatile matter content of the biocarbons are highly related to each other. This means that when the level of thermal refining of biocarbon is elevated (pyrolysis temperature is increased), the release of oxygen-containing volatiles is increased (Pienihäkkinen et al., 2021).

**Table 14. Ultimate analysis of the biocarbon samples (Modified under CC BY 4.0 license from Publication IV @2022 Authors).**

Sample	C	H	N	O	S
L600	87.9	1.73	0.97	8.5	0
L900	91.81	0.79	0.35	4.92	0
L1200	96.73	0.07	0.13	2.15	0

The identified devolatilisation products in hydrolysis lignin pyrolysis are presented in Fig. 17. The base intensity of different devolatilisation products varies, which can be seen as different starting points of the curves. The devolatilisation products in Fig. 17 were the ones that produced the highest intensities in the mass spectrometer. The main devolatilisation products in hydrolysis lignin pyrolysis were water (H<sub>2</sub>O), carbon monoxide (CO), carbon dioxide (CO<sub>2</sub>), methane (CH<sub>4</sub>) and hydrogen (H<sub>2</sub>). There might be some overlapping at specific *m/z* values. For example, the *m/z* value of 28 has accounted for CO, but this *m/z* value could also indicate the release of ethene or ethylene (C<sub>2</sub>H<sub>4</sub>). Also, strong intensities were found at *m/z* values of 32 and 36. The *m/z* value of 32 corresponds to either oxygen (O<sub>2</sub>), methanol (CH<sub>4</sub>O) or hydrazine (N<sub>2</sub>H<sub>4</sub>). According to earlier findings, methanol is the most probable thermal degradation product of hydrolysis lignin that corresponds to an *m/z* value of 32 (Zhao et al., 2014). The *m/z* signal of 36 corresponds to compounds such as hydrogen chloride (HCl) or methanol-D<sub>4</sub>, which is an isotopologue of methanol, with each hydrogen atom having an extra neutron (U.S. Secretary of Commerce, 2022). The *m/z* value of 36 may also be a signal of tri-carbon (C<sub>3</sub>), which is a transient species in lignin thermal degradation, as it is cleaved from the benzene ring to obtain saturated or unsaturated hydrocarbons (Huang et al., 2019).

The signal for vaporised water peaks at 106 °C and 330 °C. The water peak at 106 °C indicates the removal of free moisture, while the peak at 330 °C refers to water that originates from the degradation of oxygen-containing functional groups. The majority of oxygen removal in the thermal degradation of hydrolysis lignin occurs through the release of water and carbon dioxide (Zhao et al., 2014). This means that most of the oxygen is released at 330 °C as the intensity of the CO<sub>2</sub> signal also peaks at that temperature.

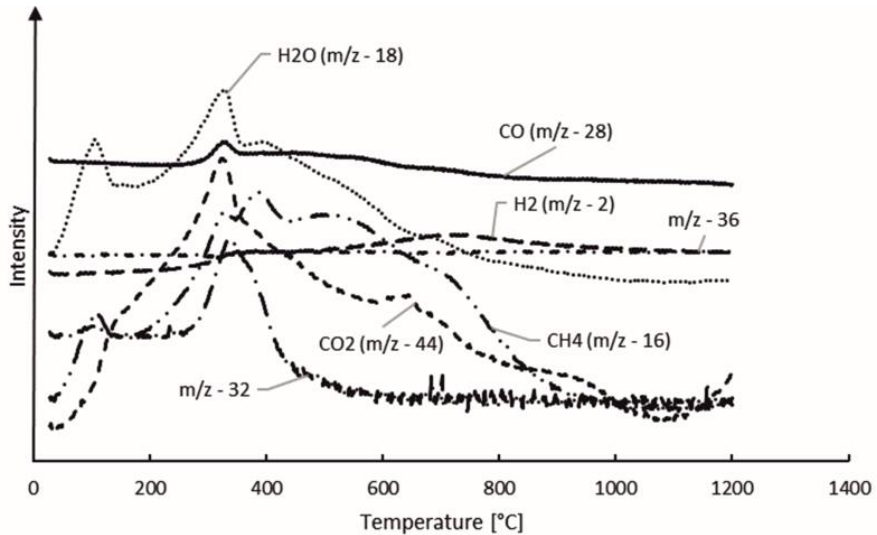
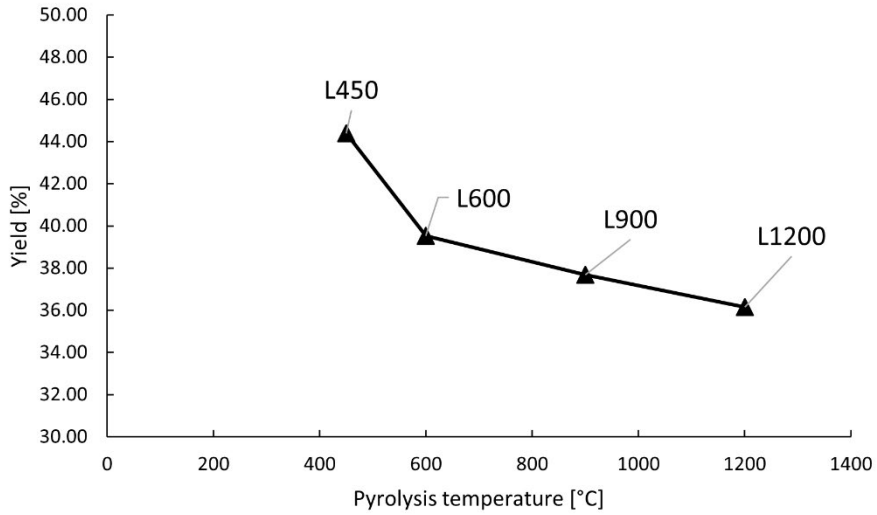


Fig. 17. Devolatilisation products in hydrolysis lignin pyrolysis (Reprinted under CC BY 4.0 license from Publication II @2021 Authors).

## 6.2 The effect of pyrolysis conditions on the solid biocarbon yield

The main single parameters affecting the distribution of the product yield are the heating rate, pyrolysis temperature and the type of biomass feedstock (Phounglamcheik et al., 2020). The feedstock in this study is hydrolysis lignin, but the effect of heating rate and final temperature in the solid biocarbon yield is investigated.

The effect of final pyrolysis temperature on the solid biocarbon yield is presented in Fig. 18. The heating rate in these experiments was 5 °C/min and the holding time at the final temperature 8 hours to ensure thorough pyrolysis of the samples. The slope of the solid yield curve is steep when moving from 450 °C to 600 °C, which can be explained by different stages of hydrolysis lignin pyrolysis. The thermal degradation stage can go as far as 550 °C, meaning that this stage is ongoing at 450 °C and has ended prior to the pyrolysis temperature of 600 °C. From 600 °C to 1200 °C the solid yield slope is more moderate. This temperature range covers the stage of amorphous carbon formation (600–900 °C) and carbon structure reformation (900–1200 °C) (Cao et al., 2013a).



**Fig. 18. Pyrolysis temperature and solid yield of biocarbons (Reprinted under CC BY 4.0 license from Publication II @2021 Authors).**

The effect of heating rate on the biocarbon solid yield is presented in Fig. 19. The effect of heating rate was investigated within the range of 5 to 20 °C/min with 5 °C/min intervals. The 5 °C/min increase in the heating rate results in an approximate 1% drop in the solid biocarbon yield, when the pyrolysis temperature is in the range of 450 °C to 1200 °C. This aspect should be considered when the conditions of pyrolysis are being designed.

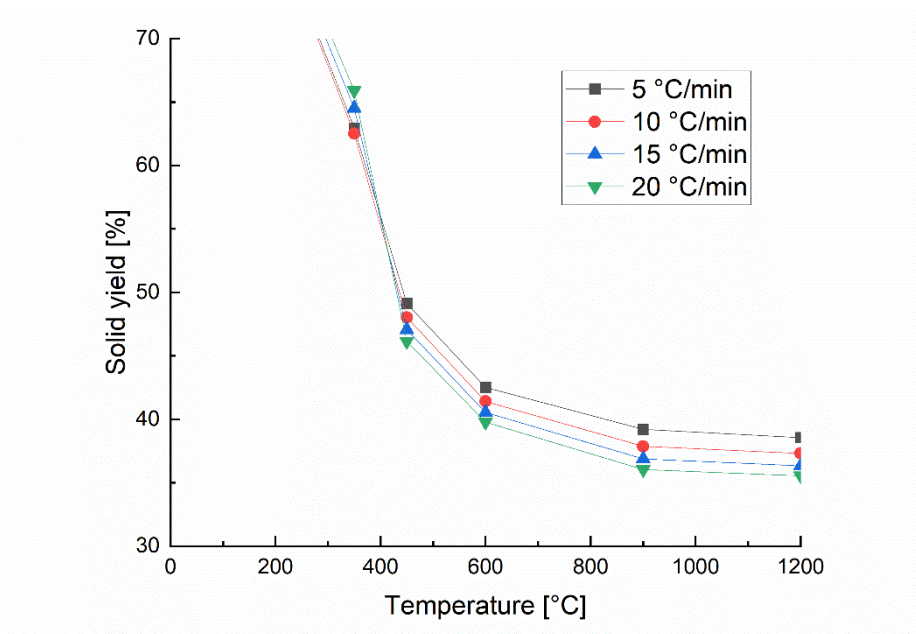


**Fig. 19. Effect of heating rate on the solid biocarbon yield (Modified under CC BY 4.0 license from Publication IV @2022 Authors).**

The effect of heating can also be observed from the mass loss rate curves that are presented in Fig. 20. The evolution of the peak of the mass loss curve begins to evolve at torrefaction temperatures below 300 °C. At this stage the curve of the lowest heating rate (5 °C/min) evolves the fastest. When the heating rate is increased, the evolution of the peak is slower, thus the mass loss rate peak evolution is shifted to higher temperatures. The mass loss rate peak temperatures of 5, 10, 15 and 20 °C/min heating rates were 320, 332, 340 and 345 °C. These findings are in agreement with an earlier study on the subject (Williams & Besler, 1996). Besides the shifting of the peaks, the peak mass loss rates are also considerably increased when moving from low to higher heating rates. This leads to a gradual decrease in the solid carbon yield, while the formation of primary pyrolysis gases is correspondingly increased. The result indicates that higher heating rates promote the cracking of organic compounds in biomass and condensable gases to form gaseous products. The released organic compounds may be further condensed either on the surface of the biocarbon to increase the solid yield, or on the liquid fraction to increase the yield of bio-oil. However, high heating rate and low

residence time are condition parameters that promote further cracking of volatiles, accounting for higher gaseous product yield.

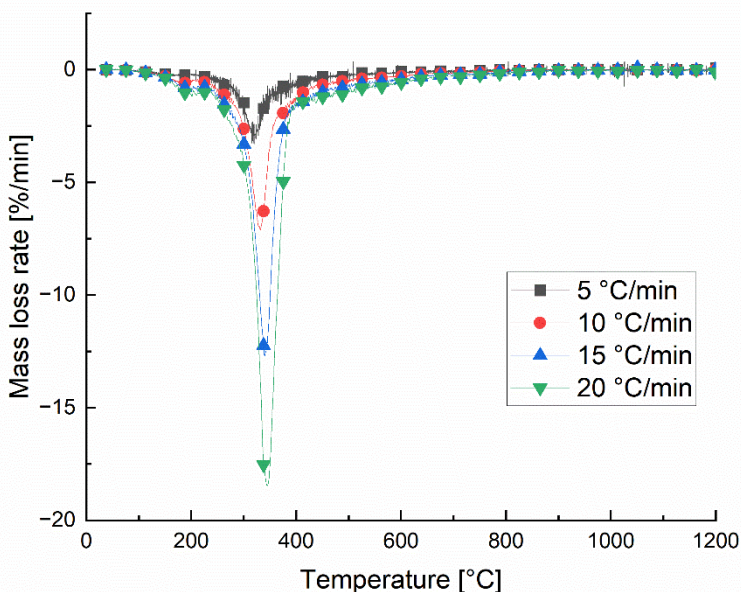


**Fig. 20. Heating rate and the evolution of mass loss rate (Modified under CC BY 4.0 license from Publication IV @2022 Authors).**

### 6.3 The structure of biocarbons

The structure of the biocarbon goes through changes at different stages of thermochemical conversion. This means that the structural characteristics of biocarbons vary when the pyrolysis temperature is different. In the temperature range of 600–1200 °C the stages of amorphous carbon formation and carbon structure reformation take place, which means that the structure of the hydrolysis lignin-based biocarbon samples densifies (Cao et al., 2013b; Otani et al., 1984). The apparent densities of L600, L900 and L1200 biocarbon briquettes were 1102, 1255 and 1364 g/dm<sup>3</sup>, respectively. Meanwhile, the apparent density of nut coke was 1084 g/dm<sup>3</sup>. The specific surface areas of the non-briquetted (L450p, L600p and L1200p) biocarbon samples, briquetted biocarbon samples (L600 and L1200) and nut coke are presented in Fig. 21. A temperature of 450 °C corresponds to the

temperature of the lignin thermal decomposition stage. At this stage the specific surface area (SSA) of hydrolysis lignin-based biocarbon (sample L450p) is moderate, 32 m<sup>2</sup>/g. As the temperature is elevated to 600 °C, which corresponds to the beginning of the stage of amorphous carbon formation, the SSA was increased to 245 m<sup>2</sup>/g (sample L600p). With further elevation of temperature to 1200 °C, lignin is in the structure reformation stage. At this stage the SSA was decreased to 2.8 m<sup>2</sup>/g. The effect of agglomeration on the SSA of the samples is easily observable. In comparison to non-briquetted L600p and briquetted L600 samples, the SSA decreased by 51 m<sup>2</sup>/g and L1200 had 1.2 m<sup>2</sup>/g lower SSA than L1200p. Meanwhile, nut coke had an SSA of 5.1 m<sup>2</sup>/g. The result indicates that the structure of hydrolysis lignin-based biocarbons can be modified by agglomeration and following high-temperature pyrolysis. The structural characteristics such as apparent density and SSA of L1200 even exceeded those of metallurgical nut coke.

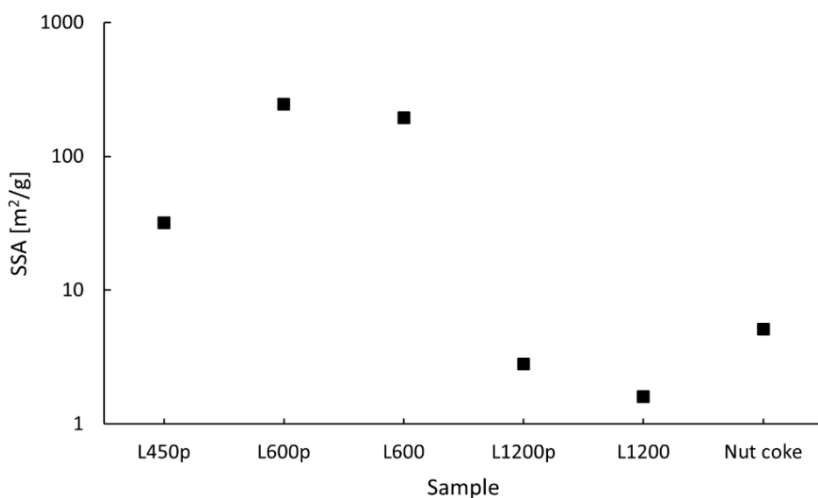


**Fig. 21. Specific surface area of the biocarbons and nut coke (Reprinted under CC BY 4.0 license from Publication II @2021 Authors).**

The surfaces of the L600, L900 and L1200 biocarbon briquettes are presented in Fig. 22. The surfaces of all the samples are smooth and dense, and porosity cannot be detected. However, several cracks can be found on the surfaces of all the biocarbon samples, with L600 having the largest cracks in terms of width, length and depth. There is no clear pattern in the orientation or location of the cracks, and

they are mainly surficial. Some cavities can be found on the surface of the L1200 sample, but they are not deep. According to these micrographs, most of the porosity or empty space inside the biocarbon structure is caused by the cracks. These surficial structure characteristics do not apply to nut coke. The surface of nut coke is rougher, consisting of a considerable number of pores and different textures. These structural changes are further analysed and discussed in Section 6.5.

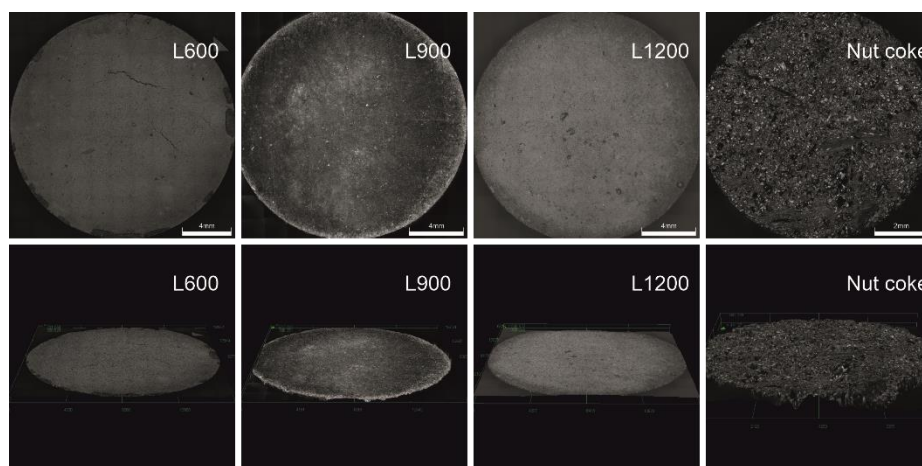


**Fig. 22. Surfaces of L600, L900, L1200 and nut coke (Modified under CC BY 4.0 license from Publication IV @2022 Authors).**

## **6.4 High temperature reactivity of biocarbons**

### **6.4.1 Dynamic reactivity tests**

The mass losses and mass loss rates of biocarbons and nut coke during the dynamic gasification experiments are presented in Fig. 23. The curves are normalised to start from a temperature of 750 °C in order to exclude the effect of volatile release from the curves. The order of the samples based on the total mass loss during the gasification experiment was: L450p, L600p, L600, L1200p, L1200 and nut coke, from highest mass loss to the lowest. The order of the samples indicates that agglomeration, high temperature pyrolysis and combination of these treatment methods modify the structure of biocarbons so that they are less reactive.

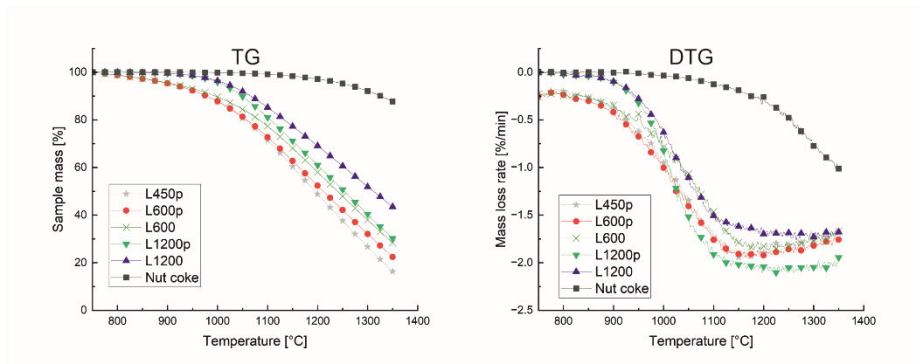


**Fig. 23. Gasification reactivity of the biocarbons and nut coke (Reprinted under CC BY 4.0 license from Publication II @2021 Authors).**

The mass loss, mass loss rate at gasification threshold temperature, and the gasification threshold temperature are collected from the data in Fig. 23 and presented in Table 15. The threshold temperature of gasification reaction was chosen based on the gasification reaction rate data set. The increase of 0.05%/min from the initial apparent reaction rate (ARR) at 750 °C was chosen. This ARR was chosen based on the mass loss data of the samples (Flores et al., 2017; Heikkilä et al., 2021).

At a pyrolysis temperature of 600 °C, the briquetting before the pyrolysis shifts the gasification threshold temperature by 26 °C. This is not, however, the case when the pyrolysis temperature is increased to 1200 °C. At the beginning of the reaction rate development, the pyrolysis temperature seems to have the biggest influence on this development. However, when gasification progresses and the temperature is elevated, the evolution of gasification rate of biocarbon briquettes is moderate in comparison to non-briquetted biocarbons. This leads to higher mass loss for non-briquetted biocarbons. Earlier, biocarbon gasification was suggested to be a phase-boundary-controlled reaction (Ahmed & Gupta, 2011; He et al., 2019; Hu et al., 2019; Luiz et al., 2018; Ortega, 1996; Struis et al., 2001). This means that the reaction rate is mainly controlled by chemical reactivity on the surface of the chars or at the edges of the pores. In this thesis, the quicker evolution of the gasification reaction rate of non-briquetted biocarbons can be partially explained by the higher surface area of non-briquetted biocarbons in comparison to briquetted biocarbons at a corresponding pyrolysis temperature. Based on the results, these treatment methods increase the material apparent density, and thus inhibit the gas penetration

into the structure of biocarbon and decrease the reactive surface area of the biocarbon.

**Table 15. Parameters from biocarbon and nut coke gasification (Reprinted under CC BY 4.0 license from Publication II @2021 Authors).**

Properties	Unit	L450p	L600p	L600	L1200p	L1200	Nut coke
Mass loss	[%]	83.68	77.55	71.64	69.77	56.48	12.21
Mass loss rate at threshold temperature	[%/min]	0.263	0.31	0.32	0.06	0.06	0.05
Threshold temperature	[°C]	847	847	873	880	872	1017

#### **6.4.2 Isothermal reactivity tests at the level of 20% mass loss**

L450p samples were left out from the isothermal reactivity tests while L900 samples were included in the tests. This decision was made based on the results of dynamic reactivity tests, as L450p samples were found to be too reactive and contain too much volatile matter. Also, only briquetted biocarbons were tested in the isothermal reactivity tests because briquetting was found to be a suitable method to modify the structural characteristics and thus the reactivity of the biocarbons.

The mass loss curves of biocarbon and nut coke samples to the level of 20% mass loss from initial volatile-free mass is presented in Fig. 24. Experimental gasification programme 1 (Table 4) was used in these isothermal reactivity tests. The gas atmosphere of programme 1 was the same as in the dynamic reactivity tests in Fig. 23. Because the temperature is kept constant in the isothermal reactivity tests, the mass loss is presented as a function of time. The time for 20% mass loss in gasification reaction was the longest for L1200 samples, approximately 80 min. L1200 was followed by L900 samples, which lost the corresponding mass percentage in approximately 63 minutes. In the case of L600 samples, the 20% mass loss took approximately 58 minutes. The results further confirm that the structural changes that were achieved by densification and high pyrolysis temperature lead to less reactive biocarbon.

Even though the gasification reactivity of L1200 biocarbon was considerably modified by densification and high pyrolysis temperature, the gasification reaction rate of nut coke was considerably lower than that of biocarbon. The gasification reaction of nut coke until 20% mass loss took approximately 391 minutes. The variation between the results of the repetitions of nut coke gasification was

considerably higher than that of biocarbons. Also, the gasification reaction time for 20% mass loss was 4.6 times longer than that of L1200 biocarbon. The long reaction time for nut coke gasification was expected from the basis of dynamic reactivity tests (Fig. 23 and Table 15).

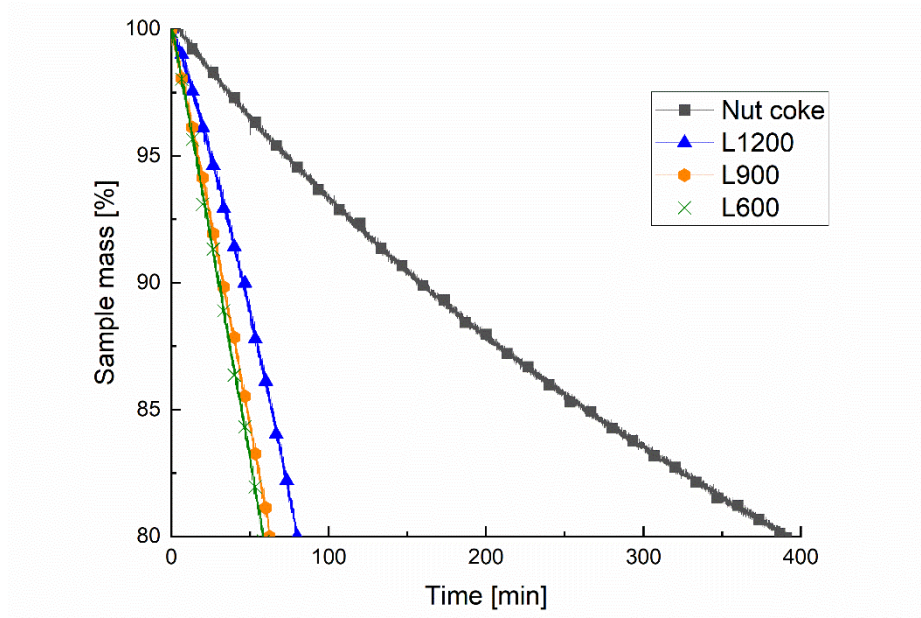


**Fig. 24. Isothermal gasification of biocarbons and nut coke (Reprinted under CC BY 4.0 license from Publication IV @2022 Authors)**

Based on the development of the reaction rate of the samples in Fig. 24, the behaviour of nut coke in gasification is different from that of biocarbons. The curves of biocarbons become steeper as a function of gasification time, i.e. the gasification reaction rate accelerates while the rate of nut coke gasification decelerates as the mass loss progresses. The evolution of the mass loss rate and other important parameters from the data of gasification experiments are collected in Table 16. The mass loss rate and the evolution of the mass loss rate data in Table 16 were collected from the equation of the linear trendline of the gasification reaction rate. The slope of the equation is the evolution of the mass loss rate, and the constant value indicates the mass loss rate at the beginning of the experiment. Based on this data, L1200 had the lowest rate of mass loss at the beginning but a high evolution rate during the gasification experiment. The result indicates that the

phase boundary reaction is slower with L1200 than with the two other biocarbon briquettes. This may be caused by the smaller surface area of L1200 at the beginning of the experiment. However, when the gasification reaction proceeds, the porosity of the samples increases, which leads to a higher surface area and a higher reaction rate.

**Table 16. Data from the isothermal gasification of biocarbons and nut coke (Reprinted under CC BY 4.0 license from Publication IV @2022 Authors).**

Sample	Volatile matter (1000 °C) [wt.%]	Time for 20% gasification [min]	Mass loss rate [%/min]	Evolution of the mass loss rate [%/min]
L600	10.47	57.68	-0.31000	-0.00090
L900	5.37	63.30	-0.26000	-0.00132
L1200	1.71	79.75	-0.18000	-0.00127
Coke	0.75	390.65	-0.06860	0.00009

The structural changes on the surface of the biocarbon briquettes (L600, L900 and L1200) and nut coke are presented in Fig. 25. All the samples went through structural changes on the sample surface. The most dramatic changes were found from the surface structure of L600 and L900 biocarbons. Before the gasification experiment, the surfaces of these samples were smooth, containing few cracks with random orientation and location. However, after gasification to the level of 20% mass loss, the surfaces of these samples were covered with cracks that were largely connected and located throughout the cross-section of the samples. The formation of the crack network of L600 and L900 could be a consequence of a few different reasons. The thermal shock at the beginning of the experiment could have led to a release of surface tension on the briquette, thus forming cracks. The release of tension could also be caused by the quick release of volatile matter, the gasification of carbon from the surface of the sample, or a combination of these. Extensive crack formation could not be found from the surfaces of L1200 or nut coke. Due to the gasification, roughness of the L1200 surface increased with the formation of short cavity holes whose appearance resembled that of pores under the microscope. In the gasification of nut coke, the surficial pores became enlarged, and enrichment of trace minerals could be detected on the edges of the pores. Based on the appearance of the minerals and usual trace mineral composition of cokes, these minerals are suggested to be either quartz ( $\text{SiO}_2$ ) or aluminium oxide ( $\text{Al}_2\text{O}_3$ ).

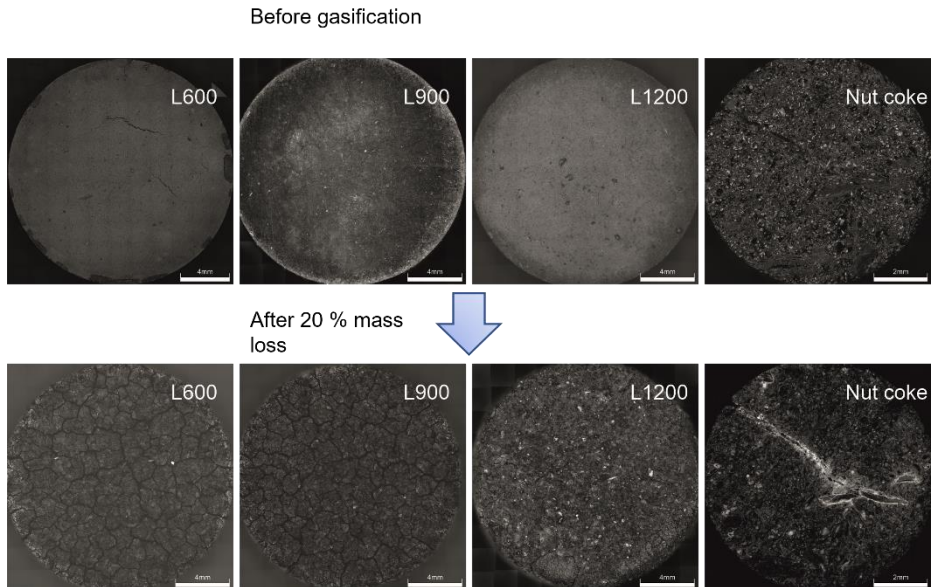


**Fig. 25. Surfaces of non-gasified and gasified samples (Reprinted under CC BY 4.0 license from Publication IV @2022 Authors).**

### **6.4.3 Inhibitive effect of CO on the gasification of biocarbon and nut coke**

Previously, CO has been reported to have an inhibitive effect on gasification of metallurgical coke as well as charcoal (Haapakangas et al., 2016; Huang et al., 2010; Roberts & Harris, 2012). The mass loss curves of L1200 and nut coke gasification are presented in Fig. 26. The gasification was performed in three different gas atmospheres with varying amounts of CO, CO<sub>2</sub> and N<sub>2</sub>. The level of 20% mass loss took the longest time when gasification was performed in a gas atmosphere that contained N<sub>2</sub>, CO and CO<sub>2</sub> with volumetric percentages of 50, 25 and 25%, respectively. When CO was replaced with N<sub>2</sub>, i.e. the N<sub>2</sub> percentage in the gas atmosphere was elevated from 50 to 75% while the CO<sub>2</sub> level remained constant and the CO level was dropped to 0%, the gasification time for 20% mass loss shortened considerably with L1200 biocarbon and nut coke. When the concentration of CO<sub>2</sub> was elevated to 100% in the reactive gas atmosphere, the gasification reaction rate of the samples was further increased, thus the reaction time for 20% mass loss shortened considerably.

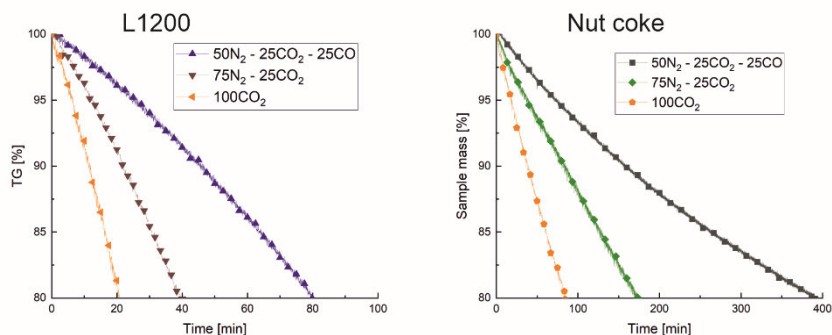


**Fig. 26. Mass loss curves of L1200 biocarbon and nut coke in gasification in different atmospheres (Reprinted under CC BY 4.0 license from Publication IV @2022 Authors).**

The shape of the mass loss curves of L1200 and nut coke differ considerably from each other. The curves of L1200 grow steeper as the gasification reaction proceeds towards 20% mass loss. In the case of nut coke, the mass loss curves become gentler, thus the mass loss rate decreases as a function of gasification reaction time. The reaction time for 20% mass loss, the mass loss rate at the beginning of the gasification experiment, and the evolution of the mass loss rate of L1200 biocarbon and nut coke are presented in Table 17. The data was collected from the curves in Fig. 26. These were the median curves of five repetitions in terms of the gasification reaction rate. Based on this data, the inhibitive effect of CO on the gasification reaction, and the increasing effect of concentration elevation of CO<sub>2</sub> on the reaction rate, is similar to biocarbon and nut coke. Earlier, the power of the inhibitive effect of CO on the gasification rate has been related to the surface area of carbonaceous material (Farid et al., 2017). In the experiments of this thesis, the SSA of L1200 and nut coke were similar, thus the inhibitive effect of CO could be expected to be similar for the samples. However, at the beginning of the experiment, the L1200 mass loss rate was approximately 2.6 times higher than that of nut coke. This indicates that fewer carbon active sites are available on the surface of nut coke than on the surface of L1200. This is suggested to occur from higher ash content of nut coke. Furthermore, the evolution of the gasification reaction rate of L1200 is the opposite to that of nut coke when CO is removed and the concentration of CO<sub>2</sub> is elevated in the reactive gas atmosphere. This makes sense when the controlling mechanism of the biocarbon gasification rate is thought to be phase boundary

reaction, while the gasification rate of nut coke is under a combined control of interfacial reaction and gas diffusion to the mineral matrix of nut coke.

**Table 17. Some of the main parameters of gasification reaction of biocarbon and nut coke.**

Sample	Experimental programme	Time for 20 % gasification [min]	Mass loss rate [%/min]	Evolution of the mass loss rate [%/min]
L1200	Programme 1	79.75	-0.18000	-0.00127
	Programme 2	39.50	-0.40000	-0.00609
	Programme 3	21.00	-0.70000	-0.02551
Nut coke	Programme 1	390.65	-0.07000	0.00009
	Programme 2	181.00	-0.13000	0.00017
	Programme 3	84.25	-0.27000	0.00083

#### **6.4.4 Gasification to higher levels of mass loss**

The mass loss curves of L1200 biocarbon and nut coke gasification to different levels of mass loss are presented in Fig. 27. The mass loss rate and the evolution of the mass loss rate do not considerably change between the gasification experiments to different mass loss levels. Based on the curves in Fig. 27, the minor differences of the curve parameters occur due to the heterogeneity of the samples rather than a change in the sample behaviour during gasification. However, the controlling mechanism of gasification varies between the L1200 biocarbon and nut coke. This can be observed from the opposite development of the slope of mass loss curves of different samples; the curves of the L1200 mass loss rate have a negative slope while the curves of nut coke have a positive slope.

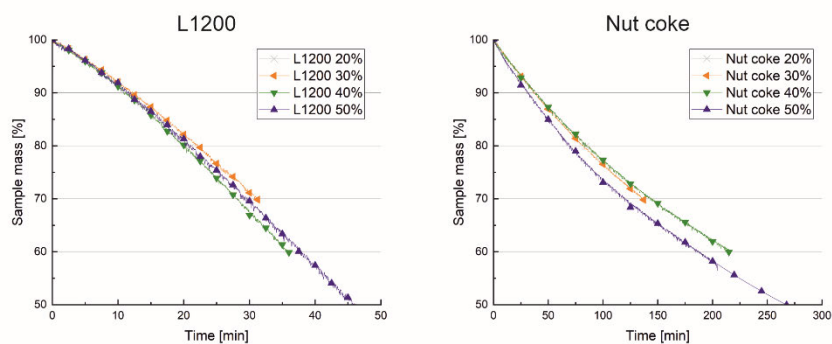


**Fig. 27. Gasification to different levels of mass loss (Reprinted under CC BY 4.0 license from Publication IV @2022 Authors).**

Because the slope between the gasification experiments to different levels did not change, it is suggested that the reaction rate controlling mechanism drifts from one mechanism to another. The contracting cylinder and random pore model were previously reported to fit well with biocarbon gasification. According to these findings and the results of this thesis, the gasification reaction rate of L1200 biocarbon is controlled by a phase boundary reaction that occurs on the surface of the samples and on the edges of the pores (Ahmed & Gupta, 2011; He et al., 2019; Hu et al., 2019; Luiz et al., 2018; Ortega, 1996; Struis et al., 2001). The mechanistic pathway of the surface reaction is as follows: the chemical adsorption of the gas to the solid char surface in the first stage, the surface reaction of  $\text{CO}_2$  with the char active sites in the second stage, and finally, the desorption of gasification reaction products from the char surface (Ahmed & Gupta, 2011). It has previously been concluded that chemical adsorption does not control the surface reaction in char gasification because the increase in partial pressure of  $\text{CO}_2$  had a negligible effect on char gasification (Ahmed & Gupta, 2011). However, in the experiments in this thesis, the increase in  $\text{CO}_2$  concentration had a significant effect on the reaction rate of the gasification of L1200 and nut coke, thus indicating that chemical adsorption was the controlling step at the beginning of gasification.

For coke, three steps have been reported to control the gasification reaction with  $\text{CO}_2$  at low temperatures ( $\leq 1000$  °C); the interfacial reaction in the first step, interfacial reaction and gas diffusion in the second step, and gas diffusion in the final step (Guo et al., 2015). The different gasification mechanisms between L1200 biocarbon and nut coke is also supported by the gasification data in Fig. 27, the macroscopic appearance of the samples after gasification and micrographs that are

presented in Fig. 28. Because of gasification, the smooth surface of L1200 becomes rougher, containing cracks and short cavities. At lower levels of gasification, at 20 and 30% mass loss, the crack formation occurs mostly on the edges of the sample while at higher levels of gasification (40 and 50% mass loss) and the cracks are also formed at the centre of the cross-section of the sample surface. The development of the nut coke surface during gasification reveals that the carbon matrix becomes gasified gradually from the surface of the sample as the level of gasification proceeds. However, nut coke includes a considerable amount of trace elements that form another matrix alongside the carbon matrix. This mineral matrix is revealed once the carbon gasification proceeds. The mineral matrix is a key factor contributing to the controlling mechanism at the second and third steps of nut coke gasification, as it upholds the porous network into which the reactive gas must diffuse in order to react with the remaining carbon.

Level of mass loss

L1200

Nut coke

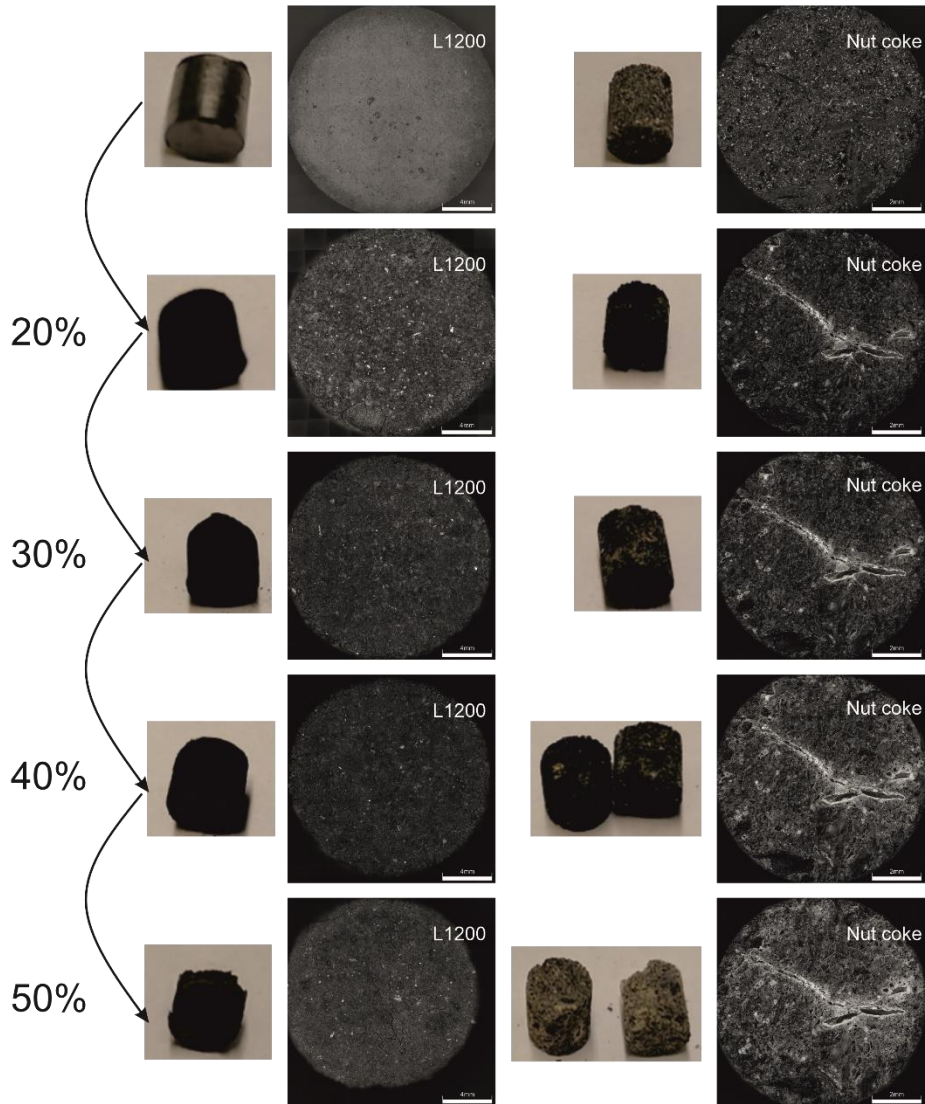
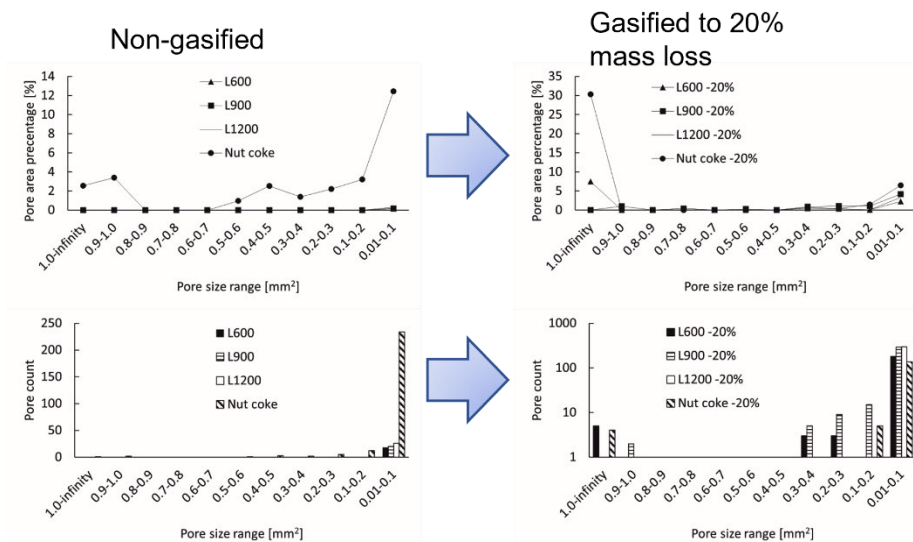


Fig. 28. Development of L1200 and nut coke structure during gasification (Modified under CC BY 4.0 license from Publication IV @2022 Authors).

## 6.5 Structural changes during gasification

The level of mass loss combined with the observations made from micrographs indicate observable changes in the structure of biocarbon samples and nut coke during gasification. In this chapter, the area percentage, pore count and pore size distribution of non-gasified and gasified samples are reported and discussed. The pore area percentage and pore count of different sized pores of biocarbon samples before and after gasification to a mass loss level of 20% are presented in Fig. 29. The pore area percentages and pore count of non-gasified biocarbons are presented on the left, while these parameters of gasified samples are presented on the right.

The total pore area percentage of L600, L900 and L1200 before gasification were 0.155, 0.171 and 0.314%, respectively. After gasification to a mass loss level of 20% the pore area percentages were 11.016, 8.887 and 3.352%, respectively. The formed cracks (Fig. 25) accounted for most of the area that was identified as pores. At this level of gasification, the large cracks accounted for most of the pore area percentage of L600, while most of the pore area percentage of L900 and L1200 is covered by small pores. The surface of nut coke also changed considerably during gasification, despite the lack of crack formation. The non-gasified nut coke sample had only one pore in the largest size range (from 1 mm to infinity) and after gasification the number of pores in that size range was four. Moreover, the pores of the largest size range of the gasified sample corresponded to 30.284% of the total surface area while the pore area percentage of the pores of corresponding size range only accounted for 2.556%. This is related to the mechanism of progression of the gasification of nut coke, as the first step of nut coke gasification is the reaction on nut coke surface and on the edges of the pores. Moreover, the fusion of the neighbouring pores increases the number of pores in the larger size ranges while the pore count of the smallest size range (from 0.01 mm<sup>2</sup> to 0.1 mm<sup>2</sup>) decreases.



**Fig. 29. The changes in porosity of biocarbons and nut coke in gasification (Modified under CC BY 4.0 license from Publication IV @2022 Authors).**

The development of structural characteristics (pore area percentage and pore count) as a function of the level of gasification is presented in Fig. 30. The pore area percentage of nut coke increased steadily until the mass loss level of 40%, after which the slope became gentler to a mass loss level of 50%. At the same time the pore count dropped from the non-gasified sample to a gasification level of 20%. From a 20% mass loss the drop stabilised until a level of 40% mass, after which there was a slight drop in the pore count at a level of 50% mass loss. The simultaneous drops in the pore count and the increased pore area percentage indicate merging of the pores on the nut coke surface during gasification. The development of the porosity (pore count and pore area percentage) of L1200 is the opposite of that of nut coke. The pore area percentage increased moderately until the mass loss level of 40%, after which the increase became steeper to the mass loss level of 50%. The pore count of L1200, on the other hand, considerably increased from the non-gasified sample to a gasification level of 20%. The increasing development of pore count continued to the gasification level of 40% and from there, it decreased as the gasification level was elevated to 50%. This development follows the pattern of pore formation, merging of the pores, and ultimately, overlapping of the pores, which is the pattern that is modelled by the random pore model (Iwaszenko et al., 2019).

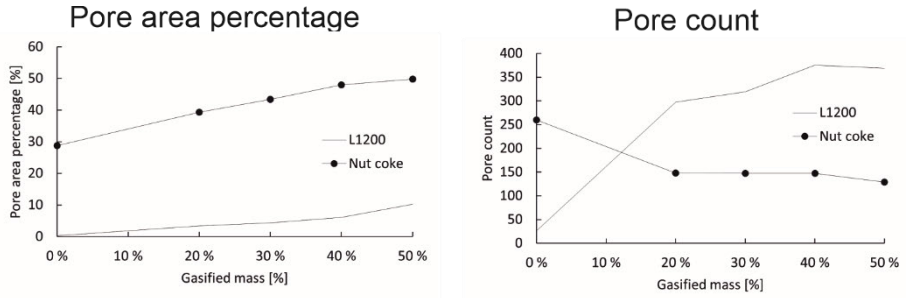


**Fig. 30. Development of the porosity of L1200 and nut coke (Modified under CC BY 4.0 license from Publication IV @2022 Authors).**

## 6.6 Compressive strength of biocarbons and nut coke

The gasification of carbonaceous material creates cavities, pores, enlargement of pores and the formation of cracks in the structure of the material. These structural changes show as empty spaces in the carbon matrix, thus creating weak points under mechanical stress. In this chapter the compressive strength test results of L600, L900, L1200 biocarbons and nut coke is reported and discussed.

The compressive strength test results of biocarbon and nut coke samples are presented in Fig. 31. The box chart presentation was chosen for illustration of the results because average or mean values, for example, do not illustrate the deviation of the results and thus the heterogeneity of the samples. The results of the non-gasified biocarbon samples directly show the significance of the pyrolysis temperature on the mechanical strength of biocarbon. L600 had slightly lower compressive strength (in average) than nut coke and considerably lower strength in comparison to L900 and L1200. The sample batch of nut coke was the most heterogeneous in terms of mechanical strength, which shows as a large cap between the extreme values and large range of the upper and lower quadrants of the results. With regard to the gasified samples, the decrease in compressive strength of nut coke and L1200 is at the same level, with the drop of average strength being 7.88 MPa for nut coke and 9.52 MPa for L1200. Meanwhile, the average strength of L900 decreased by 21.27 MPa approximately to the level of nut coke and L600 biocarbon. This could have been expected as the crack formation on the structure of L900 was approximately at the same level as that of L600, which was expected to have an impact on the structure of L900. This kind of impact on the structural changes was not found in the strength test results of L600. This is expected to be

due to the open structure of the non-gasified L600 sample, thus the sample structure does not considerably weaken after the 20% mass loss.

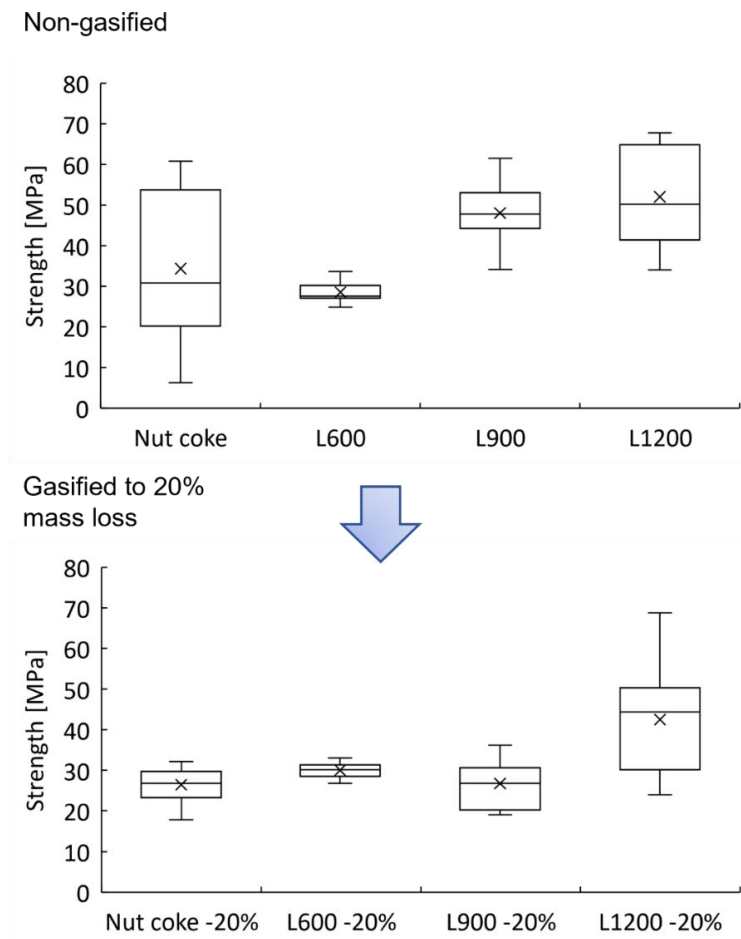


**Fig. 31. Compressive strength of non-gasified and gasified biocarbon samples and nut coke (Modified under CC BY 4.0 license from Publication IV @2022 Authors).**

The behaviour of the biocarbon and nut coke samples during the compression strength test is illustrated in stress-strain curve in Fig. 32.

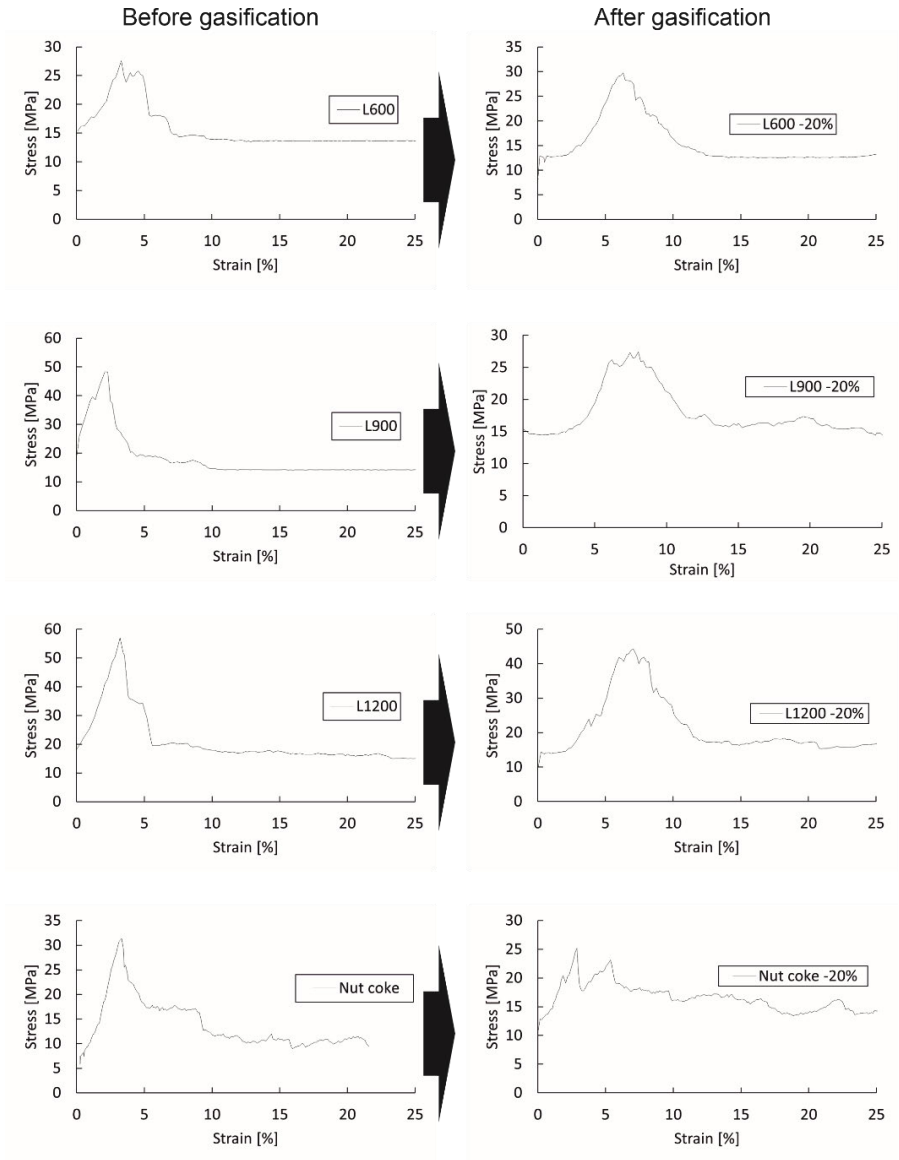


**Fig. 32. The behaviour of biocarbon and nut coke during compression (Reprinted under CC BY 4.0 license from Publication IV @2022 Authors).**

The peak stress of L600 before fracture occurs within a relatively large range, thus indicating a collapse of the structure before fracturing. This sort of behaviour is possible when there is empty space within the sample structure. The behaviour of

L600 under compression did not change considerably after gasification, which is an indication that the 20% mass loss during gasification did not considerably change the nature of porous structure of L600. The other samples, on the other hand, had a clear peak of stress before the point of fracture, indicating that their structure did not have such elasticity as L600 did. After gasification, the behaviour of L900, L1200 and nut coke changed considerably. The sharp peaks of L900 and L1200 at the point of fracture evolved to a blunt-shaped peak with a larger peak area after gasification. This shape is similar to that of L600, thus indicating that the empty space inside the structure of L900 and L1200 increased. These structural changes also affected the compressive strength of L900 and L1200 (Fig. 31 and Fig. 32). Nut coke had a different structure in comparison to biocarbon samples, thus the effect of gasification on the behaviour under compression of nut coke was different. Before gasification, nut coke had a curve evolution similar to L900 and L1200 during compression. However, after gasification, the compression strength of nut coke decreased considerably and the stress-strain curve consisted of multiple peaks, indicating multiple points of fracture. This is suggested to be a consequence of enlarged pores and increased fusion of the pores during gasification.

Gasifications to higher levels of mass loss of L1200 and nut coke revealed further changes in the compression behaviour of these samples. This is presented in Fig. 33. However, the changes between the samples were different. In the case of L1200, the peak of the fracture point became blunter, and the peak was shifted to further strain the percentage as the level of mass loss in gasification was increased. This is an indication of the surface-level porosity development during gasification, thus the formation of empty space within the structure of L1200 near the surface. This is in line with the hypothesis of gasification occurring mainly on the surface of the biocarbon and on the edges of the pores. The peak of the nut coke stress-strain curve, on the other hand, does not considerably shift to a higher percentage of strain, but became flattened as the samples were gasified to higher mass loss levels. Also, the development of multiple fracture point peaks can be observed from the curves of gasified nut coke samples. These results indicate a gasification phenomenon inside the porous structure of nut coke, which is in line with the suggested gasification mechanism of nut coke in section 6.4.4 “Gasification to higher levels of mass loss”.

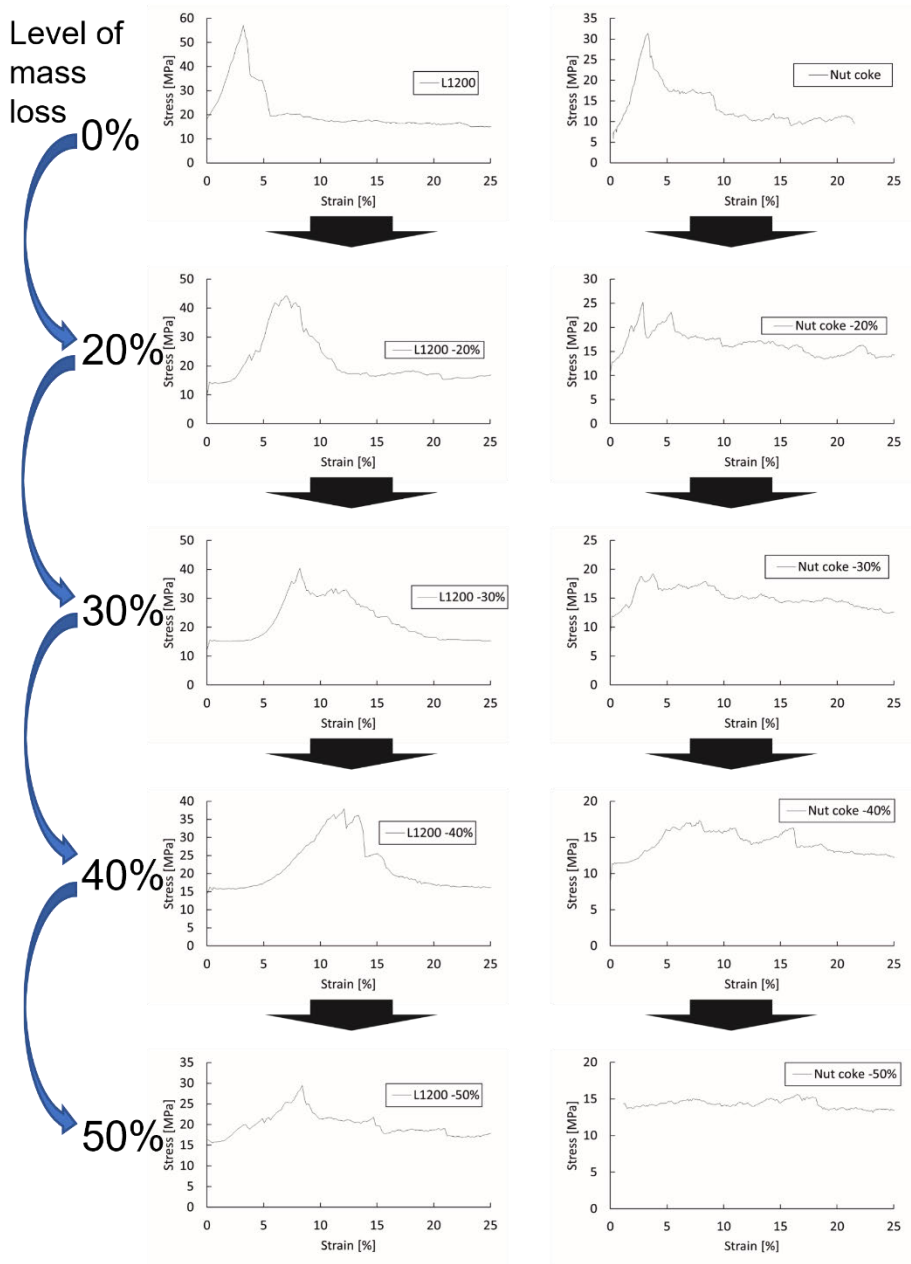


**Fig. 33. Development of the behaviour of L1200 and nut coke during the compression (Modified under CC BY 4.0 license from Publication IV @2022 Authors).**

## **6.7 Relationship between the level of gasification, structural changes and compressive strength**

The structure and mechanical strength of the samples were found to change as the level of gasification was elevated. In this section, the relationship between these properties are presented and discussed. Samples L600 and L900 were only gasified to a mass loss level of 20%, thus producing only two data points at mass loss level 0 and 20%. On the other hand, L1200 and nut coke were gasified to mass loss levels of 20, 30, 40 and 50%, thus the evolution of structural and mechanical strength properties can be followed from five different data points. Because of this, the relationships between gasification level, structural properties and compression strength were evaluated based on the results of L1200 and nut coke.

The relationships between the level of gasification and pore area percentage, the level of gasification and compression strength, and pore area percentage and compression strength are presented in Fig. 34. All the  $R^2$  values between the different properties were above 0.90, thus indicating a strong linear correlation between these properties. The relationship between the level of gasification and the pore area percentage was direct, i.e. the pore area percentage linearly increased as a function of gasification level. Meanwhile, the compression strength decreased as a function of gasification level or pore area percentage, thus indicating an inverse correlation between the compression strength and gasification level or pore area percentage.

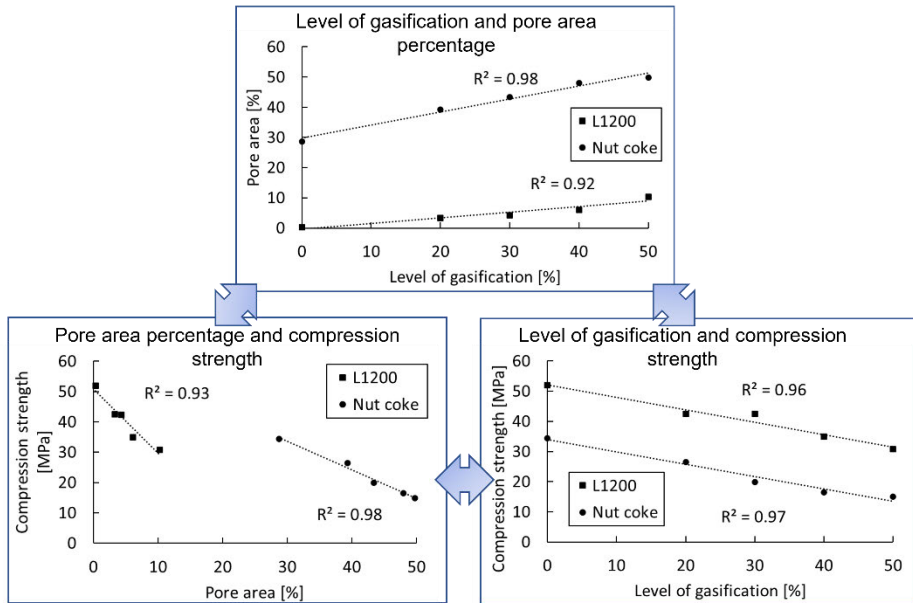


**Fig. 34. Relationships between the level of gasification, pore area percentage and compression strength (Modified under CC BY 4.0 license from Publication IV @2022 Authors).**

The level of gasification also correlated with the pore count development. However, this relationship did not follow a linear trend, but a polynomial of second order as presented in Fig. 35. In the case of L1200, the pore count increased until the level of 40% mass loss. This was the point where the pore count reached the highest number and started to decrease to the level of 50% mass loss. This is in line with the mechanistic pathway of the random pore model (Iwaszenko et al., 2019). The pore count of nut coke had the opposite development as the number of pores decreased to the level of 20% mass loss, after which the pore count remained relatively stable until the level of 50% mass loss. The result indicates that the gasification reaction occurs mainly at the surface of the nut coke at the beginning of gasification, thus leading to the enlargement and fusion of the pores. This is followed by adsorption of the reactive gas into the coke matrix. Meanwhile, the mineral matrix is left on the surface of the nut coke. This follows the mechanistic pathway of the gasification reaction of coke that was reported earlier by (Guo et al., 2015).

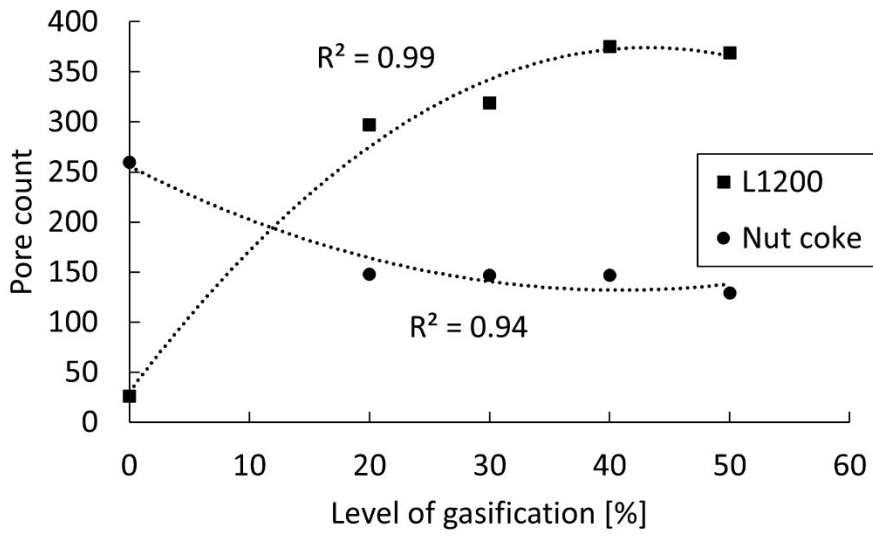


Fig. 35. Relationship between pore count and the level of gasification (Reprinted under CC BY 4.0 license from Publication IV @2022 Authors).



## 7 Evaluation of the results

Because of the different approaches of the two different branches of research in this thesis, the results of these different branches are evaluated and discussed separately.

In the first branch, the objective was to produce biocoke, i.e. metallurgical coke, in which part of the fossil-based coking coal is substituted with bio-based material. The chosen bio-based raw materials for the substitution part of fossil-based coal in coke making were hydrolysis lignin and hydrolysis lignin-based biocarbon. Hydrolysis lignin was chosen based on the following facts:

1. It is a side-stream material that is currently used mainly for combined heat and power generation (CHP).
2. It has a high carbon content and relatively low oxygen and hydrogen content compared to most biomasses.
3. It has a complex cross-linked aromatic structure that acts as a skeleton of char formation during thermal treatment.
4. It offers high yield and a wide range of thermal degradation due to the wide range of binding energies of different types of bonds within the molecular structure.
5. The adhesive nature of lignin, which leads to less mobility of the particles, means the particles stick together before pyrolysis.
6. It has low ash content, thus leading to high fixed carbon content when hydrolysis lignin is carbonised.

The results of hydrolysis lignin or hydrolysis lignin-based biocarbon utilisation as part of the coking blend in biocoke-making were not promising. The results from the interaction between coking coal and hydrolysis lignin and hydrolysis lignin-based biocarbons indicated that lower pyrolysis temperatures would be better for interaction between the materials. However, the volatiles from hydrolysis lignin were oxygen-rich, thus leading to inhibited fluidity development of coking coal and increased porosity and disoriented structure of produced cokes. Overall, the addition of hydrolysis lignin and hydrolysis lignin-based biocarbons into the coking blend led to a weakened structure, increased reactivity, and thus lower quality coke. According to the results, the methods used in this study were not suitable for development or modification of coal-lignin mixtures in such a way that the resulting coke would be sufficiently good. However, more research should be done related to the subject. For example, it would be beneficial to discover more about:

1. Optimisation of the pyrolysis temperature for optimising the oxygen content in biocarbon combined with the optimisation of the interaction between the materials.
2. Agglomeration (e.g. briquetting) of the whole coking blend to improve the proximity of the particles in the blend.
3. Substituting one or more raw material fractions in a coking blend so that the properties of the bulk blend would be compensated by the properties of other fractions.
4. Optimisation of the particle size of the biocarbon prior to co-carbonisation of the coking blend.

In the second branch of research in the utilisation of hydrolysis lignin-based biocarbon as a substitute of fossil-based carbon, the focus was on modifying the properties of biocarbon to a level that is comparable with nut coke. The main properties under investigation were the density, reactivity and mechanical strength. In order to achieve this objective, selected pre-treatment methods were performed on hydrolysis lignin. The pre-treatments in the order of their respective implementation are listed below:

1. Drying for removal of excess moisture from hydrolysis lignin biomass.
2. Grinding for homogenisation of the particle size.
3. Briquetting of hydrolysis lignin for reduction of the surface area, increasing material density and increasing the mechanical strength.
4. High pyrolysis temperatures for increasing thermal stability and density of biocarbon and decreasing the gasification reactivity.

The results of how the hydrolysis lignin-based biocarbon was modified with relatively simple pre-treatment methods were promising. The compression strength of L1200 and L900 was superior to that of metallurgical nut coke, while the compression strength of L600 was at the same level as nut coke. Also, the compression strength of biocarbons after pre-gasification were at the same level or higher than that of nut coke. The major issue when comparing the properties of fossil-based nut coke and biocarbon was the gasification reactivity. The biocarbons were considerably more reactive, which is the limiting factor of why biocarbons may not fully substitute the use of metallurgical coke in applications such as BF or SAF. In many other roles, for example as a foaming agent in EAF, as a substitute of fossil coal in pulverised coal injection in BF, and as a reductant in the reductive treatment of different residues or slags, the biocarbon could serve its purpose due

to the lower requirement of the reductant properties. The suitability of biocarbons for each application should be tested with application-centric test methods, for example with foaming tests if the objective is to utilise biocarbon as a foaming agent in EAF. When it comes to the higher gasification reactivity of biocarbons in this thesis, the difference in the mechanistic behaviour of gasification reaction between bio-based and fossil-based carbon products was addressed. Therefore, future investigation into biocarbon utilisation as a substitute of fossil-based carbon should focus on the use of inorganic binders in the agglomeration of biomass or biocarbon. The reasoning behind this is that the trace element chemistry of biocarbon would be modified, thus the relative amount of potassium (K), sodium (Na) and calcium (Ca) in the biocarbon ash would be reduced. In addition, the binder would help in the formation of mineral matrix throughout the biocarbon structure, thus changing the mechanistic pathway of biocarbon gasification to resemble that of fossil-based coke.



## 8 Conclusions and future research

The applicability of hydrolysis lignin and hydrolysis lignin-based biocarbon for substitution of fossil-based carbon in pyrometallurgical processes was studied within the research work of this thesis. Usually, carbon is utilised as a reducing agent in pyrometallurgical processes because of its capability to reduce oxides into a desired, usually metallic form. However, besides the use as a reductant, carbon can be used for example as a slag foaming agent or as an alloying element. Overall, carbonaceous materials in pyrometallurgical processes have many different roles: as a chemical reagent, the source of reducing CO gas and as a carburiser of hot metal, as a structural support material for material burden, and as a fuel to bring thermal energy for endothermic reactions. The role of being structural support material is specifically related to the BF process, while the rest of the roles apply to multiple processes. However, a certain level of mechanical strength is required even if the carbon does not act as a structural material, for example in transportation and storage. This, of course, applies in cases where the carbon is fed into the system in a shape and size of larger agglomerates and not in a pulverised form.

### 8.1 Conclusions

The applicability of hydrolysis lignin and hydrolysis lignin-based biocarbons as a substitute of fossil-based carbon was studied within two branches in this thesis: the utilisation of hydrolysis lignin and hydrolysis lignin-based biocarbon for substitution of part of the coking coal in a coking blend in production of metallurgical coke, and as an individual biocarbon for the substitution of metallurgical coke. The applicability of biocarbon and biocoke was evaluated based on the results of different tests of the properties of these materials. Gasification reactivity and compression strength were the main properties that were tested.

In terms of the formation of metallurgical coke, the formation and properties of coke depend highly on the properties of the individual fraction of the coking blend as well as the properties of the whole blend. In practice, the lack of quality of one fraction of the blend is compensated with the properties of other fractions in the blend. The major reason for the use of fractions with low quality in a coking blend is the availability and price of high-quality coking coal. The reason for substitution of part of the coking coal with bio-based material in this thesis was the mitigation of the use of fossil-based material in a coking blend, thus the mitigation of fossil-based CO<sub>2</sub> formation. However, in this thesis the properties of the blend

were not optimised, but an individual high-quality coking coal was partially replaced by bio-based materials. These bio-based materials were hydrolysis lignin and hydrolysis lignin-based biocarbon. The results indicated that the reactivity of the biocokes was higher and on the other hand the compression strength was lower than that of metallurgical coke consisting of 100% coking coal. The reactivity tests and compression strength tests were performed on biocokes in which the hydrolysis lignin-based materials were in powdered form. In these tests, the pyrolysis temperature of hydrolysis lignin biocarbon was 350 °C, which was lower than the release temperature (360 °C) of the hydrolysis lignin-originating gaseous components that have previously been reported to be major modifiers of fluidity development in coal. In the interaction studies of coal and hydrolysis lignin-based materials, the pyrolysis temperatures of the biocarbons were higher (450, 600 and 1200 °C), thus the effect of these fluidity modifiers was eliminated. Also, the non-pyrolysed hydrolysis lignin and hydrolysis lignin biocarbons were briquetted, which decreases the relative surface area, and therefore also decreases the adsorption of the fluid components from coking coal. At the same time the density of the biomaterials was increased, thus decreasing the formation of density gradients in the biocoke. These interaction studies revealed that interaction between the coking coal and hydrolysis lignin-based materials occurs mainly in the gas-gas phase. This indication was based on the observation of L1200 (hydrolysis lignin briquette pyrolysed in 1200 °C) not having a joint interface with surrounding coke, whereas other samples with milder pyrolysis temperatures had been partially fused as part of the coke matrix. Moreover, a separation between the coke matrix and L600 (hydrolysis lignin briquette pyrolysed in 600 °C) and L1200 could be detected, thus indicating a dilation of the briquette in the co-carbonisation stage followed by shrinking in the cooling stage. This was confirmed with optical dilatometry results, as clear dilation of L600 and L1200 could be detected and after the cooling, the sample volume was decreased.

In the pyrolysis of hydrolysis lignin, lignin undergoes different stages. The classification of the stages can be done in several ways, based on the TGA data, chemical reactions or structural changes. In this thesis the stages are classified as: 1) bond breaking and recombination, 2) aromatisation and 3) graphitisation. The graphitisation stage of hydrolysis covers the widest temperature range, from approximately 900 °C to over 2400 °C. The notable thing is that the biocarbon in this thesis is not graphite, although graphitic substructures have been found in lignin-based biocarbon that was pyrolysed at 1200 °C in earlier studies. These different pyrolysis stages have been used as a basis for determining the pyrolysis

temperatures of the biocarbon samples (450, 600, 900 and 1200 °C) in this thesis. The objective of this branch of research was to produce biocarbon with properties that are comparable with those of nut coke. These main properties include the density, reactivity, mechanical strength and strength after reaction. The reactivity of the samples was evaluated based on the isothermal and non-isothermal gasification reactivity tests, and the mechanical strength was evaluated based on the results of compression strength tests. Industrially produced nut coke was used as a reference material in the experiments. Also, the effect of pyrolysis conditions (heating rate and final temperature) on the yield of the sample was briefly studied.

The results clearly showed that the increase in either heating rate or final pyrolysis temperature decreased the yield of solid carbon. The solid yield in pyrolysis of hydrolysis lignin at 450, 600, 900 and 1200 °C were 44.4, 39.4, 37.7, 35.9%, respectively. It is noteworthy that the sample was not ground or agglomerated in the pyrolysis at 450 °C while the other samples were in briquetted form. Nevertheless, the most significant drop in yield can be found when the pyrolysis temperature is elevated from 450 °C to 600 °C because of the thermal degradation of hydrolysis lignin. The effect of heating rate on the yield was more moderate but still observable. The solid yield decreased for approximately one per cent when the heating rate was increased for 5 °C/min. The difference between the yields developed at relatively low temperatures, below 400 °C, after which the difference between the curves remained unchanged. The volatile matter that was released during pyrolysis mainly consisted of non-condensable gases CH<sub>4</sub>, CO<sub>2</sub>, CO, C<sub>2</sub>H<sub>4</sub> and H<sub>2</sub>. Also, H<sub>2</sub>O, methanol (CH<sub>4</sub>O) and transient species of hydrolysis lignin thermal degradation were found from the strongest signals of mass spectrometry results. Many other signals were also found from the data, but their intensities were considerably lower.

The non-isothermal reactivity experiments revealed that the gasification reactivity of the biocarbon was inhibited by agglomeration and high pyrolysis temperature (L1200, pyrolysed at 1200 °C). This was further confirmed by isothermal reactivity tests. The inhibited reactivity was based on the denser structure, thus a decreased surface area of L1200 in comparison to biocarbons of lower pyrolysis temperature. This is further related to the reaction path of biocarbon gasification. According to the literature, biocarbon gasification follows either the contracting cylinder or the random pore model, in which the controlling mechanism of gasification reaction is the phase boundary reaction. On the other hand, the reactivity of nut coke was considerably lower, even though the surface area was higher than that of L1200 biocarbon. The lower reactivity of nut coke can be

partially explained by the different trace element composition of nut coke ash, higher amount of ash, which further influence on the gasification mechanism of nut coke. In CO<sub>2</sub> gasification at 1000 °C, the coke gasification is reported to follow the pathway in which chemical reaction is the controlling mechanism in the first stage. This is followed by a combination of diffusion and chemical reaction as a controlling mechanism in the second stage and diffusion in the third stage.

The structure and mechanical strength of the samples was changed due to gasification. In the case of nut coke the pore area percentage increased while the pore count decreased as the level of gasification was increased. Gasification occurred first on the surface of the sample and at the edges of the pores, thus enlarging the pore size. Ultimately the neighbouring pores overlapped, i.e. they fused together to form a single pore. Once the carbon was gasified from the surface layers, the mineral matrix of nut coke was revealed. L1200 biocarbon, on the other hand, did not behave like this, mainly because of the lower ash content and different ash composition. The gasification pattern of L1200 seemingly followed the contracting cylinder type of gasification, in which the gasification mainly occurs on the surface layers of the sample. This was shown in microscope images. Also, the porosity development of L1200 consisted of the formation of short cavity holes on the surface of the sample, while the formation of deeper pores was not detected. The structural changes were found to affect the mechanical strength of the samples while the gasification level was found to affect the structural changes. For example, the pore area percentage of nut coke and L1200 was found to correlate with the level of gasification with R<sup>2</sup> values of 0.98 and 0.92, respectively. Meanwhile the compression strength of nut coke and L1200 correlated with pore area percentage with R<sup>2</sup> values of 0.98 and 0.93, respectively. The pore count of nut coke and L1200 also correlated with the level of gasification with R<sup>2</sup> values of 0.94 and 0.99, respectively. Similar correlations were not found between other structural parameters or pore shape factors and levels of gasification. According to the results, the pore area percentage is the dominant factor in the determination of the compression strength of the gasified samples.

These results are promising from the perspective of replacing fossil-based carbon with hydrolysis lignin-based biocarbon in pyrometallurgical processes. Looking at the mechanical strength of biocarbons, the level of compression strength is at least at the same level as that of metallurgical nut coke, thus the excessive cracking and breaking of the biocarbon in storage or transport is unlikely. The compression strength after reaction to a certain level of mass loss of L1200 was higher than that of nut coke. However, the considerably higher gasification

reactivity of L1200 would cause problems in the BF process, for example, where coke has an important role as a structural bed material for supporting the material burden in the upper layers and facilitating uniform distribution of gas and heat in the process.

## **8.2 Future research**

Overall, the results in this thesis indicate that the biocarbon research area is more promising than the area of biocoke research. Therefore, the focus should be concentrated on the development of biocarbon as a reducing agent product and not as a raw material in a coking blend. The major issues in the utilisation of hydrolysis lignin-based biocarbon in pyrometallurgical processes are related to higher gasification reactivity and poor availability of hydrolysis lignin.

The results indicated that the controlling mechanism pathway in biocarbon gasification is different from nut coke gasification. The results also indicated that the difference in the mechanistic pathway is related to the difference in ash composition and content. This indication is a motivation to use inorganic and composite binders in the agglomeration of biocarbon. By doing so, the ash chemistry of biocarbon agglomerate could be changed alongside the creation of the mineral matrix and the carbon matrix. The discovery of an applicable binder or binder mix would also enable the agglomeration of biocarbon from other biomass sources, i.e. from the biomass that does not possess similar adhesive forces to hydrolysis lignin.



## References

- Ahmed, I. I., & Gupta, A. K. (2011). Kinetics of woodchips char gasification with steam and carbon dioxide. *Applied Energy*, 88(5), 1613–1619. <https://doi.org/10.1016/j.apenergy.2010.11.007>
- Andriopoulos, N., Loo, C. E., Dukino, R., & McGuire, S. J. (2003). Micro-properties of Australian Coking Coals. *ISIJ International*, 43(10), 1528–1537. <https://doi.org/10.2355/isijinternational.43.1528>
- Babich, A., Senk, D., & Gudenau, H. W. (2009). Effect of coke reactivity and nut coke on blast furnace operation. *Ironmaking and Steelmaking*, 36(3), 222–229. <https://doi.org/10.1179/174328108x378242>
- Balakshin, M., Capanema, E. A., Zhu, X., Sulaeva, I., Potthast, A., Rosenau, T., & Rojas, O. J. (2020). Spruce milled wood lignin: linear, branched or cross-linked? *Green Chemistry*, 22(13), 3985–4001. <https://doi.org/10.1039/d0gc00926a>
- Basu, P. (2010). *Biomass gasification and pyrolysis : practical design and theory*. Academic Press.
- Bergna, D., Varila, T., Romar, H., & Lassi, U. (2022). Activated carbon from hydrolysis lignin: Effect of activation method on carbon properties. *Biomass and Bioenergy*, 159, 106387. <https://doi.org/10.1016/j.biombioe.2022.106387>
- Berlin, A., & Balakshin, M. (2014). Industrial Lignins: Analysis, Properties, and Applications. In V. K. Gupta, M. G. Tuohy, C. P. Kubicek, J. Saddler, & F. Xu (Eds.), *Bioenergy Research: Advances and Applications* (pp. 315–336). Elsevier. <https://doi.org/10.1016/b978-0-444-59561-4.00018-8>
- Boerjan, W., Ralph, J., & Baucher, M. (2003). Lignin Biosynthesis. *Annual Review of Plant Biology*, 54, 519–546. <https://doi.org/10.1146/annurev.arplant.54.031902.134938>
- Cao, J., Xiao, G., Xu, X., Shen, D., & Jin, B. (2013a). Study on carbonization of lignin by TG-FTIR and high-temperature carbonization reactor. *Fuel Processing Technology*, 106, 41–47. <https://doi.org/10.1016/j.fuproc.2012.06.016>
- Cao, J., Xiao, G., Xu, X., Shen, D., & Jin, B. (2013b). Study on carbonization of lignin by TG-FTIR and high-temperature carbonization reactor. *Fuel Processing Technology*, 106, 41–47. <https://doi.org/10.1016/j.fuproc.2012.06.016>
- Casal, M. D., Díaz-Faes, E., & Barriocanal, C. (2021). Permeability and Porosity Development during the Carbonization of Coals of Different Coking Pressures. *Energy and Fuels*, 35(7), 5808–5817. <https://doi.org/https://doi.org/10.1021/acs.energyfuels.0c04219>
- Cassel, B., & Menard, K. (2012). *Proximate Analysis of Coal and Coke using the STA 8000 Simultaneous Thermal Analyzer*.
- Chakar, F. S., & Ragauskas, A. J. (2004). Review of current and future softwood kraft lignin process chemistry. *Industrial Crops and Products*, 20(2), 131–141. <https://doi.org/10.1016/j.indcrop.2004.04.016>
- Chio, C., Sain, M., & Qin, W. (2019). Lignin utilization: A review of lignin depolymerization from various aspects. *Renewable and Sustainable Energy Reviews*, 107, 232–249. <https://doi.org/10.1016/j.rser.2019.03.008>

- Cho, J., Chu, S., Dauenhauer, P. J., & Huber, G. W. (2012). Kinetics and reaction chemistry for slow pyrolysis of enzymatic hydrolysis lignin and organosolv extracted lignin derived from maplewood. *Green Chemistry*, *14*(2), 428–439. <https://doi.org/10.1039/c1gc16222e>
- Collard, F. X., & Blin, J. (2014). A review on pyrolysis of biomass constituents: Mechanisms and composition of the products obtained from the conversion of cellulose, hemicelluloses and lignin. *Renewable and Sustainable Energy Reviews*, *38*, 594–608. <https://doi.org/10.1016/j.rser.2014.06.013>
- De Carvalho, D. M., & Colodette, J. L. (2017). Comparative Study of Acid Hydrolysis of Lignin and Polysaccharides in Biomasses. *Bioresources*, *12*(4), 6907–6923.
- Díaz, M. C., Zhao, H., Kokonya, S., Dufour, A., & Snape, C. E. (2012). The Effect of Biomass on Fluidity Development in Coking Blends Using High-Temperature SAOS Rheometry. *Energy and Fuels*, *26*(3), 1767–1775. <https://doi.org/10.1021/ef2018463>
- Díez, M. A., Alvarez, R., & Barriocanal, C. (2002). Coal for metallurgical coke production: predictions of coke quality and future requirements for cokemaking. *International Journal of Coal Geology*, *50*(1–4), 389–412. [https://doi.org/10.1016/s0166-5162\(02\)00123-4](https://doi.org/10.1016/s0166-5162(02)00123-4)
- Diez, M. A., Alvarez, R., & Fernández, M. (2012). Biomass derived products as modifiers of the rheological properties of coking coals. *Fuel*, *96*, 306–313. <https://doi.org/10.1016/j.fuel.2011.12.065>
- Díez, M. A., Barriocanal, C., & Álvarez, R. (2005). Plastic wastes as modifiers of the thermoplasticity of coal. *Energy and Fuels*, *19*(6), 2304–2316. <https://doi.org/10.1021/ef0501041>
- Diez, M. A., & Borrego, A. G. (2013). Evaluation of CO<sub>2</sub>-reactivity patterns in cokes from coal and woody biomass blends. *Fuel*, *113*, 59–68. <https://doi.org/10.1016/j.fuel.2013.05.056>
- Ding, L., Zhang, Y., Wang, Z., Huang, J., & Fang, Y. (2014). Interaction and its induced inhibiting or synergistic effects during co-gasification of coal char and biomass char. *Bioresource Technology*, *173*, 11–20. <https://doi.org/10.1016/j.biortech.2014.09.007>
- Dresselhaus, M. S., & Dresselhaus, G. (2002). Intercalation compounds of graphite. *Advances in Physics*, *51*(1), 1–186. <https://doi.org/10.1080/00018730110113644>
- Echterhof, T. (2021). Review on the Use of Alternative Carbon Sources in EAF Steelmaking. *Metals*, *11*(2), 222. <https://doi.org/10.3390/met11020222>
- Eom, I. Y., Kim, J. Y., Kim, T. S., Lee, S. M., Choi, D., Choi, I. G., & Choi, J. W. (2012). Effect of essential inorganic metals on primary thermal degradation of lignocellulosic biomass. *Bioresource Technology*, *104*, 687–694. <https://doi.org/10.1016/j.biortech.2011.10.035>
- Evans, R. J., & Milne, T. A. (1987). Molecular Characterization of the Pyrolysis of Biomass. *Energy and Fuels*, *1*(2), 123–137. <https://doi.org/10.1021/ef00002a001>
- Figuroa-Gerstenmaier, S., Siperstein, F. R., Celzard, A., & Fierro, V. (2014). Application of Density Functional Theory for Determining Pore-Size Distributions of Microporous Activated Carbons. *Adsorption Science & Technology*, *32*(1), 23–35. <https://doi.org/10.1260/0263-6174.32.1.23>

- Flores, B. D., Flores, I. V., Guerrero, A., Orellana, D. R., Pohlmann, J. G., Diez, M. A., Borrego, A. G., Osório, E., & Vilela, A. C. F. (2017). Effect of charcoal blending with a vitrinite rich coking coal on coke reactivity. *Fuel Processing Technology*, *155*, 97–105. <https://doi.org/10.1016/j.fuproc.2016.04.012>
- Flores, R. M. (2014). Coalification, Gasification, and Gas Storage. In R. M. Flores (Ed.), *Coal and Coalbed Gas* (pp. 167–233). Elsevier. <https://doi.org/10.1016/b978-0-12-396972-9.00004-5>
- Geerdes, M., Lingiardi, O., Ricketts, J., Chaigneau, R., & Kurunov, I. (2015). Coke. In *Modern Blast Furnace Ironmaking: An Introduction* (3rd ed., pp. 43–57). IOS Press.
- Gornostayev, S., Heikkinen, E. P., Heino, J., & Fabritius, T. (2018). Occurrence and Behavior of Sulfur-Bearing Minerals in Metallurgical Coke. *Steel Research International*, *89*(4), 1700470. <https://doi.org/10.1002/srin.201700470>
- Gornostayev, S. S., Heikkinen, E. P., Heino, J. J., Huttunen, S. M. M., & Fabritius, T. M. J. (2016). Behavior of Alkali-Bearing Minerals in Coking and Blast Furnace Processes. *Steel Research International*, *87*(9), 1144–1153. <https://doi.org/10.1002/srin.201500295>
- Guo, W., Xue, Q., Liu, Y., Guo, Z., She, X., Wang, J., Zhao, Q., & An, X. (2015). Kinetic analysis of gasification reaction of coke with CO<sub>2</sub> or H<sub>2</sub>O. *International Journal of Hydrogen Energy*, *40*(39), 13306–13313. <https://doi.org/10.1016/j.ijhydene.2015.07.048>
- Haapakangas, J. A., Uusitalo, J. A., Mattila, O. J., Gornostayev, S. S., Porter, D. A., & Fabritius, T. M. J. (2014). The Hot Strength of Industrial Cokes - Evaluation of Coke Properties that Affect Its High-Temperature Strength. *Steel Research International*, *85*(12), 1608–1619. <https://doi.org/10.1002/srin.201300450>
- Haapakangas, J., Suopajarvi, H., Iljana, M., Kempainen, A., Mattila, O., Heikkinen, E. P., Samuelsson, C., & Fabritius, T. (2016). Coke Reactivity in Simulated Blast Furnace Shaft Conditions. *Metallurgical and Materials Transactions B: Process Metallurgy and Materials Processing Science*, *47*(4), 2357–2370. <https://doi.org/10.1007/s11663-016-0677-y>
- Habibi, R., Kopyscinski, J., Masnadi, M. S., Lam, J., Grace, J. R., Mims, C. A., & Hill, J. M. (2013). Co-gasification of biomass and non-biomass feedstocks: Synergistic and inhibition effects of switchgrass mixed with sub-bituminous coal and fluid coke during CO<sub>2</sub> gasification. *Energy and Fuels*, *27*(1), 494–500. <https://doi.org/10.1021/ef301567h>
- Haensel, T., Comouth, A., Lorenz, P., Ahmed, S. I. U., Krischok, S., Zydzia, N., Kauffmann, A., & Schaefer, J. A. (2009). Pyrolysis of cellulose and lignin. *Applied Surface Science*, *255*(18), 8183–8189. <https://doi.org/10.1016/j.apsusc.2009.05.047>
- He, Q., Guo, Q., Ding, L., Wei, J., & Yu, G. (2019). CO<sub>2</sub> gasification of char from raw and torrefied biomass: Reactivity, kinetics and mechanism analysis. *Bioresource Technology*, *293*, 122087. <https://doi.org/10.1016/j.biortech.2019.122087>
- Heikkilä, A. M., Koskela, A. M., Iljana, M. O., Lin, R., Bartusch, H., Heikkinen, E. P., & Fabritius, T. M. J. (2021). Coke Gasification in Blast Furnace Shaft Conditions with H<sub>2</sub> and H<sub>2</sub>O Containing Atmospheres. *Steel Research International*, *92*(3), 2000456. <https://doi.org/10.1002/srin.202000456>

- Hu, J., Xiao, R., Shen, D., & Zhang, H. (2013). Structural analysis of lignin residue from black liquor and its thermal performance in thermogravimetric-Fourier transform infrared spectroscopy. *Bioresource Technology*, *128*, 633–639. <https://doi.org/10.1016/j.biortech.2012.10.148>
- Hu, Q., Yang, H., Wu, Z., Lim, C. J., Bi, X. T., & Chen, H. (2019). Experimental and modeling study of potassium catalyzed gasification of woody char pellet with CO<sub>2</sub>. *Energy*, *171*, 678–688. <https://doi.org/10.1016/j.energy.2019.01.050>
- Huang, J., Fu, S., & Gan, L. (Eds.). (2019). Lignin Chemicals and Their Applications. In *Lignin Chemistry and Applications* (pp. 79–134). Elsevier. <https://doi.org/10.1016/b978-0-12-813941-7.00004-7>
- Huang, Y., Wei, Z., Qiu, Z., Yin, X., & Wu, C. (2012). Study on structure and pyrolysis behavior of lignin derived from corncob acid hydrolysis residue. *Journal of Analytical and Applied Pyrolysis*, *93*, 153–159. <https://doi.org/10.1016/j.jaap.2011.10.011>
- Huang, Z., Zhang, J., Zhao, Y., Zhang, H., Yue, G., Suda, T., & Narukawa, M. (2010). Kinetic studies of char gasification by steam and CO<sub>2</sub> in the presence of H<sub>2</sub> and CO. *Fuel Processing Technology*, *91*(8), 843–847. <https://doi.org/10.1016/j.fuproc.2009.12.020>
- Huo, W., Zhou, Z., Chen, X., Dai, Z., & Yu, G. (2014). Study on CO<sub>2</sub> gasification reactivity and physical characteristics of biomass, petroleum coke and coal chars. *Bioresource Technology*, *159*, 143–149. <https://doi.org/10.1016/j.biortech.2014.02.117>
- Hussein, A., Fafard, M., Ziegler, D., & Alamdari, H. (2017). Effects of Charcoal Addition on the Properties of Carbon Anodes. *Metals*, *7*(3), 98. <https://doi.org/10.3390/met7030098>
- Iwaszenko, S., Howaniec, N., & Smoliński, A. (2019). Determination of random pore model parameters for underground coal gasification simulation. *Energy*, *166*, 972–978. <https://doi.org/10.1016/j.energy.2018.10.156>
- Jeguirim, M., & Limousy, L. (2019). *Char and Carbon Materials Derived from Biomass: Production, Characterization and Applications*. Elsevier.
- Jones, F., Jones, P., De Marco, R., Pejčić, B., & Rohl, A. L. (2008). Understanding barium sulfate precipitation onto stainless steel. *Applied Surface Science*, *254*(11), 3459–3468. <https://doi.org/10.1016/j.apsusc.2007.11.062>
- Kaliyan, N., & Morey, R. V. (2010). Natural binders and solid bridge type binding mechanisms in briquettes and pellets made from corn stover and switchgrass. *Bioresource Technology*, *101*(3), 1082–1090. <https://doi.org/10.1016/j.biortech.2009.08.064>
- Kandiyoti, R., Herod, A., Bartle, K., & Morgan, T. (2017). Elements of thermal breakdown: Heating rate effects and retrogressive reactions. In *Solid Fuels and Heavy Hydrocarbon Liquids* (pp. 251–283). Elsevier. <https://doi.org/10.1016/b978-0-08-100784-6.00006-0>
- Kato, K., & Seiji, N. (2009). Coal Pre-treating Technologies for Improving Coke Quality. *International Congress on the Science and Technology of Iron Making*, 361–366.
- Kawamoto, H. (2017). Lignin pyrolysis reactions. *Journal of Wood Science*, *63*(2), 117–132. <https://doi.org/10.1007/s10086-016-1606-z>

- Kemppainen, K., Ranta, L., Sipilä, E., Östman, A., Vehmaanperä, J., Puranen, T., Langfelder, K., Hannula, J., Kallioinen, A., Siika-Aho, M., Sipilä, K., & von Weymarn, N. (2012). Ethanol and biogas production from waste fibre and fibre sludge - The FibreEtOH concept. *Biomass and Bioenergy*, *46*, 60–69. <https://doi.org/10.1016/j.biombioe.2012.03.027>
- Khan, T. A., Lee, J. H., & Kim, H. J. (2019). Lignin-Based Adhesives and Coatings. *Lignocellulose for Future Bioeconomy*, 153–206. <https://doi.org/10.1016/b978-0-12-816354-2.00009-8>
- Kifani-Sahban, F., Kifani, A., Belkbir, L., Zoulalian, A., Arauzo, J., & Cardero, T. (1997). A physical approach in the understanding of the phenomena accompanying the thermal treatment of lignin. *Thermochimica Acta*, *298*(1–2), 199–204. [https://doi.org/10.1016/S0040-6031\(97\)00115-9](https://doi.org/10.1016/S0040-6031(97)00115-9)
- Kokonya, S., Castro-Díaz, M., Barriocanal, C., & Snape, C. E. (2013). An investigation into the effect of fast heating on fluidity development and coke quality for blends of coal and biomass. *Biomass and Bioenergy*, *56*, 295–306. <https://doi.org/10.1016/j.biombioe.2013.05.026>
- Konno, S., Kubota, Y., Nomura, S., Uebo, K., Dobashi, A., & Doi, K. (2020). *Effect of Coal Size on Coking Pressure and Coke Strength*.
- Koskela, A., Heikkilä, A., Bergna, D., Salminen, J., & Fabritius, T. (2021). Effects of Briquetting and High Pyrolysis Temperature on Hydrolysis Lignin Char Properties and Reactivity in CO-CO<sub>2</sub>-N<sub>2</sub> Conditions. *Minerals*, *11*(2), 187. <https://doi.org/10.3390/min11020187>
- Koskela, A., Suopajarvi, H., & Fabritius, T. (2022a). Interaction between coal and lignin briquettes in co-carbonization. *Fuel*, *324*, 124823. <https://doi.org/10.1016/j.fuel.2022.124823>
- Koskela, A., Suopajarvi, H., Gornostayev, S., Uusitalo, J., & Fabritius, T. (2022b). Improvement of coke strength by HDPE addition. *International Journal of Coal Preparation and Utilization*. <https://doi.org/10.1080/19392699.2022.2066088>
- Koskela, A., Suopajarvi, H., Mattila, O., Uusitalo, J., & Fabritius, T. (2019). Lignin from Bioethanol Production as a Part of a Raw Material Blend of a Metallurgical Coke. *Energies*, *12*(8), 1533. <https://doi.org/10.3390/en12081533>
- Koskela, A., Suopajarvi, H., Uusitalo, J., & Fabritius, T. (2023). Evolution of biocarbon strength and structure during gasification in CO<sub>2</sub> containing gas atmosphere. *Fuel Communications*, *14*, 100082. <https://doi.org/10.1016/j.jfueco.2022.100082>
- Krebs, V., Furdin, G., Marêché, J. F., & Dumay, D. (1996). Effects of coal moisture content on carbon deposition in coke ovens. *Fuel*, *75*(8), 979–986. [https://doi.org/10.1016/0016-2361\(96\)00039-7](https://doi.org/10.1016/0016-2361(96)00039-7)
- Kumar, M., & Gupta, R. C. (1997). Industrial Uses of Wood Char. *Energy Sources*, *20*(7), 575–589. <https://doi.org/10.1080/00908319808970079>
- Li, J., Bai, X., Fang, Y., Chen, Y., Wang, X., Chen, H., & Yang, H. (2020). Comprehensive mechanism of initial stage for lignin pyrolysis. *Combustion and Flame*, *215*, 1–9. <https://doi.org/10.1016/j.combustflame.2020.01.016>

- Li, K., Khanna, R., Zhang, J., Liu, Z., Sahajwalla, V., Yang, T., & Kong, D. (2014). The evolution of structural order, microstructure and mineral matter of metallurgical coke in a blast furnace: A review. *Fuel*, *133*, 194–215. <https://doi.org/10.1016/j.fuel.2014.05.014>
- Li, K., Zhang, J., Barati, M., Khanna, R., Liu, Z., Zhong, J., Ning, X., Ren, S., Yang, T., & Sahajwalla, V. (2015). Influence of alkaline (Na, K) vapors on carbon and mineral behavior in blast furnace cokes. *Fuel*, *145*, 202–213. <https://doi.org/10.1016/j.fuel.2014.12.086>
- Liu, Q., Wang, S., Zheng, Y., Luo, Z., & Cen, K. (2008). Mechanism study of wood lignin pyrolysis by using TG–FTIR analysis. *Journal of Analytical and Applied Pyrolysis*, *82*(1), 170–177. <https://doi.org/10.1016/j.jaap.2008.03.007>
- Loison, R., Foch, P., & Boyer, A. (1989a). Coal in general. In R. Loison, P. Foch, & A. Boyer (Eds.), *Coke: quality and production* (2nd ed., pp. 1–58). Elsevier. <https://books.google.com/books/about/Coke.html?hl=fi&id=WIYjBQAAQBAJ>
- Loison, R., Foch, P., & Boyer, A. (1989b). Coke quality criteria. In R. Loison, P. Foch, & A. Boyer (Eds.), *Coke: quality and production* (2nd ed., pp. 158–200). Elsevier.
- Loison, R., Foch, P., & Boyer, A. (1989c). Phenomena of carbonization in a coke oven chamber. Theory of relationship to coke quality. In R. Loison, P. Foch, & A. Boyer (Eds.), *Coke: quality and production* (2nd ed., pp. 117–157).
- Lu, L., Adam, M., Sarath, H., Somerville, M., Hapugoda, S., Jahanshahi, S., & Mathieson, J. G. (2012). Iron Ore Sintering With Charcoal. *6th International Congress on the Science and Technology of Ironmaking – ICSTI*, 1121–1131.
- Luiz, J., Alves, F., De, R., Peralta, F., Moreira, M., Constantino Gomes Da Silva, J., Felix De Sena, R., De Fátima, R., Muniz Moreira, P., & José, H. J. (2018, May). *CO<sub>2</sub> Gasification of Biochars Prepared from Agroindustrial Waste: a Kinetic Study*. <https://doi.org/10.5071/26thEUBCE2018-2CV.4.20>
- Lyalyuk, V. P., Sokolova, V. P., Lyakhova, I. A., & Kassim, D. A. (2012). Ensuring Stable Quality of Blast Furnace Coke. *Coke and Chemistry*, *55*(8), 304–308. <https://doi.org/10.3103/s1068364x12080054>
- Mahmood, N., Yuan, Z., Schmidt, J., & Xu, C. (2016). Depolymerization of lignins and their applications for the preparation of polyols and rigid polyurethane foams: A review. *Renewable and Sustainable Energy Reviews*, *60*, 317–329. <https://doi.org/10.1016/j.rser.2016.01.037>
- Mahoney, M., Andriopoulos, N., Keating, J., Loo, C. E., & McGuire, S. (2005). Pilot scale simulation of cokemaking in integrated steelworks. *Ironmaking & Steelmaking*, *32*(6), 468–478. <https://doi.org/10.1179/174328105x48098>
- Mahony, B., Moulson, I., & Wilkinson, H. C. (1981). Study of the relation between the phosphorus content of coal and coke. *Fuel*, *60*(4), 355–358. [https://doi.org/10.1016/0016-2361\(81\)90206-4](https://doi.org/10.1016/0016-2361(81)90206-4)
- Mandlekar, N., Cayla, A., Rault, F., Giraud, S., Salaün, F., Malucelli, G., & Guan, J.-P. (2018). An overview on the use of lignin and its derivatives in fire retardant polymer systems. In M. Poletto (Ed.), *Lignin - Trends and Applications* (pp. 207–231). InTech Open.

- Manousiouthakis, V. I., & Choi, S. H. (2021). A carbon cycle optimization method for fossil and biomass energy utilization. *Korean Journal of Chemical Engineering*, 38(10), 2003–2008. <https://doi.org/10.1007/S11814-021-0899-9>
- Marcos, M., Bianco, L., Cirilli, F., Reichel, T., Baracchini, G., Echterhof, T., Rekersdrees, T., Mirabile, D., Griessacher, T., & Sommerauer, H. (2019). *Biochar for a sustainable EAF steel production (GREENEAF2) : final report*.
- Massoudi Farid, M., Kang, M. S., & Hwang, J. (2017). The effect of CO on coal–biomass co-gasification with CO<sub>2</sub>. *Fuel*, 188, 98–101. <https://doi.org/10.1016/j.fuel.2016.10.025>
- Mathews, J. P., & Chaffee, A. L. (2012). The molecular representations of coal – A review. *Fuel*, 96, 1–14. <https://doi.org/10.1016/j.fuel.2011.11.025>
- McGrath, T. E., Geoffrey Chan, W., & Hajaligol, M. R. (2003). Low temperature mechanism for the formation of polycyclic aromatic hydrocarbons from the pyrolysis of cellulose. *Journal of Analytical and Applied Pyrolysis*, 66(1–2), 51–70. [https://doi.org/10.1016/s0165-2370\(02\)00105-5](https://doi.org/10.1016/s0165-2370(02)00105-5)
- Mili, M., Hashmi, S. A. R., Ather, M., Hada, V., Markandeya, N., Kamble, S., Mohapatra, M., Rathore, S. K. S., Srivastava, A. K., & Verma, S. (2022). Novel lignin as natural-biodegradable binder for various sectors—A review. *Journal of Applied Polymer Science*, 139(15), 51951. <https://doi.org/10.1002/app.51951>
- Mochizuki, Y., & Tsubouchi, N. (2019). Preparation of pelletized coke by co-carbonization of caking coal and pyrolyzed char modified with tar produced during pyrolysis of woody biomass. *Fuel Processing Technology*, 193, 328–337. <https://doi.org/10.1016/j.fuproc.2019.05.036>
- Mousa, E., Wang, C., Riesbeck, J., & Larsson, M. (2016). Biomass applications in iron and steel industry: An overview of challenges and opportunities. *Renewable and Sustainable Energy Reviews*, 65, 1247–1266. <https://doi.org/10.1016/j.rser.2016.07.061>
- Naderi, M. (2015). Surface Area: Brunauer-Emmett-Teller (BET). In *Progress in Filtration and Separation* (pp. 585–608). Elsevier Ltd. <https://doi.org/10.1016/b978-0-12-384746-1.00014-8>
- Negi, S., & Pandey, A. K. (2015). Ionic Liquid Pretreatment. In A. K. Pandey, S. Negi, P. Binod, & C. Larroche (Eds.), *Pretreatment of Biomass: Processes and Technologies* (pp. 137–155). Elsevier. <https://doi.org/10.1016/b978-0-12-800080-9.00008-6>
- Nomura, S., Arima, T., & Kato, K. (2004). Coal blending theory for dry coal charging process. *Fuel*, 83(13), 1771–1776. <https://doi.org/10.1016/j.fuel.2004.03.006>
- Nomura, S., Naito, M., & Yamaguchi, K. (2007). Post-reaction Strength of Catalyst-added Highly Reactive Coke. *ISIJ International*, 47(6), 831–839. <https://doi.org/10.2355/isijinternational.47.831>
- Ortega, A. (1996). Some successes and failures of the methods based on several experiments. *Thermochimica Acta*, 284(2), 379–387. [https://doi.org/10.1016/0040-6031\(95\)02766-1](https://doi.org/10.1016/0040-6031(95)02766-1)
- Otani, C., Polidoro, H. A., Otani, S., & Craievich, A. (1984). Structure variations of carbonizing lignin. *Journal de Chimie Physique*, 81, 887–891. <https://doi.org/10.1051/jcp/1984810887>

- Pastorova, I., Botto, R. E., Arisz, P. W., & Boon, J. J. (1994). Cellulose char structure: a combined analytical Py-GC-MS, FTIR, and NMR study. *Carbohydrate Research*, 262(1), 27–47. [https://doi.org/10.1016/0008-6215\(94\)84003-2](https://doi.org/10.1016/0008-6215(94)84003-2)
- Patisson, F., & Mirgaux, O. (2020). Hydrogen Ironmaking: How It Works. *Metals*, 10(7), 922. <https://doi.org/10.3390/met10070922>
- Patrick, J. W. (1974). The coking of coal. *Science Progress*, 61(243), 375–399.
- Patwardhan, P. R., Dalluge, D. L., Shanks, B. H., & Brown, R. C. (2011). Distinguishing primary and secondary reactions of cellulose pyrolysis. *Bioresource Technology*, 102(8), 5265–5269. <https://doi.org/10.1016/j.biortech.2011.02.018>
- Phounglamcheik, A., Wang, L., Romar, H., Kienzl, N., Broström, M., Ramser, K., Skreiberg, Ø., & Umeki, K. (2020). Effects of Pyrolysis Conditions and Feedstocks on the Properties and Gasification Reactivity of Charcoal from Woodchips. *Energy and Fuels*, 34(7), 8353–8365. <https://doi.org/10.1021/acs.energyfuels.0c00592>
- Pienihäkkinen, E., Lindfors, C., Ohra-Aho, T., Lehtonen, J., Granström, T., Yamamoto, M., & Oasmaa, A. (2021). Fast Pyrolysis of Hydrolysis Lignin in Fluidized Bed Reactors. *Energy and Fuels*, 35(18), 14758–14769. <https://doi.org/10.1021/acs.energyfuels.1c01719>
- Raj, T., Chandrasekhar, K., Naresh Kumar, A., Rajesh Banu, J., Yoon, J. J., Kant Bhatia, S., Yang, Y. H., Varjani, S., & Kim, S. H. (2022). Recent advances in commercial biorefineries for lignocellulosic ethanol production: Current status, challenges and future perspectives. *Bioresource Technology*, 344, 126292. <https://doi.org/10.1016/j.biortech.2021.126292>
- Roberts, D. G., & Harris, D. J. (2012). High-pressure char gasification kinetics: CO inhibition of the C-CO<sub>2</sub> reaction. *Energy and Fuels*, 26(1), 176–184. <https://doi.org/10.1021/ef201174k>
- Robinson, R., Brabie, L., Pettersson, M., Amovic, M., & Ljunggren, R. (2020). An Empirical Comparative Study of Renewable Biochar and Fossil Carbon as Carburizer in Steelmaking. *ISIJ International*, ISIJINT-2020-135. <https://doi.org/10.2355/isijinternational.isijint-2020-135>
- Rowell, R. M., Pettersen, R., & Tshabalala, M. A. (2012). Cell Wall Chemistry. In *Handbook of Wood Chemistry and Wood Composites, Second Edition* (pp. 33–72). CRC Press. <https://doi.org/10.1201/b12487-5>
- Ryu, Z., Zheng, J., & Wang, M. (1998). Porous structure of pan-based activated carbon fibers. *Carbon*, 36(4), 427–432. [https://doi.org/10.1016/s0008-6223\(97\)00225-x](https://doi.org/10.1016/s0008-6223(97)00225-x)
- Sakaranaho, M., Heikkilä, A., Suopajarvi, H., Päätaalo, M., & Fabritius, T. (2018). Charcoal Use in Chromite Pellets – Effect on Sintering Process, Pellet Properties, and Electrical Conductivity. *Steel Research International*, 89(2), 1700260. <https://doi.org/10.1002/srin.201700260>
- Schweinfurth, S. P. (2009). An Introduction to Coal Quality . In B. S. Pierce & K. O. Dennen (Eds.), *The National Coal Resource Assessment Overview: U.S. Geological Survey Professional Paper 1625–F, Chapter C* (p. 16). <http://www.usgs.gov/pubprod>

- Solar, J., Caballero, B. M., Barriocanal, C., Lopez-Urionabarrenechea, A., & Acha, E. (2021). Impact of the Addition of Pyrolysed Forestry Waste to the Coking Process on the Resulting Green Biocoke. *Metals*, *11*(4), 613. <https://doi.org/10.3390/met11040613>
- Spreitzer, D., & Schenk, J. (2019). Reduction of Iron Oxides with Hydrogen—A Review. *Steel Research International*, *90*(10), 1900108. <https://doi.org/10.1002/srin.201900108>
- Struis, R. P. W. J., Von Scala, C., Stucki, S., & Pins, R. (2001). Gasification Reactivity of Charcoal with CO<sub>2</sub> at Elevated Conversion Levels. In A. V. Bridgwater (Ed.), *Progress in Thermochemical Biomass Conversion* (Vol. 1, pp. 73–91). Wiley Blackwell. <https://doi.org/10.1002/9780470694954.ch5>
- Suarez-Ruiz, I., Diez, M. A., & Rubiera, F. (2018). Coal. In I. Suárez-Ruiz, M. A. Diez, & F. Rubiera (Eds.), *New Trends in Coal Conversion: Combustion, Gasification, Emissions, and Coking* (pp. 1–30). Elsevier. <https://doi.org/10.1016/b978-0-08-102201-6.00001-7>
- Suárez-Ruiz, I., & Ward, C. R. (2008). Basic Factors Controlling Coal Quality and Technological Behavior of Coal. In I. Suárez-Ruiz & J. C. Crelling (Eds.), *Applied Coal Petrology* (pp. 19–59). Elsevier. <https://doi.org/10.1016/b978-0-08-045051-3.00002-6>
- Suopajarvi, H., Dahl, E., Kemppainen, A., Gornostayev, S., Koskela, A., & Fabritius, T. (2017). Effect of Charcoal and Kraft-Lignin Addition on Coke Compression Strength and Reactivity. *Energies*, *10*(11), 1850. <https://doi.org/10.3390/en10111850>
- Thommes, M., Kaneko, K., Neimark, A. V., Olivier, J. P., Rodriguez-Reinoso, F., Rouquerol, J., & Sing, K. S. W. (2015). Physisorption of gases, with special reference to the evaluation of surface area and pore size distribution (IUPAC Technical Report). *Pure and Applied Chemistry*. <https://doi.org/10.1515/pac-2014-1117>
- Toloue Farrokh, N., Suopajarvi, H., Mattila, O., Umeki, K., Phounglamcheik, A., Romar, H., Sulasalmi, P., & Fabritius, T. (2018). Slow pyrolysis of by-product lignin from wood-based ethanol production— A detailed analysis of the produced chars. *Energy*, *164*, 112–123. <https://doi.org/10.1016/j.energy.2018.08.161>
- U.S. Secretary of Commerce. (2022). *NIST Chemistry WebBook*. <https://doi.org/https://doi.org/10.18434/t4d303>
- Van de Velden, M., Baeyens, J., Brems, A., Janssens, B., & Dewil, R. (2010). Fundamentals, kinetics and endothermicity of the biomass pyrolysis reaction. *Renewable Energy*, *35*(1), 232–242. <https://doi.org/10.1016/j.renene.2009.04.019>
- Vogl, V., Åhman, M., & Nilsson, L. J. (2018). Assessment of hydrogen direct reduction for fossil-free steelmaking. *Journal of Cleaner Production*, *203*, 736–745. <https://doi.org/10.1016/j.jclepro.2018.08.279>
- Wang, Y., Sridhar, S., & Valdez, M. (2002). Formation of CaS on Al<sub>2</sub>O<sub>3</sub>-CaO inclusions during solidification of steels. *Metallurgical and Materials Transactions B*, *33*(4), 625–632. <https://doi.org/10.1007/s11663-002-0042-1>
- Ward, C. R. (2003). Coal Geology. In R. A. Meyers (Ed.), *Encyclopedia of Physical Science and Technology* (3rd ed., pp. 45–77). Elsevier. <https://doi.org/10.1016/b978-0-12-409548-9.05437-3>

- Ward, C. R., Corcoran, J. F., Saxby, J. D., & Read, H. W. (1996). Occurrence of phosphorus minerals in Australian coal seams. *International Journal of Coal Geology*, 30(3), 185–210. [https://doi.org/10.1016/0166-5162\(95\)00055-0](https://doi.org/10.1016/0166-5162(95)00055-0)
- Ward, C. R., & Suárez-Ruiz, I. (2008). Introduction to Applied Coal Petrology. In I. Suárez-Ruiz & J. C. Crelling (Eds.), *Applied Coal Petrology* (pp. 1–18). Elsevier. <https://doi.org/10.1016/b978-0-08-045051-3.00001-4>
- Williams, P. T., & Besler, S. (1996). The Influence of Temperature and Heating Rate on the Slow Pyrolysis of Biomass. *Renewable Energy*, 7(3), 233–250. [https://doi.org/10.1016/0960-1481\(96\)00006-7](https://doi.org/10.1016/0960-1481(96)00006-7)
- Wiser, W. H. (1984). Conversion of bituminous coals to liquids and gases. In L. Petrakis & J. Fraissard (Eds.), *Magnetic Resonance: Introduction, Advanced Topics and Applications to Fossil Energy (NATO ASI Series C): Vol. 124. D.* (p. 325). Reidel Publishing Company.
- Yan, M., Song, X., Tian, J., Lv, X., Zhang, Z., Yu, X., & Zhang, S. (2020). Construction of a New Type of Coal Moisture Control Device Based on the Characteristic of Indirect Drying Process of Coking Coal. *Energies*, 13(16), 4162. <https://doi.org/10.3390/en13164162>
- Yang, H., Yan, R., Chen, H., Lee, D. H., & Zheng, C. (2007). Characteristics of hemicellulose, cellulose and lignin pyrolysis. *Fuel*, 86(12–13), 1781–1788. <https://doi.org/10.1016/j.fuel.2006.12.013>
- Yang, Y., Raipala, K., & Holappa, L. (2014). Ironmaking. In S. Seetharaman (Ed.), *Treatise on Process Metallurgy* (Vol. 3, pp. 2–88). Elsevier. <https://doi.org/10.1016/b978-0-08-096988-6.00017-1>
- Yu, J., Wang, D., & Sun, L. (2021). The pyrolysis of lignin: Pathway and interaction studies. *Fuel*, 290, 120078. <https://doi.org/10.1016/j.fuel.2020.120078>
- Zevallos Torres, L. A., Lorenci Woiciechowski, A., de Andrade Tanobe, V. O., Karp, S. G., Guimarães Lorenci, L. C., Faulds, C., & Soccol, C. R. (2020). Lignin as a potential source of high-added value compounds: A review. *Journal of Cleaner Production*, 263, 121499. <https://doi.org/10.1016/j.jclepro.2020.121499>
- Zhang, C., Shao, Y., Zhang, L., Zhang, S., Westerhof, R. J. M., Liu, Q., Jia, P., Li, Q., Wang, Y., & Hu, X. (2020). Impacts of temperature on evolution of char structure during pyrolysis of lignin. *Science of The Total Environment*, 699, 134381. <https://doi.org/10.1016/j.scitotenv.2019.134381>
- Zhao, J., Xiuwen, W., Hu, J., Liu, Q., Shen, D., & Xiao, R. (2014). Thermal degradation of softwood lignin and hardwood lignin by TG-FTIR and Py-GC/MS. *Polymer Degradation and Stability*, 108, 133–138. <https://doi.org/10.1016/j.polymdegradstab.2014.06.006>
- Zheng, Q., Zhang, D., Fu, P., Wang, A., Sun, Y., Li, Z., & Fan, Q. (2022). Insight into the fast pyrolysis of lignin: Unraveling the role of volatile evolving and char structural evolution. *Chemical Engineering Journal*, 437, 135316. <https://doi.org/10.1016/j.cej.2022.135316>

## Original publications

- I Koskela, A., Suopajarvi, H., Mattila, O., Uusitalo, J., & Fabritius, T. (2019). Lignin from bioethanol production as a part of a raw material blend of a metallurgical coke. *Energies*, *12*(8), 1533. <https://doi.org/10.3390/en12081533>
- II Koskela, A., Heikkilä, A., Bergna, D., Salminen, J., & Fabritius, T. (2021). Effects of briquetting and high pyrolysis temperature on hydrolysis lignin char properties and reactivity in CO-CO<sub>2</sub>-N<sub>2</sub> conditions. *Minerals*, *11*(2), 187. <https://doi.org/10.3390/min11020187>
- III Koskela, A., Suopajarvi, H., & Fabritius, T. (2022). Interaction between coal and lignin briquettes in co-carbonization. *Fuel*, *324*, 124823. <https://doi.org/10.1016/j.fuel.2022.124823>
- IV Koskela, A., Suopajarvi, H., Uusitalo, J., & Fabritius, T. (2023). Evolution of biocarbon strength and structure during gasification in CO<sub>2</sub> containing gas atmosphere. *Fuel Communications*, *14*, 100082. <https://doi.org/10.1016/j.jfueco.2022.100082>

Reprinted under Creative Commons CC BY 4.0 license<sup>1</sup> (Publications I–IV © 2019, 2021, 2022 and 2022 Authors).

Original publications are not included in the electronic version of the thesis.

---

<sup>1</sup> <https://creativecommons.org/licenses/by/4.0/>



866. Shi, Henglin (2023) Learning-based human action and affective gesture analysis
867. Pálvölgyi, Petra (2023) Synthesis of porous dielectric materials for future wireless high frequency applications
868. Kovacevic, Ivana (2023) Advanced network slicing and computational offloading for latency limited communications
869. Ikkala, Lauri (2023) Airborne remote sensing as a tool for monitoring topographical and hydrological changes on northern degraded and restored peatlands
870. Virpiranta, Hanna (2023) Development of biological treatment for sulfate- and metals-containing cold mining-impacted waters
871. Alzaza, Ahmad (2023) Cementitious binders for construction in northern cold regions
872. Kantanen, Pekka (2023) The role of finely divided retained austenite on the mechanical properties of QP and ART processed novel 0.3C ultrahigh strength steels
873. Markkula, Juho (2023) Communicating smart grid demand response and control data through LTE network related solutions
874. Laukkanen, Johanna (2023) Alkali-activation of industrial aluminosilicate sidestreams : application for mine water treatment and sediment remediation
875. Ismail, Mostafa (2023) Advanced imaging of lignocellulosic and cellulose materials
876. Abdelrahim, Ahmed (2023) Towards lower CO<sub>2</sub> emissions in iron and steelmaking : hydrogen-assisted reduction and cement-free briquettes
877. Zhou, Jin (2023) Conductive composites of engineered nanomaterials with excellent gas sensing properties
878. Ali, Farooq (2023) A framework for analyzing, developing, and managing stakeholder network relationships in collaborative hospital construction projects
879. Rönkkö, Pasi (2023) Circular economy as an enabler of improved resilience and material availability in supply chains
880. Isteri, Visa (2023) Alternative ye'elimate (CSA) cement clinkers from industrial byproducts
881. Aprialdi, Dwinata (2023) Forest hydrological studies to improve water management in marine lowlands in Palembang, Indonesia

Book orders:

Virtual book store

<https://verkkokauppa.omapumu.com/fi/>

S E R I E S E D I T O R S

**A**  
**SCIENTIAE RERUM NATURALIUM**

*University Lecturer Mahmoud Filali*

**B**  
**HUMANIORA**

*University Lecturer Santeri Palviainen*

**C**  
**TECHNICA**

*Senior Research Fellow Antti Kaijalainen*

**D**  
**MEDICA**

*University Lecturer Pirjo Kaakinen*

**E**  
**SCIENTIAE RERUM SOCIALIUM**

*University Lecturer Henri Pettersson*

**E**  
**SCRIPTA ACADEMICA**

*Strategy Officer Mari Katvala*

**G**  
**OECONOMICA**

*University Researcher Marko Korhonen*

**H**  
**ARCHITECTONICA**

*Associate Professor Anu Soikkeli*

**EDITOR IN CHIEF**

*University Lecturer Santeri Palviainen*

**PUBLICATIONS EDITOR**

*Publications Editor Kirsti Nurkkala*

ISBN 978-952-62-3667-4 (Paperback)

ISBN 978-952-62-3668-1 (PDF)

ISSN 0355-3213 (Print)

ISSN 1796-2226 (Online)